Wear and friction studies of alumina: Correlation with electron triboemission

Dan A. Mazilu

Dissertation submitted to the Faculty of the Virginia Polytechnic Institute and State University in partial fulfillment of the requirements for the degree of

DOCTOR OF PHILOSOPHY

in

PHYSICS

A. L. Ritter, Chair

M. J. Furey

R. K. P. Zia

J. R. Heflin

T. Mizutani

December 12, 2002

Blacksburg, Virginia

Keywords: alumina, wear, friction, triboemission, lognormal

Wear and friction studies of alumina: Correlation with electron triboemission

by

Dan A. Mazilu

Abstract

The first question addressed in this thesis is whether the cumulative triboemission from the abrasion of alumina by a diamond indenter (repeat-pass sliding) correlates with the volume of material removed and, in particular, whether transitions in the rate of material removal are mirrored in the cumulative triboemission rate. As a function of load and number of diamond passes, several wear regimes are observed that are characterized from SEM micrographs by different relative proportions of plastic flow material and fractured surface in the wear scar. In all but one wear regime, the correlation between the wear volume and cumulative triboemission is modest (linear regression coefficient $R^2 = 0.71$); including the one atypical wear regime worsens the correlation. The wear volume and cumulative triboemission are shown to be random variables with normal and lognormal distributions, respectively. Again, excluding the atypical wear regime, the correlation between the logarithms of the estimated population means is significantly better ($R^2 = 0.91$) than the correlation between wear volume and cumulative triboemission for individual samples. In addition to the overall correlation between wear volume and cumulative triboemission, transitions from one wear regime to another are marked by changes in the slope of the mean cumulative triboemission versus pass number. These transitions correlate with the relative fraction of plastic flow debris in the wear scar.

The second question addressed in this thesis is whether the introduction of the chemical vapor aluminum tri-sec butoxide, $[C_2H_5CH(CH_3)O]_3Al \equiv$ ATSB, into the boundary layer of an alumina-on-alumina sliding contact can reduce wear and friction. A split-plot factorial experiment was conducted; the factors tested, in addition to the presence or absence of ATSB, were normal load, sliding speed, and surface roughness. The main conclusions of the experiment are that ATSB has no statistically significant effect on specific wear, but that the presence of ATSB reduces friction by 21% at low sliding speed (0.02 m/s) and increases friction by 26% at high sliding speed (1.2 m/s).

To my wife Irina

Acknowledgements

I would like to express my sincere gratitude to Dr. A. L. Ritter for all his help during my graduate studies at Virginia Tech. Without his constant support, this work could not have been accomplished.

I would also like to thank the members of my advisory committee, Dr. M. J. Furey, Dr. R. K. P. Zia, Dr. J. R. Heflin and Dr. T. Mizutani for their time and support. In particular, I would like express my appreciation to Dr. Furey for all his assistance and suggestions.

I am indebted and would like to thank to Dr. Gustavo Molina for building the experimental apparatus and for all his help. I also want to thank Melvin Shaver, John Miller, Scott Allen, Fred Mahone and Judy Faw for all their help and Chris Thomas for her constant support.

Finally, a special thank you goes to my wife Irina and to my parents and sister.

Contents

List of Figures

List of Tables

Chapter 1. Introduction and Overview

Traditionally, the material of choice for applications involving wear and friction is a strengthened metal or alloy, generally with the aid of a lubricant. However, ceramic materials offer some unique advantages as tribomaterials and are increasingly employed over conventional materials in tribological systems. Because of their outstanding physical and chemical properties (strength, hardness, chemical inertness, thermal shock resistance), ceramics are ideal candidates for using in adiabatic diesel engines, turbine components, roller and slider bearings, pump seals, cutting tools, replacement hip joints [1] and numerous other applications in severe conditions. However, there are challenges that limit the use of ceramics as tribomaterials and that have to be overcome before ceramics can be used in such practical applications. A better understanding of the microstructural and compositional characteristics that govern the wear behavior of ceramics is demanded.

One such challenge to be overcome has to do with difficulties in the lubrication of ceramics. Ceramics do not respond to conventional lubricants, which are designed to function by a chemical reaction with the surface. In particular, traditional lubricants are not suitable for use at very high operating temperatures. Several dry lubricants exist (graphite, DLC, MoS2), but they do not have desired combination of wear and friction characteristics. Desirable material properties for low wear and low friction appear to be antithetical – soft material for low friction and hard material for low wear. There is, accordingly, an increased interest in the development of lubrication alternatives for ceramics, and in understanding the tribochemical fundamentals by which new lubrication processes can be designed and controlled. The research described in the second chapter of this thesis, *Correlation between wear and triboemission in the abrasive wear of alumina by diamond*, is motivated by a novel lubrication mechanism developed by Furey and Kajdas [2] called tribopolymerization. This mechanism provides boundary lubrication to ceramics by the continuous formation of a protective polymeric film on the surfaces in

contact. Triboemitted particles may have a dramatic, if not controlling influence on some tribochemical reactions that occur in the contact region; in particular, the mechanism of tribopolymerization for some addition-type monomers is thought to be initiated and controlled by low-energy electrons [3] that are emitted when ceramic or oxide surfaces are perturbed during tribological contact. Therefore, a strong interest exists in characterizing the charged-particle triboemission from ceramics. This characterization becomes even more important if a correlation were found to exist between the intensity of the charged particle triboemission and the wear of the material under tribological contact. Such an observation would suggests the potential of using the triboemission as a real-time probe [4] for the wear behavior of the ceramic.

The reason for wanting to do this stems from the fact that a wear measurement is by necessity post-hoc (the technical difficulties in trying to measure the wear volume in real time would be considerable, if not insurmountable). On the other hand, a triboemission measurement can take place in real time. A good correlation between the registered triboemission and the wear of the material would, conceivably, allow one to predict when catastrophic wear and failure occur or when certain prescribed limits on the wear volume have been reached that terminate the useful life of the ceramic component. At the same time, provided a reliable correlation were found, changes in the triboemission rate could be linked to transitions between different wear regimes for the ceramic.

For all these reasons, we designed this experiment to address the question of whether the cumulative triboemission and the wear volume are correlate for the abrasion of alumina with diamond; in particular, we wanted to investigate whether transition in the rates of material removal were accompanied by similar transitions in the cumulative triboemission rate. Chapter 2 of this thesis gives a detailed description of this experiment. In summary, we abraded a disk-shaped alumina sample with a diamond indenter in a pin-on-disk configuration and we measured the ensuing triboemission and the wear volume.

We found that significant variability exists both in the cumulative triboemission and the wear volume for samples tested under the same conditions of load and speed. The sample-to-sample distribution of the cumulative triboemission and wear volume are lognormal [5] and normal, respectively. A correlation exists between the population mean of the cumulative triboemission and the population mean of the wear volume even though the total emission and the total wear for individual samples are only modestly correlated. The answer to the question, does a correlation exist between the mean cumulative triboemission and the mean wear volume, is a qualified yes. The results and the qualification are discussed in detail in section 2.5.

The third chapter of this thesis, *Friction and wear of alumina in the presence of the chemical vapor aluminum-tri-sec butoxide*, describes an experiment that was designed to study the feasibility of wear and friction reduction in the sliding contact of alumina-on-alumina. This is accomplished by the growth of fresh ceramic material on the surfaces in contact from an appropriate chemical vapor, using tribological stress as a source of energy for decomposing the vapor. We introduced the chemical vapor aluminum tri-sec butoxide, $[C_2H_5CH(CH_3)O]_3Al \equiv$ ATSB, into the boundary layer of an alumina-on-alumina sliding contact using a ball-on-cylinder geometry. Since the efficacy of ATSB in the boundary layer might depend on other factors, we conducted a split-plot factorial experiment using the surface roughness as the plot variable. The other factors tested (sub-plot variables) were the presence or absence of ATSB, the normal load, and the sliding speed. The product of normal load and sliding distance was constant in these experiments.

The main conclusions of the experiment are that ATSB has no statistically significant effect on the specific wear, but that the presence of ATSB reduces friction by 21% at low sliding speed (0.02 m/s) and increases friction by 26% at high sliding speed (1.2 m/s). Secondary conclusions regarding the dependence of specific wear and friction on surface roughness, sliding speed and normal load are also discussed in section 3.4.

References

[1] O.O. Ajayi and K.C. Ludema, *Surface damage of structural ceramics: Implications for wear modeling*, Wear **124**, 237-257 (1988).

[2] M.J. Furey and C. Kajdas, *Models of tribopolymerization as an anti-wear mechanism*, Proc. Japan International Tribology Conference, Nagoya, Japan, pp. 1089-1094 (1990).

[3] C. Kajdas, *Importance of anionic reactive intermediates for lubricant component reactions with friction surfaces*, Lubrication Science **6-3**, pp. 203-228 (1994).

[4] J.T. Dickinson, L. Scudiero, K. Yasuda, M.W. Kim and S.C. Langford, *Dynamic tribological probes: particle emission and transient electrical measurements*, Tribology Letters **3**, 53-67 (1997).

[5] E. Limpert, W.A. Stahel and M. Abbt, *Log-normal Distributions across the Sciences: Keys and Clues*, Bioscience **51** No. 5, 341-352 (2001).

Chapter 2. Correlation between wear and triboemission in the abrasive wear of alumina by diamond

2.1 Introduction

The question addressed by this study is whether the cumulative triboemission from the abrasion of alumina correlates with the volume of material removed and, in particular, whether transitions in the rate of material removal are mirrored in the cumulative triboemission rate. The term "triboemission" refers to the emission of electrons, ions, neutral particles, photons and acoustic emission from the interface between materials under tribological stress. In this thesis, the term triboemission is used to refer to electron emission. The source of energy for ejecting the emitted electron may be localized surface excitations due to the creation of cracks, slip dislocations and micro-twinning or chemical reactions between atmosphere and freshly exposed surfaces.

To our knowledge, no one has attempted to demonstrate the correlation between the wear of alumina or other material and triboemission. The importance of this correlation stems from the fact that triboemission can provide a real-time probe of the wear process. Friction measurements can be made in real time, but friction and wear are not correlated, and therefore friction does not provide insight into the evolution of the wear process. Other ways to examine the processes leading to catastrophic wear and/or failure, such as optical or scanning electron microscopy are difficult to employ in real time, when the wear is occurring, and therefore have the disadvantage of being post-hoc. Electron emission measurements, however, can be made in real time, much like friction measurements, and they can provide insight into the evolution of the surfaces prior to the

onset of the catastrophic wear and the termination of the useful life of the ceramic components in practical applications. We used the abrasion of alumina by diamond to study whether such a correlation between wear and triboemission exists.

The abrasive wear of alumina by diamond and the triboemission of charged particles were studied using a tribometer with a conical indenter-on-disk contact geometry. The tribometer allows the variation and control of the applied load and sliding speed over a broad range of values. The instrument is equipped with a channel electron multiplier (CEM) to detect the charged particles emitted from the contact region. The tests were carried out inside a vacuum chamber at pressures lower than 10^{-4} Pa and at room temperature. The disk-shaped alumina samples were scratched by a conical diamond indenter under two different loads (10 N and 30 N) and for different numbers of passes. The triboemission measurements consisted of recording the number of particles emitted before the disk began rotating (background), while the disk was rotating and being scratched with the diamond indenter, and after the disk stopped (post-emission). After the tests, the surface profiles of the scratched specimens were obtained by means of stylus profilometry and the volume of material removed from the samples was calculated from the surface profiles of the wear tracks. The samples were also examined by scanning electron microscopy (SEM).

For both loads, the wear volume was initially a linear function of pass number. For the 10 N load, however, the rate of material removal decreased dramatically 20 passes. The residuals of the wear volume with respect to the linear regression fit were normally distributed for both loads. The normality of the wear volume distribution bears emphasizing because we found the cumulative triboemission count to be distributed not normally, but rather lognormally.

For both loads, the measured wear profile exhibited significant variability at different positions along the circular wear scar. However, even though the standard deviation of

the wear volume increased in absolute value with the number of passes, the relative variability given by the coefficient of variation decreased for both loads with the number of passes. This observation agrees qualitatively with the features observed in the SEM micrographs of the samples. For low numbers of passes the variations in the track cross-sectional area were significant with respect to the actual track size. After more passes however, variability in the track cross-section still existed, but it was less significant compared with the actual size of the wear track.

Examination of the SEM micrographs of the samples revealed a pattern of successive wear regimes when the normal load is 10 N. Initially, the wear track is covered primarily with plastic flow material interspersed with much smaller areas of intergranular and intragranular fracture. After approximately two passes a transition occurs; the plastic flow material has delaminated from the wear scar surface which now is made up almost entirely of fractured surface. Then, after approximately 20 passes, another transition occurs. The wear scar is a mixture of plastic flow film and fractured surface. We infer that a steady state is achieved after 20 passes, in which the delamination of plastic material is balanced by the continuous re-formation of plastic film from the wear debris. The SEM pictures capture a particular moment of this balancing process. Our interpretation of these data is that the triboemission rate is low when the wear scar surface is free of plastic film and high when the plastic film is present and cracking and delaminating from the wear track during subsequent passes. The data for 30 N load does not show clear wear transitions, but suggests instead that the wear process mode is similar to the mode observed at 10 N load after 20 passes.

The triboemission is characterized by burst-type features at random times and by the presence of a component with approximately constant rate over several passes that results in a nearly linear cumulative emission. The non-burst emission rate may either increase or decrease, sometimes in conjunction with a burst and sometimes not, with concomitant change in the slope of the cumulative emission.

The cumulative electron count as a function of load and the number of passes exhibited significant variability from sample to sample under ostensibly identical testing conditions, emphasizing the necessity of treating it as a random variable with an underlying population characterized by a population mean and standard deviation. A significant finding of this thesis is that the distribution of the cumulative emission population is lognormal. The estimated population means do correlate well with pass number in contrast to the poor correlation between these two quantities for individual samples. Hypothesis testing performed on the cumulative triboemission data corroborated that the distribution is lognormal. The determination of the population distribution is critical in order to draw statistically valid inferences regarding the population parameters and their dependence on experimental variables [1].

We hypothesize that the cumulative triboemission for a given load and number of passes is proportional to the number of debris particles that are created during the abrasion process. The cumulative wear volume from sample-to-sample for specified load and number of passes is a random variable with normal, or near normal, distribution. But for a given cumulative wear volume, the number of debris particles can vary and, in fact, we argue that this number is a random variable with lognormal distribution.

The cumulative emission and the cumulative wear volume for each individual sample appear to be poorly correlated. The mean cumulative wear volume correlates, however, with the mean cumulative triboemission even though the distributions of these two quantities are different. Only in the last wear regime after 20 passes at 10 N load does the correlation break down. We infer that wear debris is continually ground but not ejected from the wear scar in this regime and as a consequence the triboemission rate remains high but the wear rate is low. The goal of this thesis is to provide a basis for understanding the macroscopic parameters that influence wear and ultimately to relate them to the underlying microscopic interactions between two surfaces sliding across each other.

2.2 Background

2.2.1 Wear

Three mechanisms of material removal from abrasion of alumina have been reported: brittle fracture, plastic deformation followed by delamination of the plastic flakes, and a "tribochemical" mechanism [2]. These mechanisms may act concurrently or in succession [3], [4].

The first mechanism, and perhaps the most important [2], is brittle fracture. Two types of cracks have been observed when an indenter is pressed into a ceramic substrate. One type consists of cracks that are normal to the surface and extend in a radial direction from the small region of contact. The second type is represented by lateral cracks that are parallel to the surface but relatively deep in the material [5], [6]. Some authors suggest that the interaction of the lateral and radial cracks results in material removal [5]-[7], but some argue that radial and lateral cracks do not contribute to wear. Instead, they argue that wear is a consequence of the fracture and fragmentation of material nearer the surface than the radial and lateral cracks. This scale of fracture is of the order of grain sizes whereas the radial and lateral cracks are of the order of the size of indentations and are usually below the indentation [2].

Ajayi and Ludema found that the damage due to successive passes of alumina on alumina consisted of plastic deformation with some grain boundary microfracture followed by fatigue-like flake removal (delamination) in the wear track. [2]. Although ceramic materials are considered to be brittle, plastic deformation has been observed during static and sliding contact. Plastic strain arises from dislocation motion and micro-twins and is seen clearly in the worn surface of alumina specimens. It is also evident in the broadening of X-ray diffraction patterns [8]. Plastic flow is seen in some cutting processes [8], some fatigue processes [9] and in "mild" wear processes [10]. Some authors suggest that

plasticity is enhanced by frictional heating, which has the effect of reducing the yield strength of materials [11], [12].

The plastic flow in alumina depends on the crystallographic orientation and is strongly anisotropic. In the case of single crystals of Al_2O_3, sliding parallel to prismatic planes in the c-axis direction leads to extensive fracture. However, sliding in other directions on these planes, or on the basal plane, is accompanied by plastic flow [13]. Therefore, the abraded surface of a polycrystalline alumina specimen can be expected to exhibit regions of intergranular fracture alongside areas of predominantly plastic flow, associated with differences in the crystallographic orientation of the grains.

The third mechanism of material removal is a "tribochemical" mechanism [2], [14], [15], which involves interfacial chemical reaction at the sliding interface, followed by removal of material by sliding contact. Our measurements were done in vacuum (pressure less than 10^{-6} torr) and though a film of water vapor initially existed on the surfaces of the alumina specimens, we do not expect significant contribution to the wear process from this mechanism after the first pass of the diamond tip.

An important aspect of the wear of alumina is the large variation observed by different investigators in the coefficient of friction and wear rate. Sharp transitions are observed in the wear rate as a function of pass number over the surface. However, these transitions in wear rate do not follow a consistent pattern. Numerous investigators reported a transition from mild to severe wear in repeat-pass sliding of alumina [16], [3]. This transition is characterized by a significant change in the coefficient of friction and an increase in the wear rate by as much as several orders of magnitude [3]. But Ajayi and Ludema [18] found the opposite behavior; during repeat-pass sliding, the wear rate was high at the beginning of the wear measurement and then decreased to a lower value after a few passes.

Several mechanisms for the mild-to-severe wear transition have been suggested. Wang et al. [19] introduced the "tensile stress model". They hypothesized that a wear transition occurs when the tensile stress at the contact exceeds a critical value. The transition is from a plastic deformation-controlled to a microcrack or microfracture-controlled wear mechanism. A sudden change occurs in the coefficient of friction and the wear rate. After the transition, wear is controlled by the microfracture or grain pullout. Blomberg et al. [16] found that the main wear mechanism was microfracture in the mild regime and surface macrofracture in the severe regime. Xu and Jahanmir [4] noted that repeated scratching of a polycrystalline alumina specimen with a diamond indenter causes damage accumulation in the material beneath the sliding contact area due to intergranular fracture. After a critical number of passes, a percolation-like transition was observed from a damage accumulation process with little material loss to a material removal process that involves mainly grain dislodgement (mild wear). At large loads, the removal process exhibited a second transition as a function of the number of passes, from grain dislodgement to a more severe wear process by lateral crack chipping. Cho et al. [17] also observed an abrupt mild-to-severe transition in the wear of alumina-on-alumina during sliding. They found that during the initial stage, surface material is removed by a plastic grooving process and is accompanied by the accumulation of subsurface dislocations arrays and twins. With continued sliding, internal stresses associated with this accumulating damage eventually resulted in grain boundary cracking and grain pull-out, which leads to the onset of fracture-dominated, severe wear. They noted that the observed change in wear behavior from a mild abrasive process to one involving fracture and grain pull-out can be alternatively described as a ductile to brittle transition.

Ajayi and Ludema [18] noted that the opposite behavior, severe-to-mild wear, might be due to the high contact pressure at the beginning of sliding. The contact pressure decreases with time as the nominal contact area between the wearing surfaces increases. They proposed, however, that a more likely source of wear rate reduction with time is the reattachment of some of the wear debris to form the so-called "transfer film" [18].

Through this process, some of the materials that become detached from the surfaces by wear (wear debris particles) remain in the wearing system. The film was observed to be continuous and adherent when an ionic material slid over an ionic material, whereas adherent islands formed when an ionic material slid over a covalent material. No distinct film formed when a covalent material slid over a covalent material. Sometimes the debris particles were deposited in surface pits produced by wear, without forming a continuous film. Whenever formed, the film was strongly attached, enough to resist being wiped off by the slider. The authors' calculations suggest that the fine particles are attached primarily by van der Waals forces and to a lesser extent by electrostatic attractive forces. The formation of this "transfer film" leads to a decrease in the wear rate because of the "protecting" role of the film. It was also reported that the formation of the transfer film in some ceramic materials in sliding contact coincided with transitions in friction and wear behavior [20].

The significant variability in the coefficients of friction and the wear rates of alumina, as well as the nature of their transitions, is due in part to the range of test conditions (e.g. load, sliding speed and material microstructure) and contact geometries used by the experimenters [17], [3] but also to the heterogeneous characteristic of this material.

2.2.2 Triboemission

The term "triboemission" refers to the emission of electrons, ions, neutral particles, photons and acoustic emission from the interface between materials under tribological stress. In this paper we will use the term triboemission to refer to electron emission. The source of energy for ejecting the emitted electron may be localized surface excitations due to the creation of cracks, slip dislocations and micro-twinning or chemical reactions between atmosphere and freshly exposed surfaces.

Triboemission of electrons as well as other charged particles was reported from early experimentation on exoemission [21]. Exoemission is the emission of electrons by solid surfaces that are subjected to mechanical work or tensile deformation. The emitted electrons are often named "exoelectrons" and they are typically of low energy. Exoemission often involves an Auger-like process in which an electron in a weakly bound surface state is ejected when a second electron drops into an empty state created by the material deformation process. The rate of exoemission decreases with time after the material deformation with a material-dependent time constant that varies from milliseconds to seconds [22].

Numerous investigators [23], [24], [25], [26], [27] have reported electron triboemission from a series of different materials (metals, ceramics, polymers, etc.). Electron emission is not observed during tribological stress of metals that do not have an oxide surface layer; it is observed from the fracture and abrasion of insulators, as well as from the interfacial failure of two bonded materials if one or both of the materials is an insulator. Triboemission also occurs in the fracture [28], [29] and abrasion [30] of semiconductors such as Si and Ge.

Similar to the findings of Dickinson et al. [24], [25], Molina et al. [31], [32] found that the electron triboemission in the abrasion of alumina with diamond occurred in large

bursts superimposed on a constant lower level of emission consisting of smaller bursts. The lower level emission was found not to vary significantly between different specimens. However, the magnitude of the large emission bursts was found to vary by as much as two orders of magnitude between different specimens of the same material, tested under identical conditions. The emission occurred at all times during the sliding of the diamond indenter on the alumina specimen and it continued at lower levels after the contact ceased. Retarded energy measurements by Molina [31] found that the kinetic energies of most triboemitted electrons were less than 5 eV, but the energy spectrum extended to 48 eV, the limit of the measurement. In the abrasion of MgO with diamond, Dickinson [24] found that the distribution of emitted electron kinetic energy extended to over 800 eV. They suggested that the very high energy electrons were emitted from surface patches that were negatively charged, created by charge transfer between the tip and substrate and by fracture.

The microscopic mechanism responsible for triboemission is not known, although various models have been proposed. Gieroszynski et al. [33]-[34] suggested a so-called "electrified fissure" mechanism according to which charge separation occurs between the walls of propagating cracks in ionic materials. Intense electric fields arise between the oppositely charged walls of the cracks and electrons are then ejected by field emission from the crack faces. Arnott and Ramsey [35] proposed that the strain energy released at the tip of the propagating crack may lead the emission of electrons, but they did not specify a detailed mechanism for the emission.

The wear of alumina involves crack formation due to tribological stress and triboemission is closely correlated with crack formation and propagation. Dickinson et al. demonstrated the causal relation between the creation and propagation of cracks in the oxide surface layer of aluminum due to tensile stress and the emission of electrons [23], [36], [37]. They used an acoustic transducer attached to the specimen that registered acoustic emission bursts that accompany the propagation of the tip of the crack through the

surface oxide layer. They found that the electron emission was strongly correlated with the acoustic emission for both long time scales (minutes) and short time scales (microseconds) [37]. The coincidence between the acoustic emission and the electron emission was interpreted as proof of the correlation between crack formation and propagation and electron emission [23], [36].

Dickinson et al. reviewed the characteristic features of the electron emission accompanying cleavage or fracture of materials [24]. Emission begins and is most intense during fracture; i.e., the rate of production and decay of excitations is highest during crack propagation. The negatively charged particles that are emitted are electrons and not negative ions, as demonstrated by the influence of an applied magnetic field on the detected emission. The emission associated with the fracture continues after fracture. This "post-emission" indicates that the fracture surfaces are still in an activated state and at least some of the relaxation processes are non-radiative. The "time-constants" for the decay of this post-emission depend strongly on the material and vary over orders of magnitude from milliseconds to tens or hundreds of seconds.

2.2.3 Correlation between wear of alumina and triboemission

To our knowledge, no one has attempted to demonstrate the correlation between the wear of alumina or other material and triboemission. We used the abrasion of alumina by diamond to study whether such a correlation exists. The importance of this correlation stems from the fact that triboemission can provide a real-time probe of the wear process.

When a hard diamond indenter abrades a softer alumina specimen in repeat-pass sliding, the alumina substrate can either deform plastically without material removal, or material may be removed by the processes discussed in section 2.2.1. Cracks are initiated and begin to propagate in the substrate. This eventually may lead to severe and even catastrophic wear of the alumina, which equates with the termination of the useful life of the substrate in tribological applications [24], [25].

Friction measurements can be made in real time, but friction and wear are not correlated, and therefore friction does not provide insight into the evolution of the wear process. Other ways to examine the processes leading to failure, such as optical or scanning electron microscopy are difficult to employ in real time, when the wear is occurring, and therefore have the disadvantage of being post-hoc. Electron emission measurements, however, can be made in real time, much like friction measurements, and they can provide insight into the evolution of the surfaces prior to the onset of the catastrophic wear regime. Due to the correlation between triboemission and the initiation and propagation of cracks in the material, electron emission can be used as a probe to examine in real time the dynamic interactions between interfaces in tribological contact. Such a time-resolved method of investigation of the wear process is desirable if alumina and other ceramics are to be used as tribomaterials in practical applications. The electron triboemission can yield insight on the evolution of ceramic substrates during wear and on the sequence of events that ultimately lead to failure [24], [25].

2.3 Experimental Procedures

The triboemission of electrons due to the abrasive wear of alumina by a diamond indenter in vacuum was studied using a tribometer designed and constructed by G.J. Molina [31]. The apparatus is schematically illustrated in Figures 2.1 and 2.2. As shown in Figure 2.1, the diamond indenter is attached to a pin and held stationary. The sample is attached to a rotating shaft that slides in a vacuum feedthrough as shown in Figure 2.2. A lever arm applies the load to the shaft that, in turn, presses the sample up against the diamond indenter. The lower limit of the load is restricted to a few newtons because of friction in the sliding seals and the upper limit is restricted by the stability of the diamond indenter. The range of the sliding speed is 0.3 mm/sec to several cm/sec. The instrument is equipped with a channel electron multiplier (CEM) to detect the charged particles emitted from the contact region.

All the tests were carried out inside a vacuum chamber and at room temperature. The vacuum for these experiments, between 6.5×10^{-7} and 9.5×10^{-7} torr, was obtained using an ion pump in conjunction with a turbomolecular pump. The ion pump was turned off during the measurements because it creates charged particles that register as background for the CEM. This background was a major problem for previous experiments and the addition of the turbomolecular pump to the tribometer for these experiments significantly improved the collection of data.

The ceramic chosen for this study was a commercially available 99.8% alumina from LSP Industrial Ceramics. The disk samples were 1" in diameter and 0.118" thick. The samples were not polished and the, as received, surface roughness R_a was measured to be 1.8 ± 0.8 μm. The average grain size of the ceramic was estimated from SEM micrographs to be 2.8 μm and had a lognormal distribution with a standard deviation of

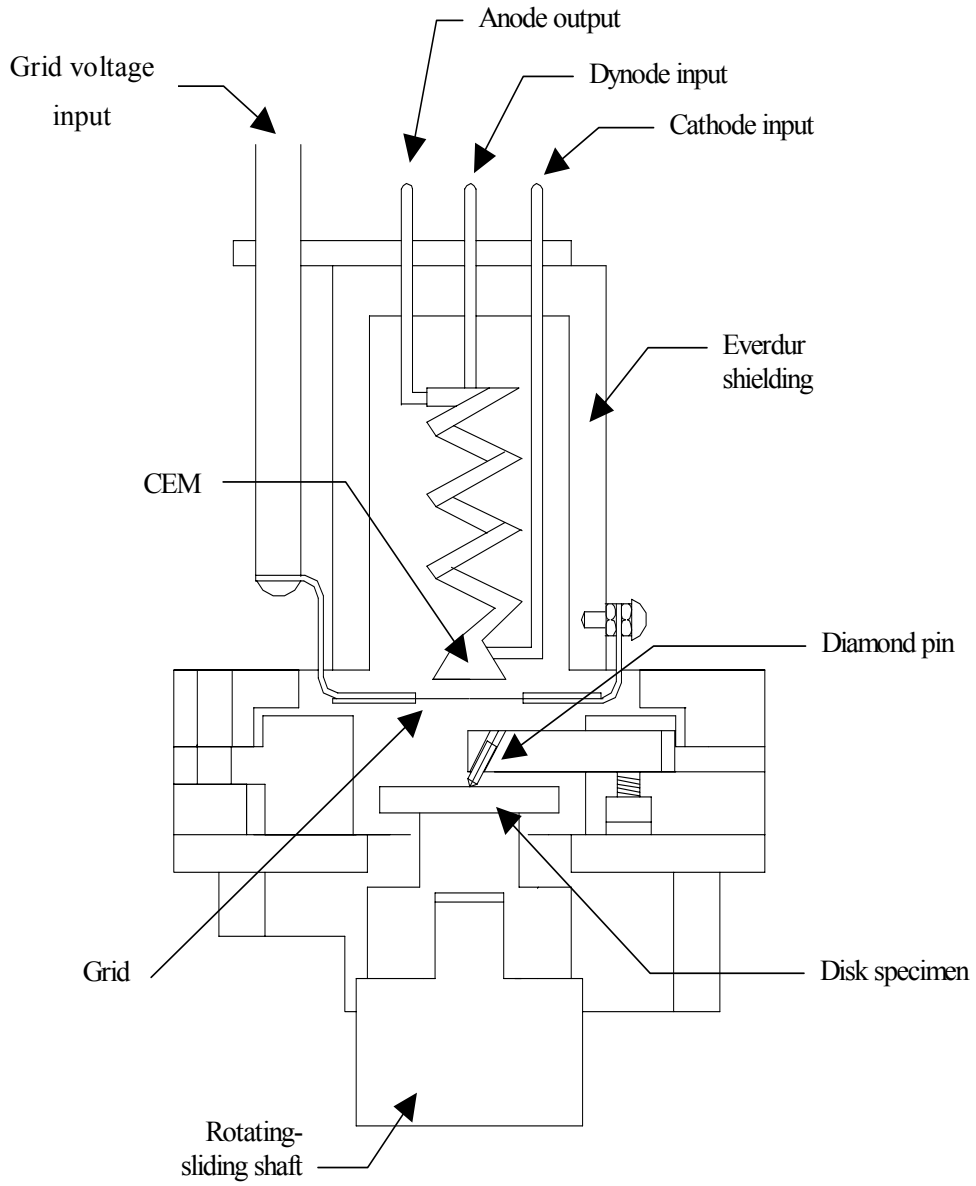

Figure 2.1. Schematic view of the sample, diamond indenter and CEM. The diamond indenter is attached to a pin and held stationary while the disk-shaped sample is pressed against it. (G.J. Molina, Ref. [31])

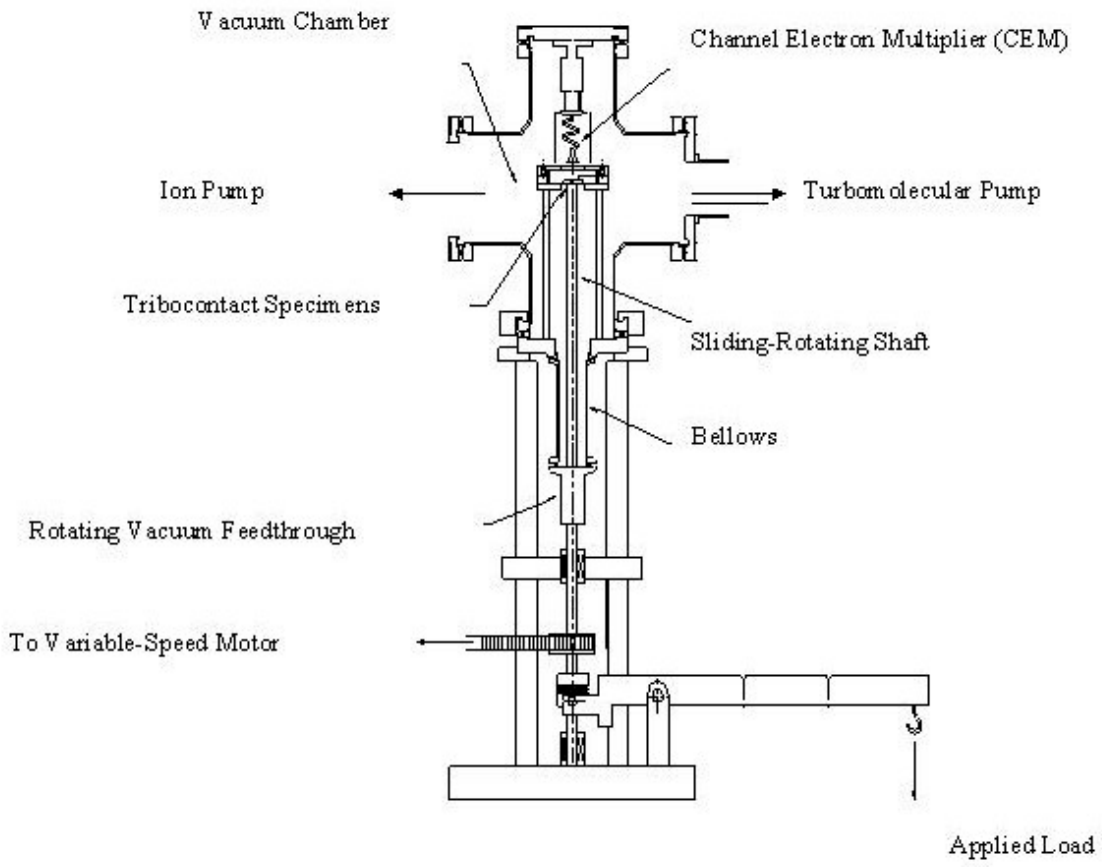

Figure 2.2. Schematic view of the pin-on-disk tribometer. The sample is attached to a rotating shaft that slides in a vacuum feedthrough. A lever arm applies the load to the shaft, which, in turn, presses the sample up against the diamond indenter. (G.J. Molina, Ref. [31]).

3.4 μm. The abrasion of the alumina surface was done with a diamond indenter from Bruce Diamonds (Figure 2.3). The diamond was conical, with an apex angle of 120°. Prior to the experiments the samples were cleaned with acetone in an ultrasonic bath and then rinsed with methanol.

The experiment consisted of measurements on 25 samples as summarized in Table 2.1. Each experiment is characterized by the load, either 10 N or 30 N, and the number of revolutions (passes) of the ceramic disk. The linear sliding speed in each case, 0.28 ± 0.03 mm/s, was chosen to minimize the frictional heating of the sample. The wear-track radius was 2.36 ± 0.24 mm. The values for the load were chosen to bracket a mild-to-severe wear transition that has been observed in the abrasive wear of alumina.

The triboemission measurements consisted of recording the number of particles emitted before the disk began rotating (background), while the disk was rotating and being scratched with the diamond indenter, and after the disk stopped (post-emission). The time window for counting particles was 1 second. The average number of events in a one-second window was 3, and the range was 0 to 4054. All the runs included a measurement of the background emission registered by the CEM before scratching the sample and then post-emission after the abrasion ended. For all the measurements, a retarding potential of – 4 V was applied to the grid in front of the CEM in order to minimize the detection of secondary electrons. Molina [31] found that the detected emission decreased exponentially with the retarding potential. The emission at -4 V was approximately 50% of the emission at zero retarding potential.

The CEM was calibrated prior to each measurement in order to correct for variations in the fraction of pulses from the detector that did not exceed the discriminator setting and for fluctuations in the gain of the detector. Every charged particle that reaches the CEM

Figure 2.3. View of the conical diamond indenter and the alumina disk. The abrasion of the alumina surface was done with a diamond indenter from Bruce Diamonds. The diamond was conical, with an apex angle of 120°. (G.J. Molina, Ref. [31]).

Normal Load	Run number	Number of passes	Cumulative Count	Wear Volume (mm^3/m)
10 N	1	1	14	0.16
	11	1	63	0.17
	3	3	28	0.45
	7	3	119	0.51
	4	7	179	0.48
	9	7	79	1.02
	2	20	276	2.29
	6	20	932	1.46
	5	54	14122	2.95
	10	54	982	2.80
	8	148	26345	2.63
	12	148	16685	3.45
30 N	11	1	144	1.16
	12	1	443	0.77
	1	2	4054	2.26
	2	2	582	1.14
	5	3	5825	2.38
	10	6	2796	3.85
	13	6	496	2.27
	3	9	298	3.39
	4	9	4996	3.13
	8	13	1886	5.71
	9	13	761	4.71
	6	18	3184	5.27
	7	18	4104	12.13

Table 2.1. Experimental measurements on different samples as a function of load and the number of passes (revolutions of the sample). The linear sliding speed in each case was 0.28 ± 0.03 mm/sec. The order of the measurements was randomized.

creates a voltage pulse. The amplitudes of the pulses are normally distributed and the mean and standard deviation of the Gaussian distribution depend on the gain of the detector. For the calibration, we found the mean and the standard deviation of the pulse size distribution, using the ion pump as a source of charged particles. We varied the discriminator voltage setting from zero, where the pulses from all the charged particles that reached the detector were registered, to high values (~40 mV), where none of the pulses registered and the count was zero (Figure 2.4). In the figure, this amounts to translating the vertical line that represents the discriminator setting from left to right. For a given mean and standard deviation of the Gaussian distribution of pulse amplitudes, and for a given number of particles that reach the CEM, the number of particles that create pulses that are registered is proportional with the area under the probability density curve to the right of the discriminator setting [38]. Changing this setting affects the number of pulses detected by the CEM. In our experiments, the discriminator voltage was set to 8.8 ± 1.9 mV and we detected 85% ± 9% of the pulses, i.e. the area to the right of the discriminator setting was 85% ± 9% of the total area under the probability density curve. We then corrected the count based on the fraction of events that fell below the discriminator setting. We did not set the discriminator to zero in order to avoid the detection of electrical noise.

The specimens were ultrasonically cleaned in acetone after scratching, in order to remove loosely attached debris from the wear tracks. The profiles of the wear tracks were then measured using a Tencor Alpha-Step 500 profilometer with a horizontal resolution of 1.00 μm and a vertical resolution of 25Å. For each sample, 20 profile traces of the wear-track were measured at evenly spaced positions along the track in order to calculate the volume of material removed.

Table 2.1 is a compilation of the data, showing the cumulative electron count and wear volume as a function of load and number of passes. The cumulative electron count is a

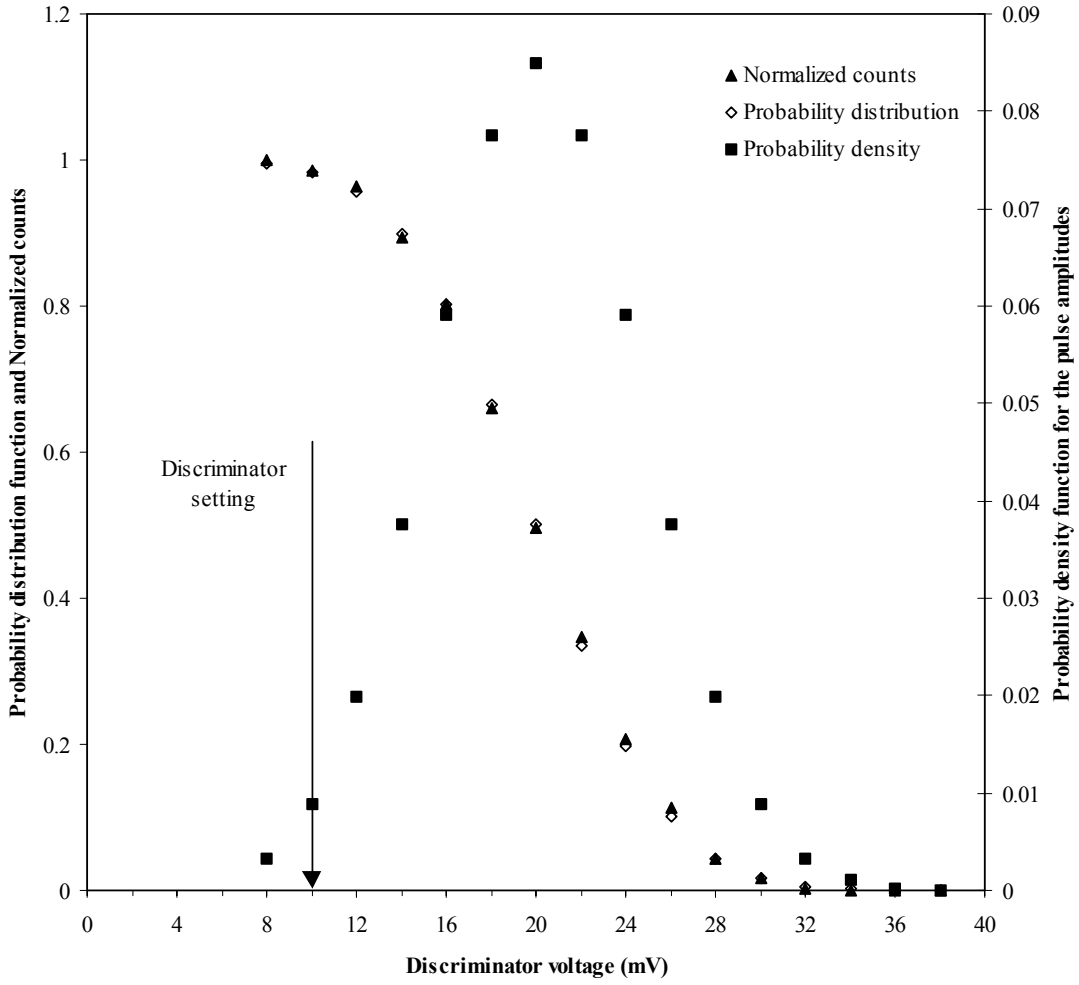

Figure 2.4 Typical calibration curve for the CEM. Of all the charged particles that reach the CEM, the number of particles that create pulses that are registered is proportional with the area under the probability density curve to the right of the discriminator setting.

sum over the number of events in the one-second bins from the initiation to the end of abrasion. Significant variability exists in the number of events from one bin to the next for a given sample [31], [24], [32]. The frequency distribution of these events is not Poisson [31] implying a temporal correlation of the emission. In addition, the cumulative emission from measurements on different samples at the same load and number of passes has considerable variability. We have identified the structure of this variability as a lognormal distribution. The discovery, that wear and the concomitant triboemission are lognormal random variables, is a major point of this research and will be discussed in section 2.5.

Finally, the samples were examined by scanning electron microscopy (SEM) at magnifications ranging from 25x to 5000x. These pictures reveal a striking transition in the nature of the wear track surface that correlates with a transition in the triboemission rate. This observation is a second major point of this research and will be discussed in section 2.4.

2.4 Results

2.4.1 Wear Data

The volume of material removed from the samples by the diamond indenter was determined from the measured profiles of the wear tracks. In Figure 2.5, the volume of material removed per unit scratch length (i.e. wear volume) is plotted versus the number of passes for 10 N and 30 N. Each point on this plot is from a different sample and is determined from 20 profiles measured at different positions around the wear track. The wear volume for 10 N load increases linearly with pass number up to 20 passes, but then the rate of material removal decreases dramatically from 20 passes to 148 passes. This transition in wear rate after 20 passes is associated with changes in the appearance of the wear scar surface observed by SEM and discussed below. A linear regression fit to the 10 N load data from one to 20 passes gives a wear volume rate with pass number of 0.09 mm^3/m. The residuals of the wear volume with respect to the linear regression fit from one to 20 passes are normally distributed for 10 N load as shown in the normal plot Figure 2.6. The standard deviation of the residuals for 10 N load is 0.27 mm^3/m. The wear volume increases linearly as a function of pass number for 30 N load. A linear regression fit to the data gives a wear volume rate with pass number of 0.41 mm^3/m. The residuals of the wear volume with respect to the linear regression fit are also normally distributed for the 30 N load, as shown in the normal plot Figure 2.7. The standard deviation of the residuals is 1.60 mm^3/m. We emphasize the normality of the wear volume distribution because the cumulative triboemission count is not a normally distributed, but is a lognormal distribution as discussed in section 2.5.2.

For both loads, the values of the measured cross section for any given sample exhibited significant variability at different positions along the circular wear scar. In Figure 2.8 we

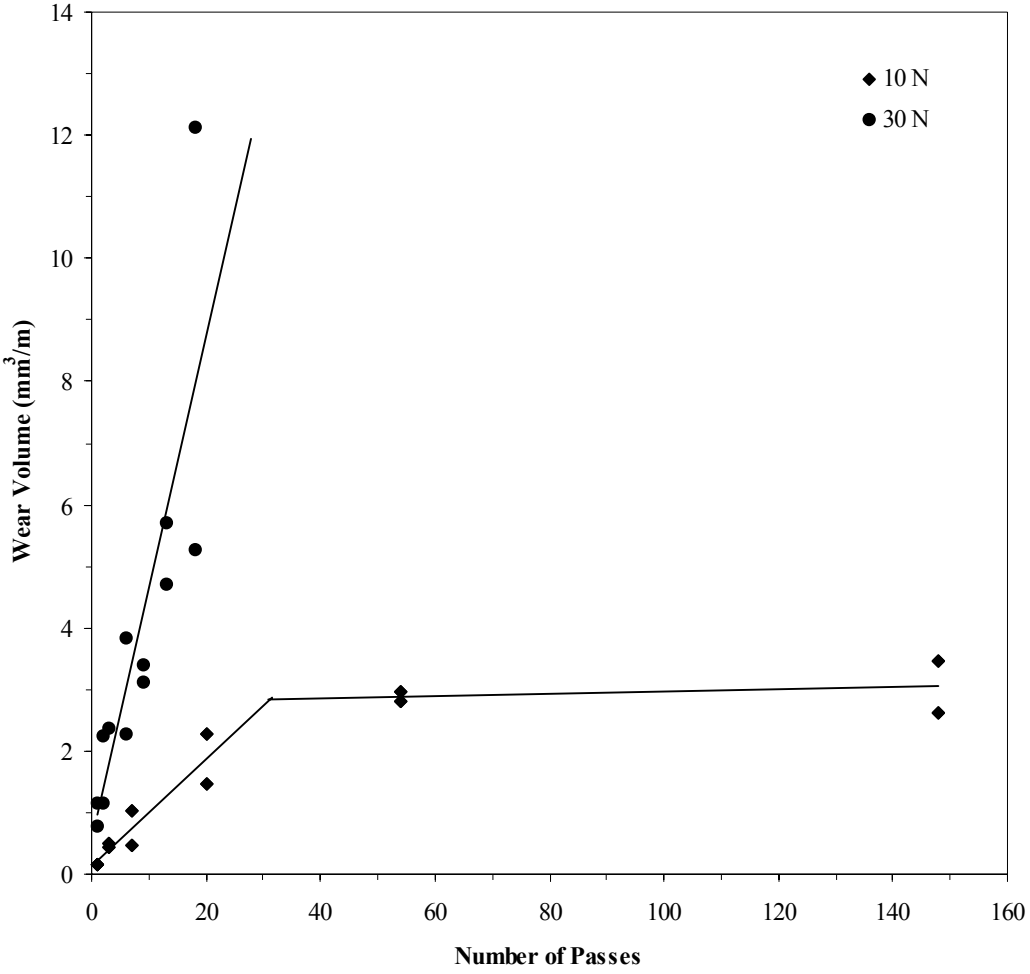

Figure 2.5. The volume of material removed per unit scratch length versus the number of passes for the two loads. The wear volume increases linearly as a function of pass number for the 30 N load. For the 10 N load, the wear volume increases linearly with the pass number up to 20 passes, after which the rate of material removal decreases dramatically.

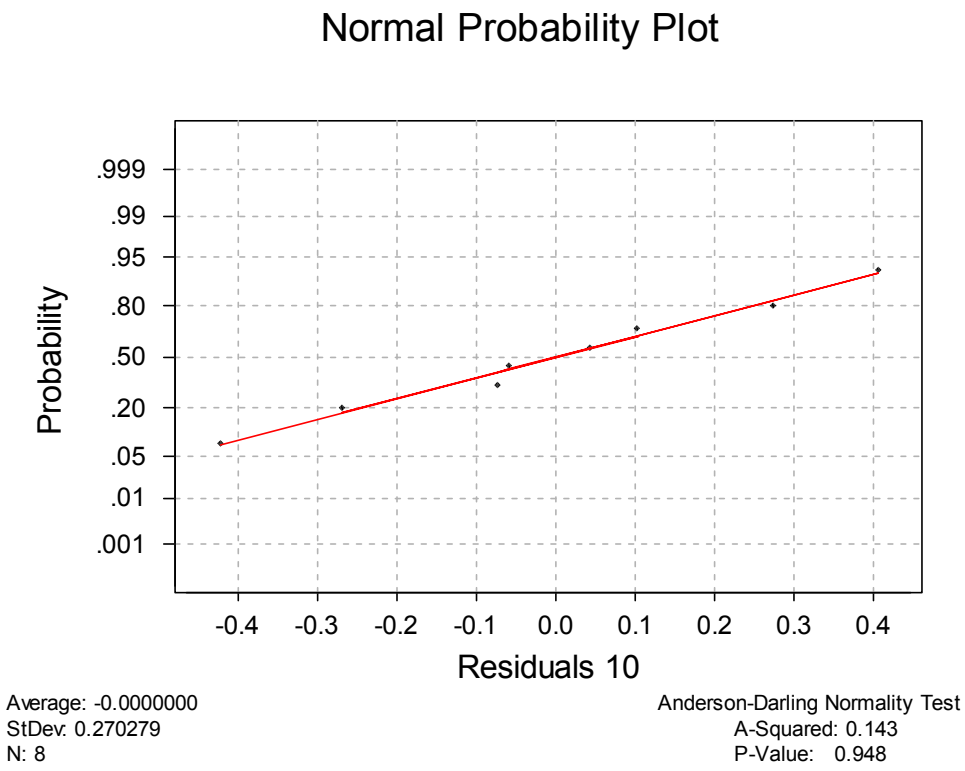

Figure 2.6. Normal probability plot for the residuals of the wear volume with respect to the linear regression fit for the 10 N load. The residuals are normally distributed.

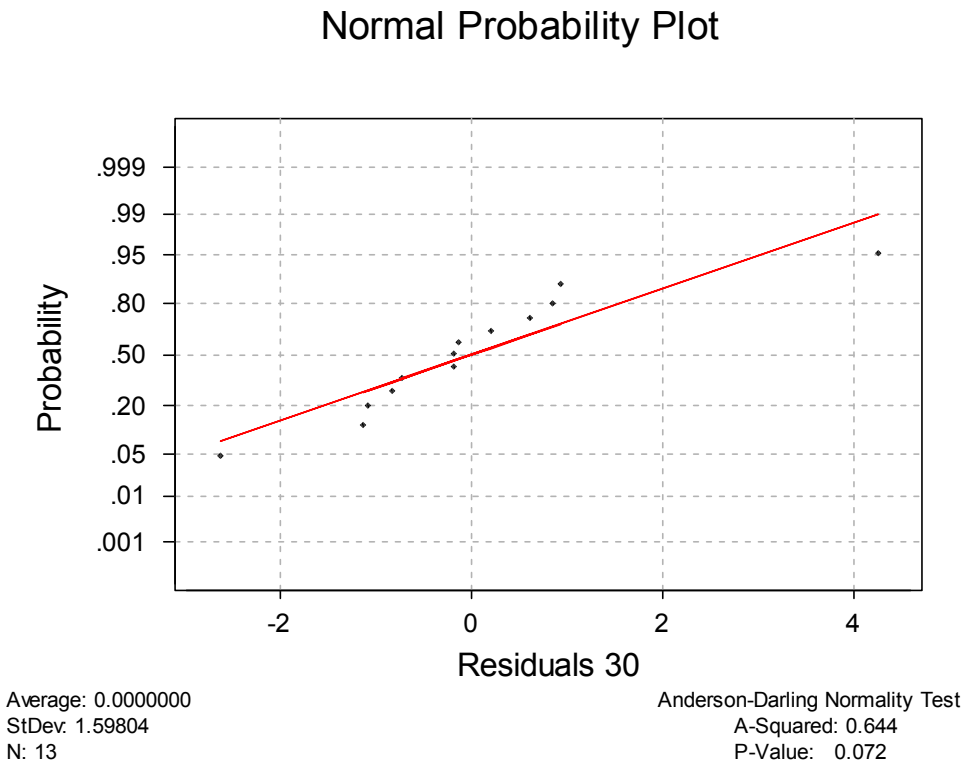

Figure 2.7. Normal probability plot for the residuals of the wear volume with respect to the linear regression fit for the 30 N load. The residuals are also normally distributed.

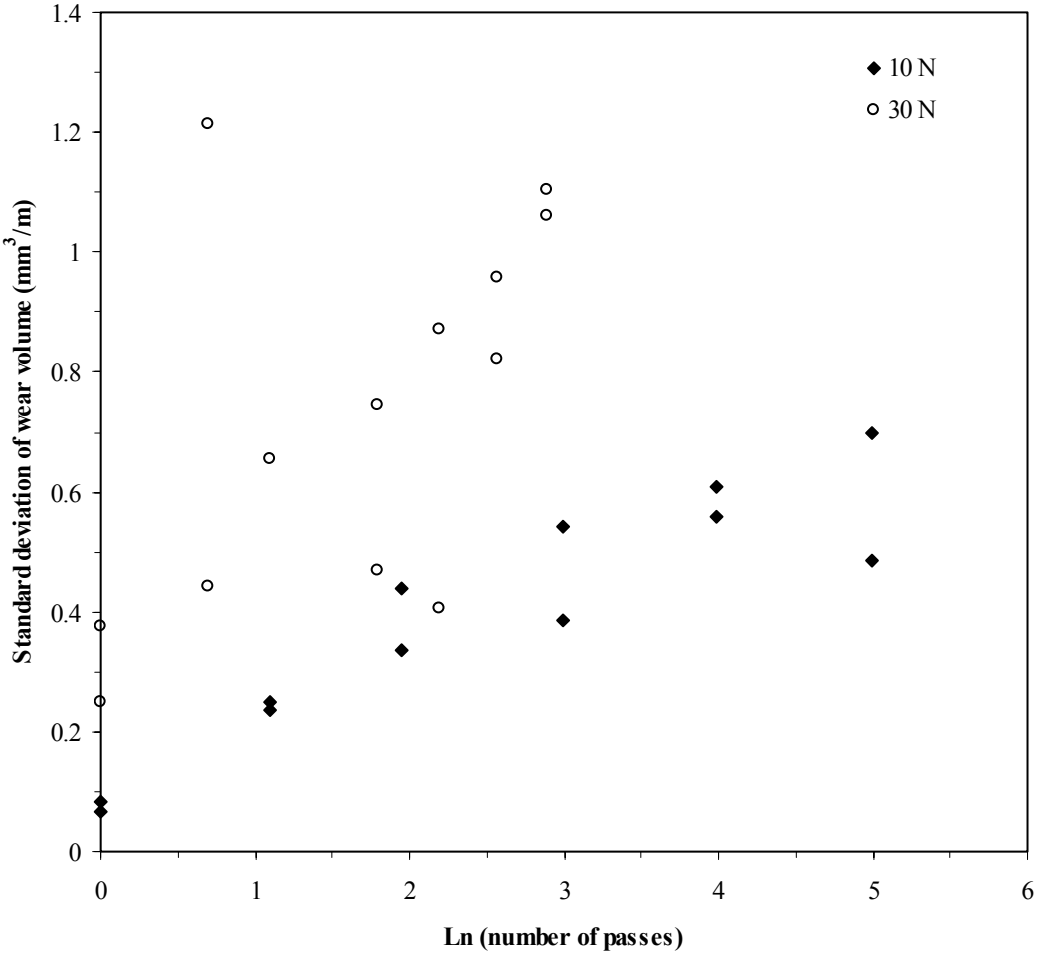

Figure 2.8. Standard deviation of the wear volume versus the natural logarithm of the number of passes. For both the 10 N and 30 N load, the variability increases with the number of passes. For the 10 N load, the slope of the graph appears to decrease after approximately 20 passes. For any given number of passes, the variability in the wear volume is greater for 30 N than for 10 N.

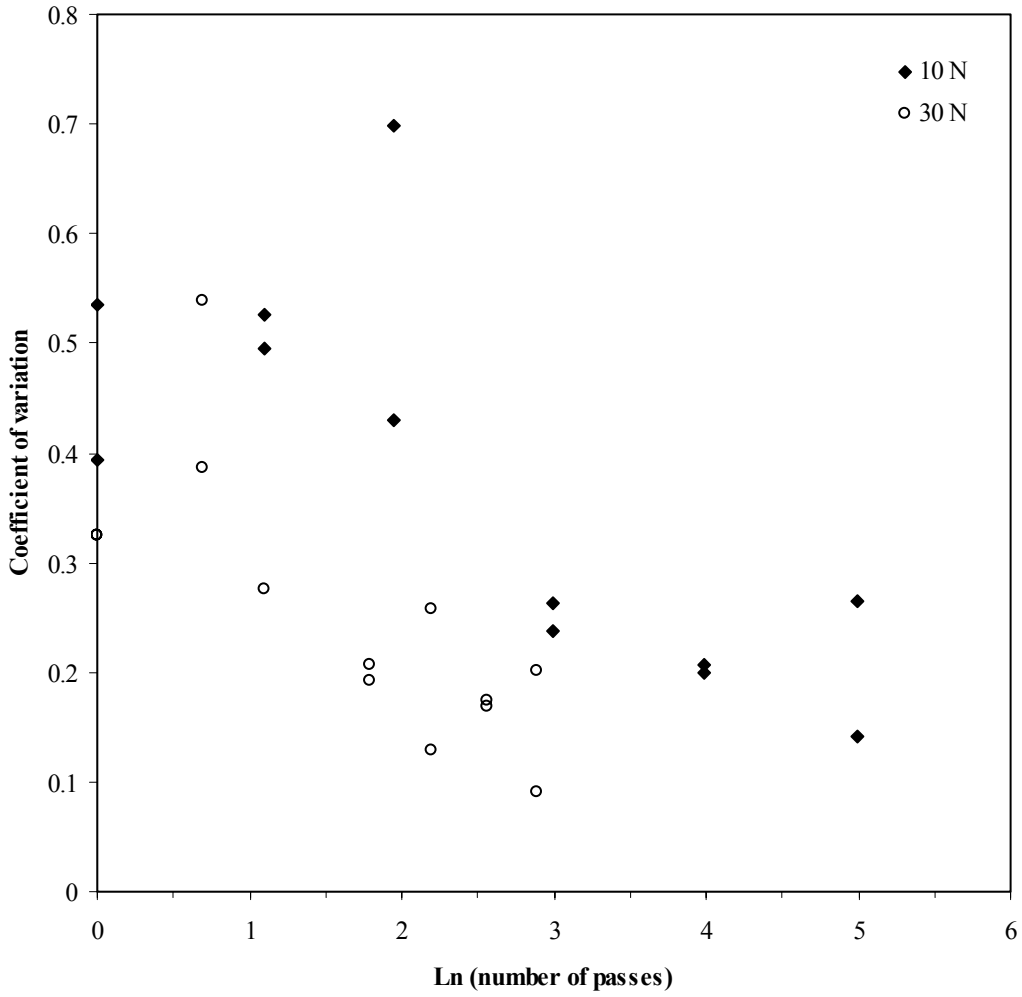

Figure 2.9. Coefficient of variation of the wear volume versus the natural logarithm of the number of passes.

plotted the standard deviation of the wear volume versus the natural logarithm of the number of passes for each sample. For both the 10 N and 30 N load, the variability tends to increase with the number of passes. For the 10 N load, the slope of the graph appears to decrease after approximately 20 passes. Also, for any given number of passes, the variability in the wear volume is greater for the higher load.

In Figure 2.9 we plotted the coefficient of variation of the wear volume versus the number of passes. The coefficient of variation is defined as the standard deviation divided by the mean and is a useful measure of relative dispersion or scatter of the data with respect to the mean. The mean and standard deviation usually change together in experiments; therefore, knowledge of the relative variation is valuable. Even though the standard deviation of the wear volume increases in absolute value with the number of passes, the mean wear volume is increasing faster and, therefore, the coefficient of variation decreases for both loads.

SEM pictures of the wear scars for 10 N load on the alumina samples are shown in Figures 2.10a to 2.10v for 1, 3, 7, 20, 54 and 148 passes. The steps in pass number were chosen to give evenly spaced steps in the natural logarithm of the pass number. The wear scars are not perfectly circular because of play in the shaft that rotates the sample. A pattern emerges from these pictures that correlates with the change in wear rate discussed above and in the emission data to be discussed in sections 2.4.2 and 2.5.2. For one pass, the wear track consists almost entirely of plastic flow material in one sample (Figures 2.10a and 2.10b) or areas of plastic flow interspersed with smaller areas of intergranular and intragranular fracture in the second sample (Figures 2.10c and 2.10d). Then, after 3 and 7 passes, the plastic flow material has delaminated from all four samples (Figures 2.10e to 2.10j) and the wear scar is made up almost entirely of fractured surface. The two samples that went through 20 passes are qualitatively different. Sample 6 (Figures 2.10k and 2.10l) has almost no plastic flow material in the wear scar, similar in appearance to

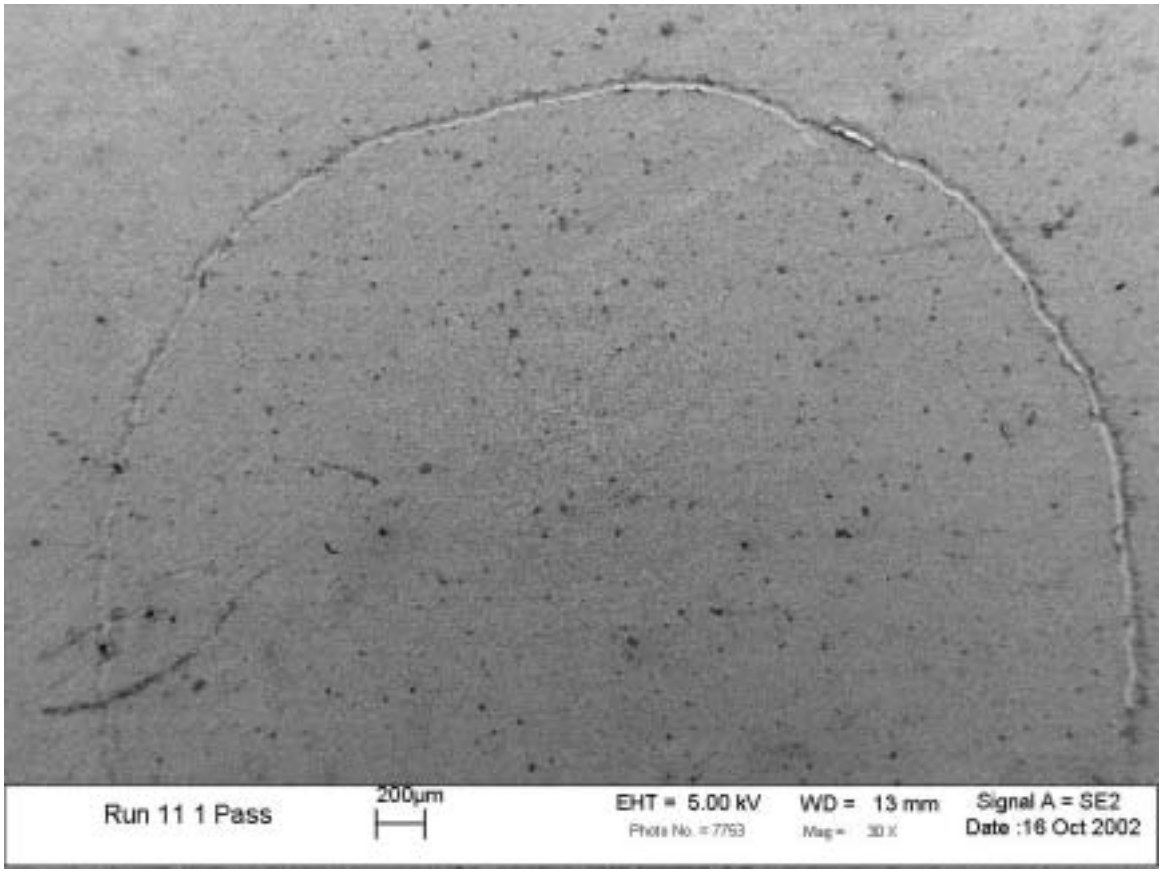

Figure 2.10a. Typical circular wear scar on the alumina sample left by the diamond indenter after one pass. The photo is an SEM micrograph at a 30x magnification. Load is 10 N. The wear scar is not perfectly circular because of play in the shaft that rotates the sample. The wear track is almost entirely covered by plastic flow material.

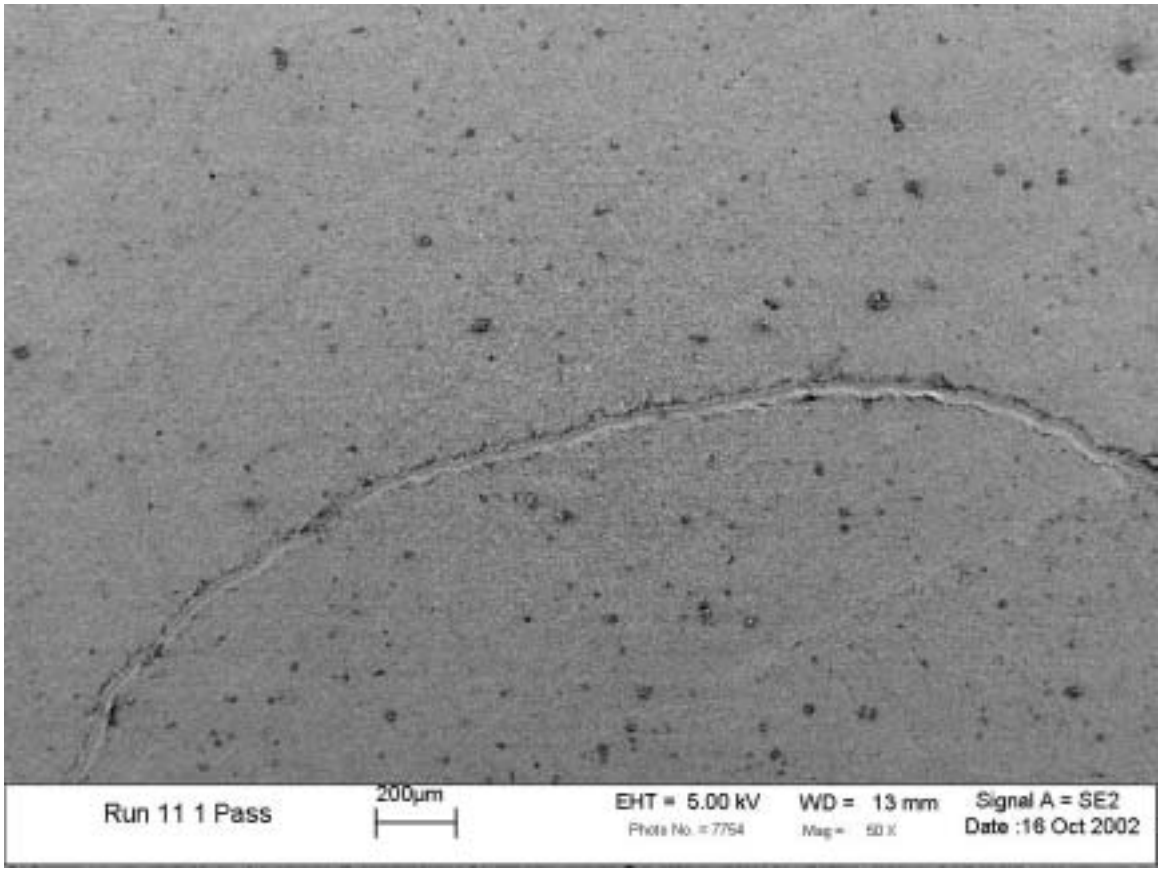

Figure 2.10b. The same wear scar as in Figure 2.10a, at 50x magnification.

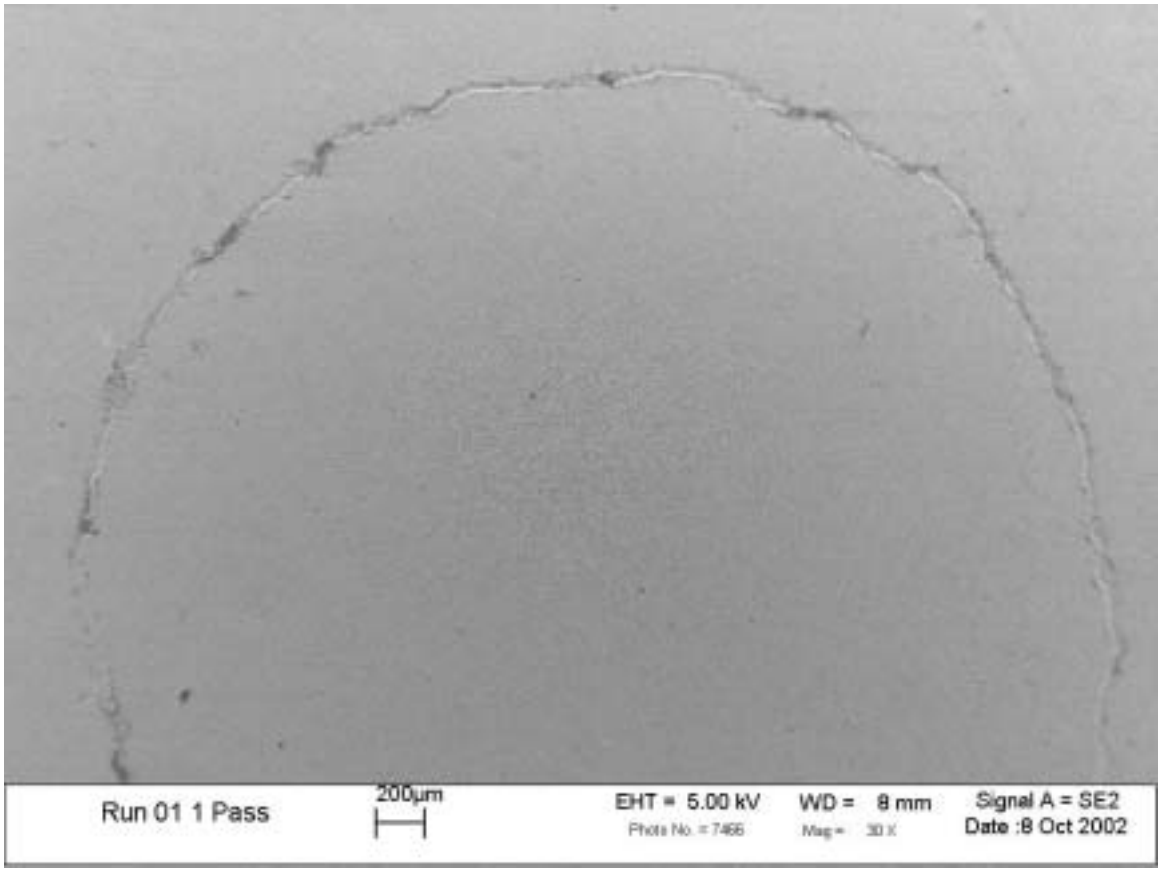

Figure 2.10c. Wear scar after one pass consists of areas of plastic flow interspersed with smaller areas of intergranular and intragranular fracture.

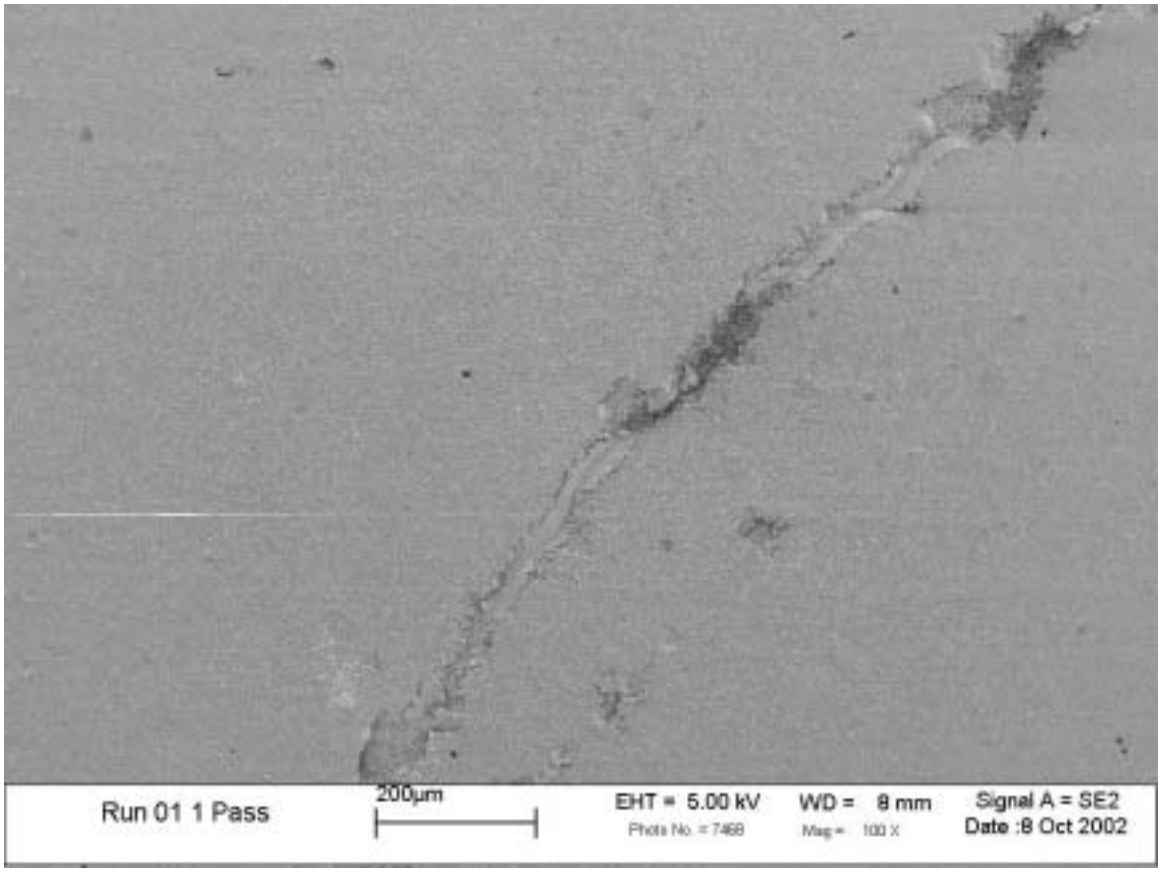

Figure 2.10d. The same wear scar as in Figure 2.10c, at 100x magnification.

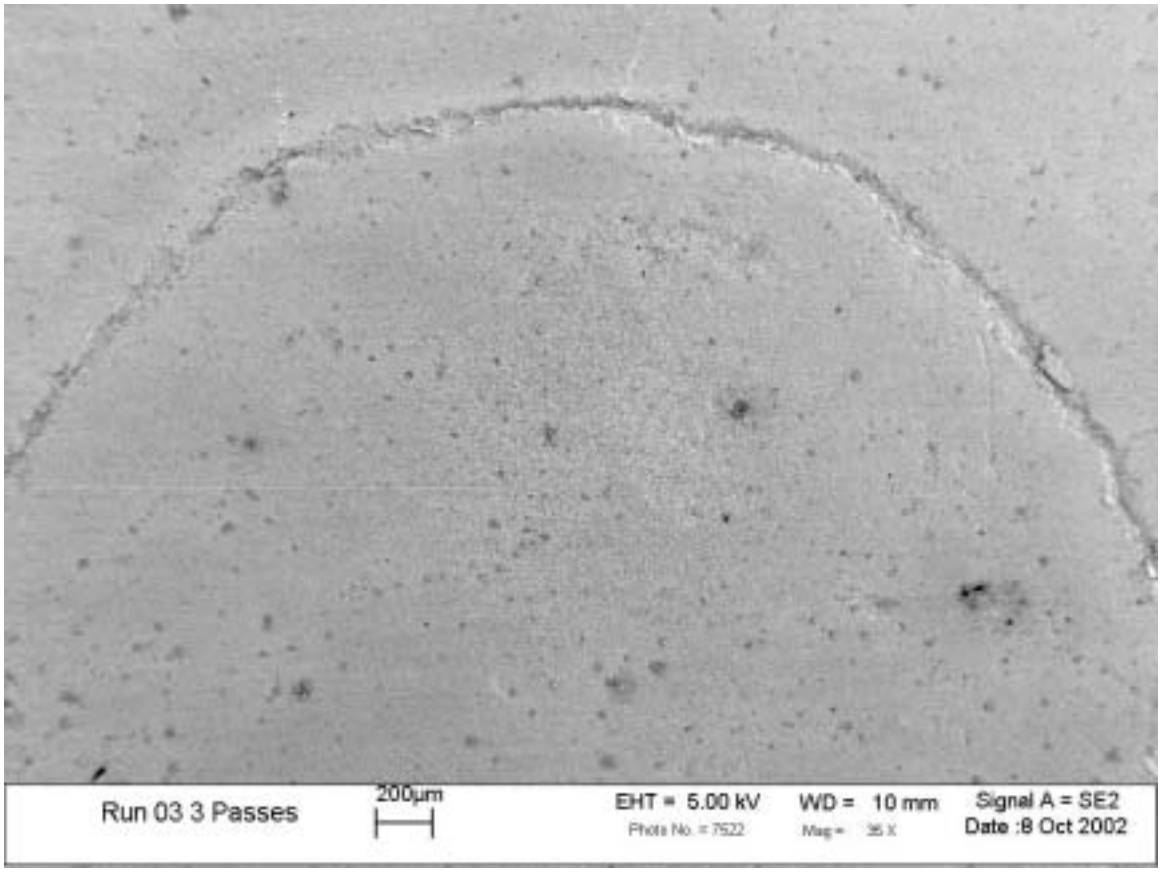

Figure 2.10e. Wear scar after 3 passes. The plastic flow material has delaminated and the wear scar is made up almost entirely of fractured surface.

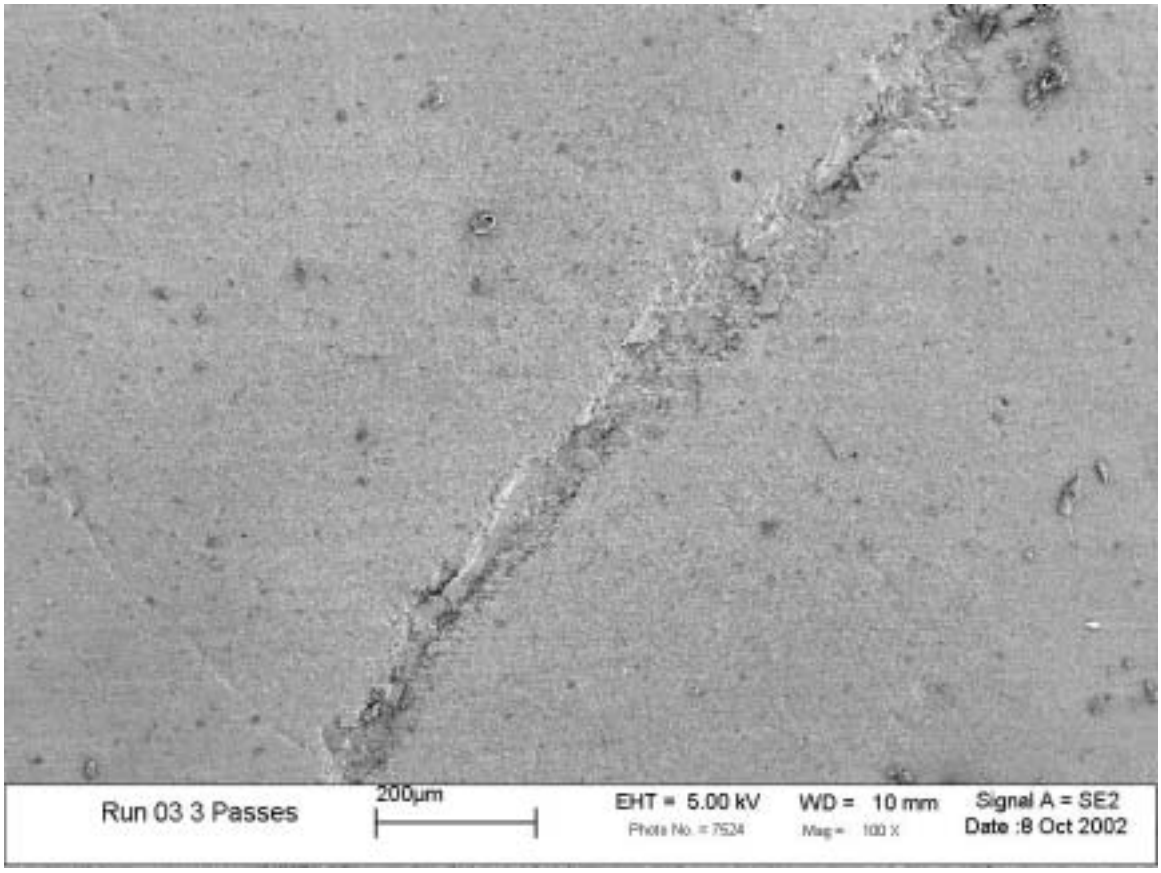

Figure 2.10f. The same wear scar as in Figure 2.10e, at 100x magnification.

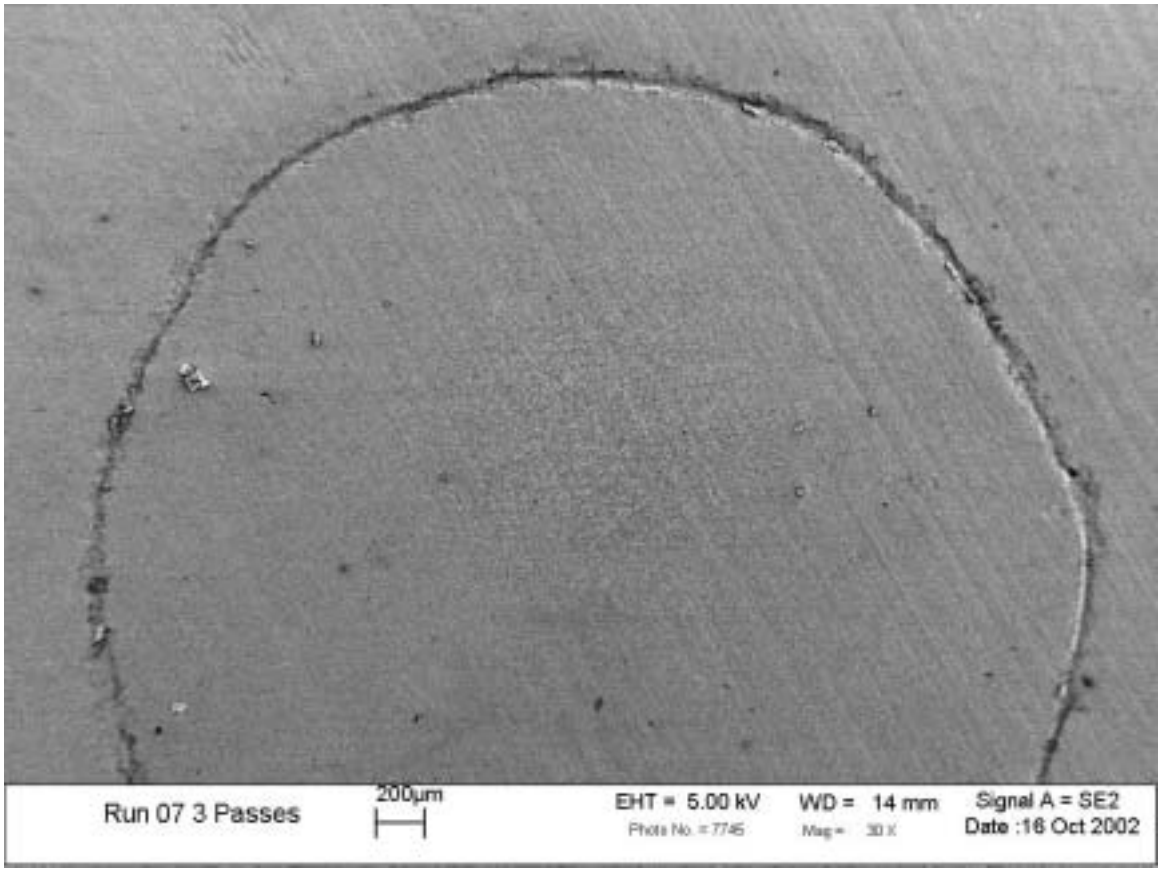

Figure 2.10g. Wear scar after 3 passes. The plastic flow material has delaminated and the wear scar is made up almost entirely of fractured surface.

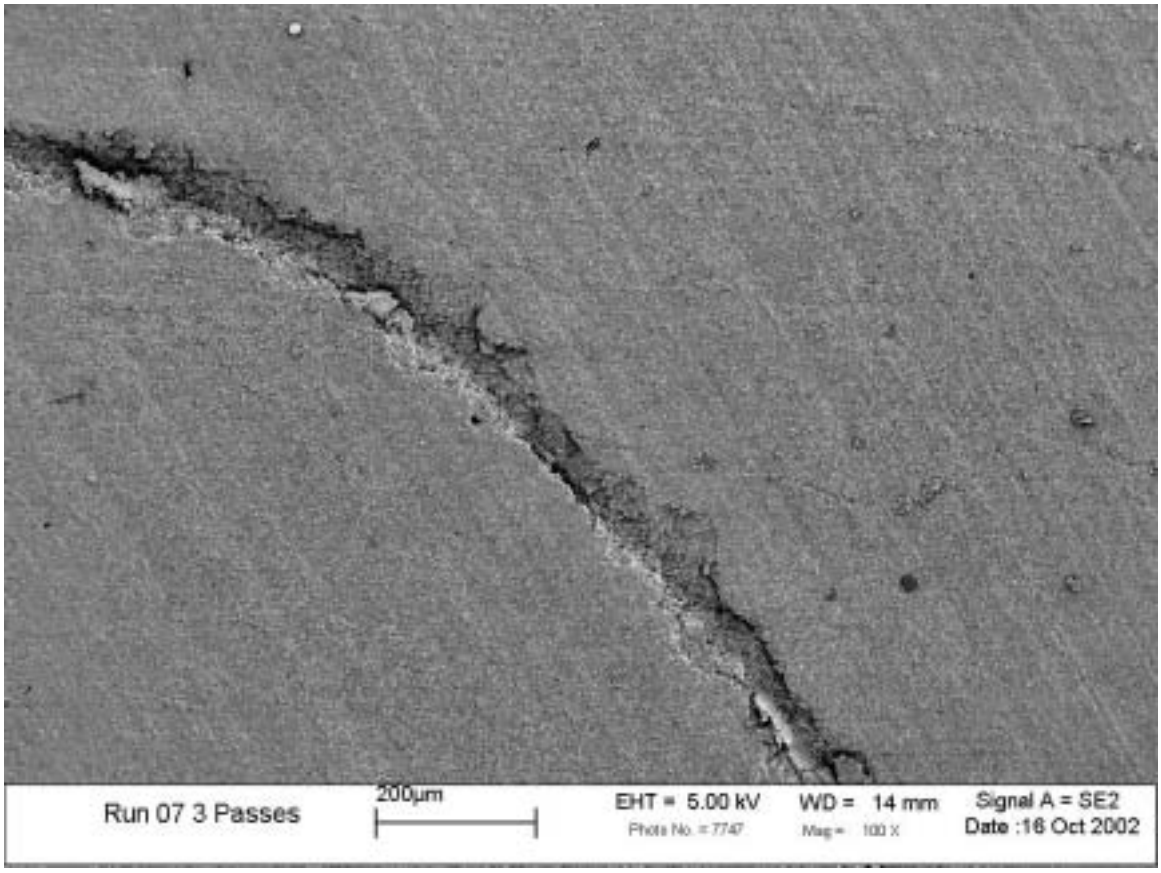

Figure 2.10h. The same wear scar as in Figure 2.10g, at 100x magnification.

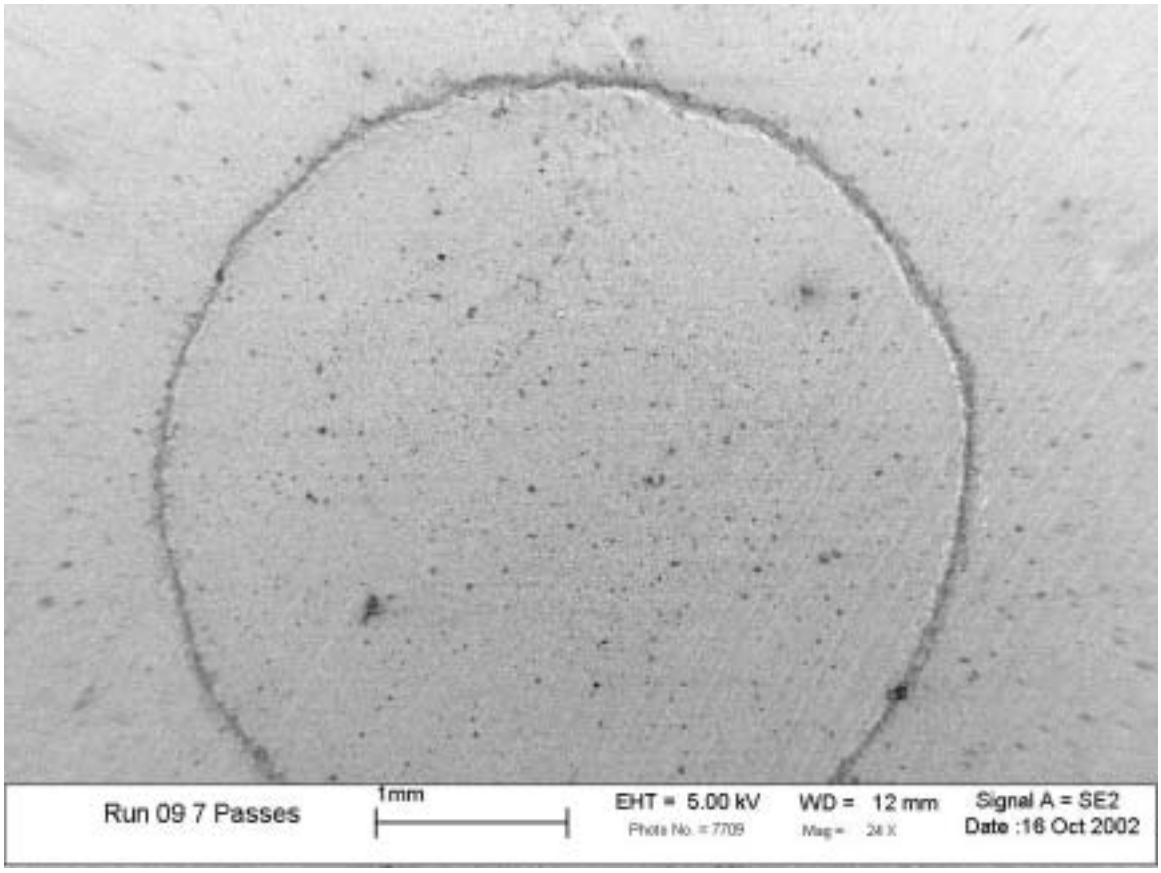

Figure 2.10i. Wear scar after 7 passes. The plastic flow material has delaminated and the wear scar is made up almost entirely of fractured surface.

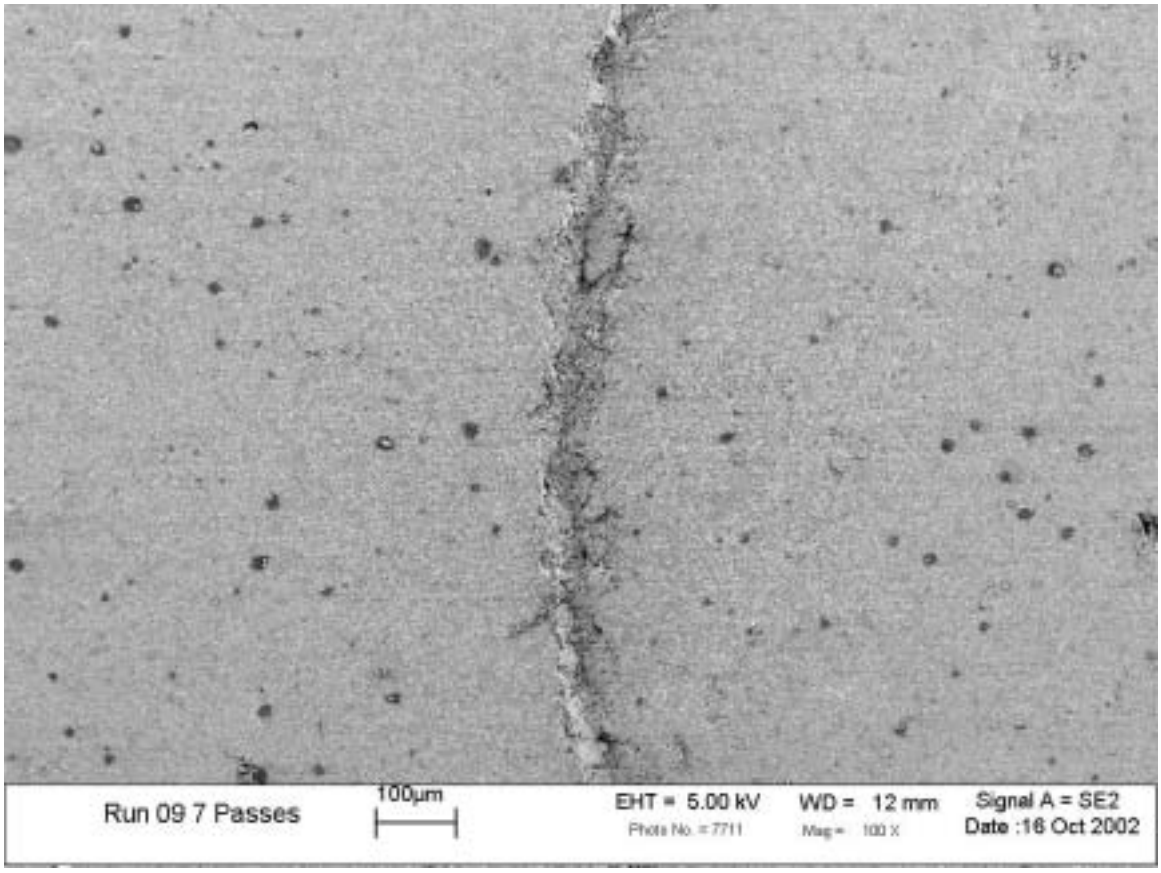

Figure 2.10j. The same wear scar as in Figure 2.10i, at 100x magnification.

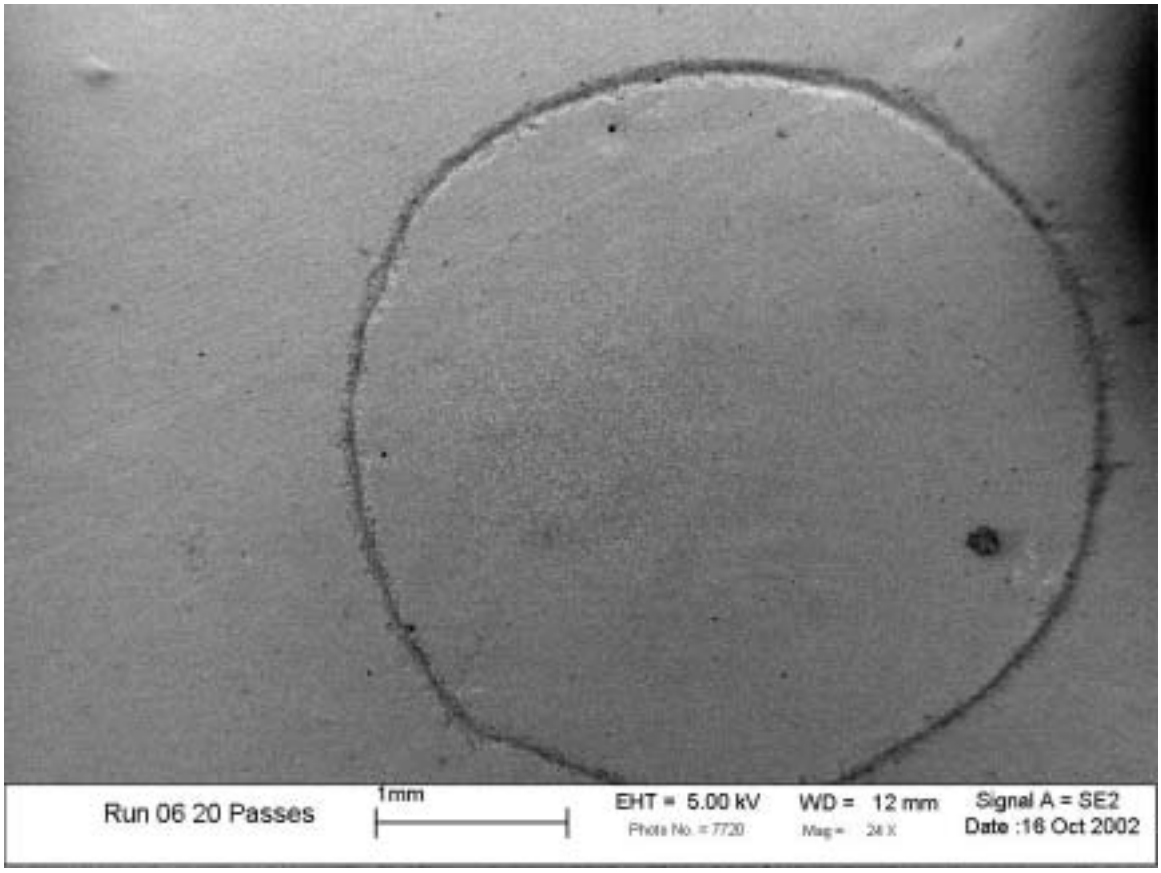

Figure 2.10k. Wear scar after 20 passes. For this sample, the wear track has almost no plastic flow material, similar in appearance to the 3 and 7 pass samples. We hypothesize that this is one of the samples on the boundary of a wear transition. For this particular sample, the transition has not occurred.

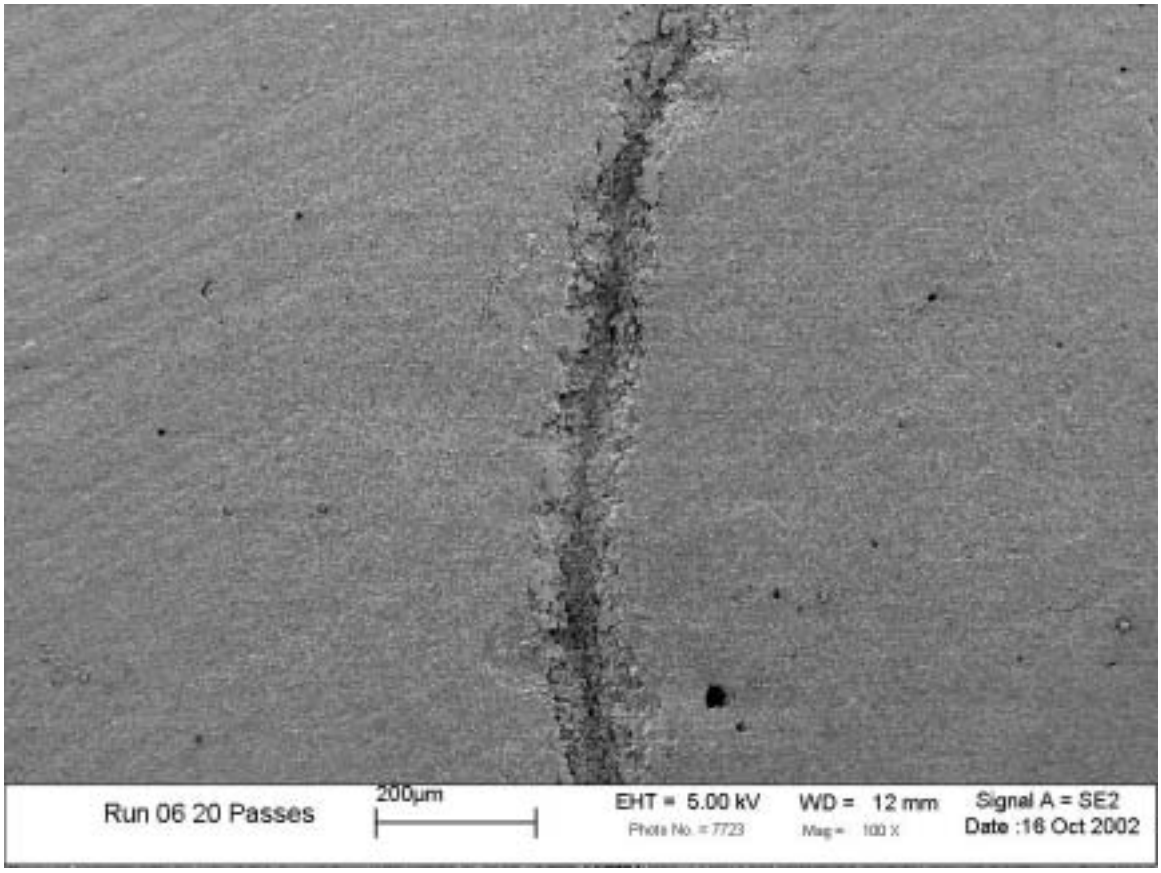

Figure 2.10l. The same wear scar as in Figure 2.10k, at 100x magnification.

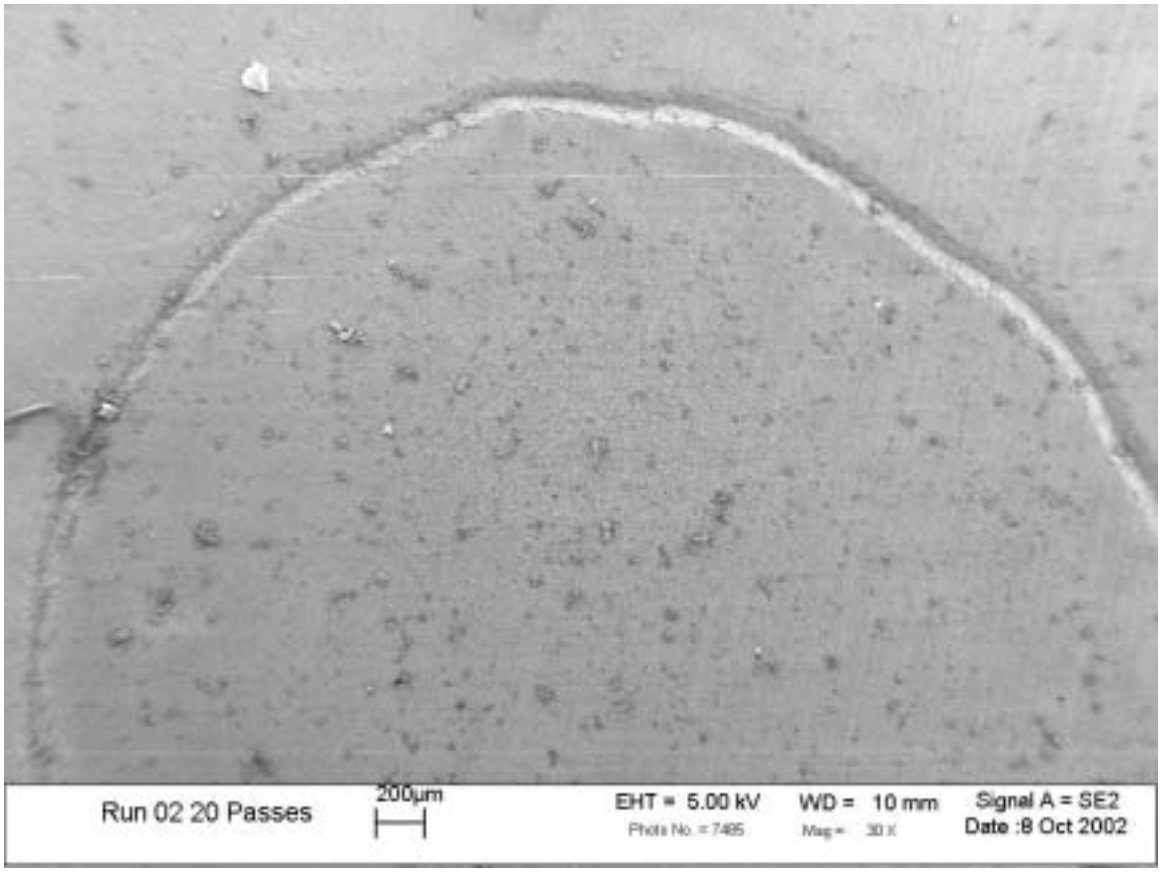

Figure 2.10m. Wear scar after 20 passes. Here, the wear track is almost entirely covered with plastic flow debris. We hypothesize that this is the second sample on the boundary of a wear transition. In the case of this sample, the transition has already occurred.

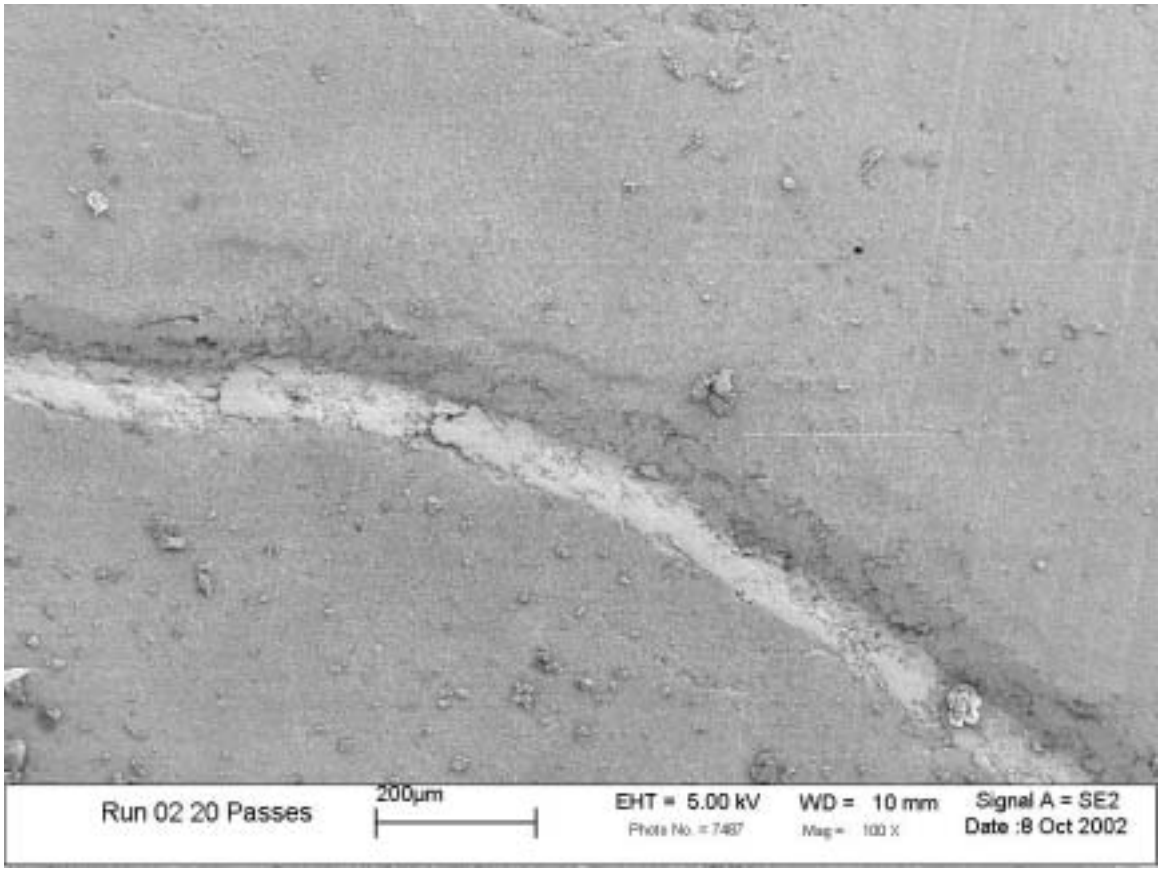

Figure 2.10n. The same wear scar as in Figure 2.10m, at 100x magnification.

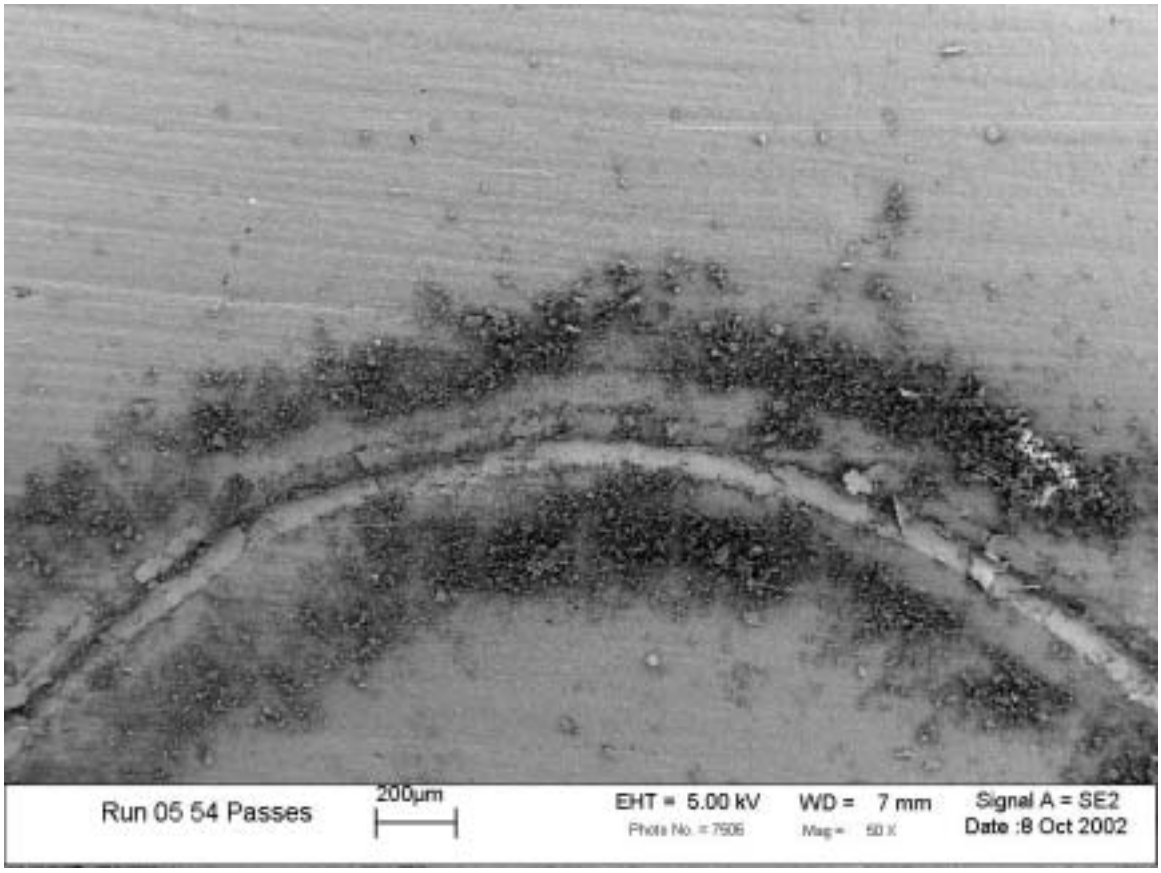

Figure 2.10o. The wear scar after 54 passes consists of a mixture of fractured and plastic flow surfaces. We hypothesize that this, and the following SEM micrographs (Figures 2.10q to 2.10v) are snapshots of a steady state process in which the delamination of the plastic material is balanced by re-formation of plastic film from the wear debris.

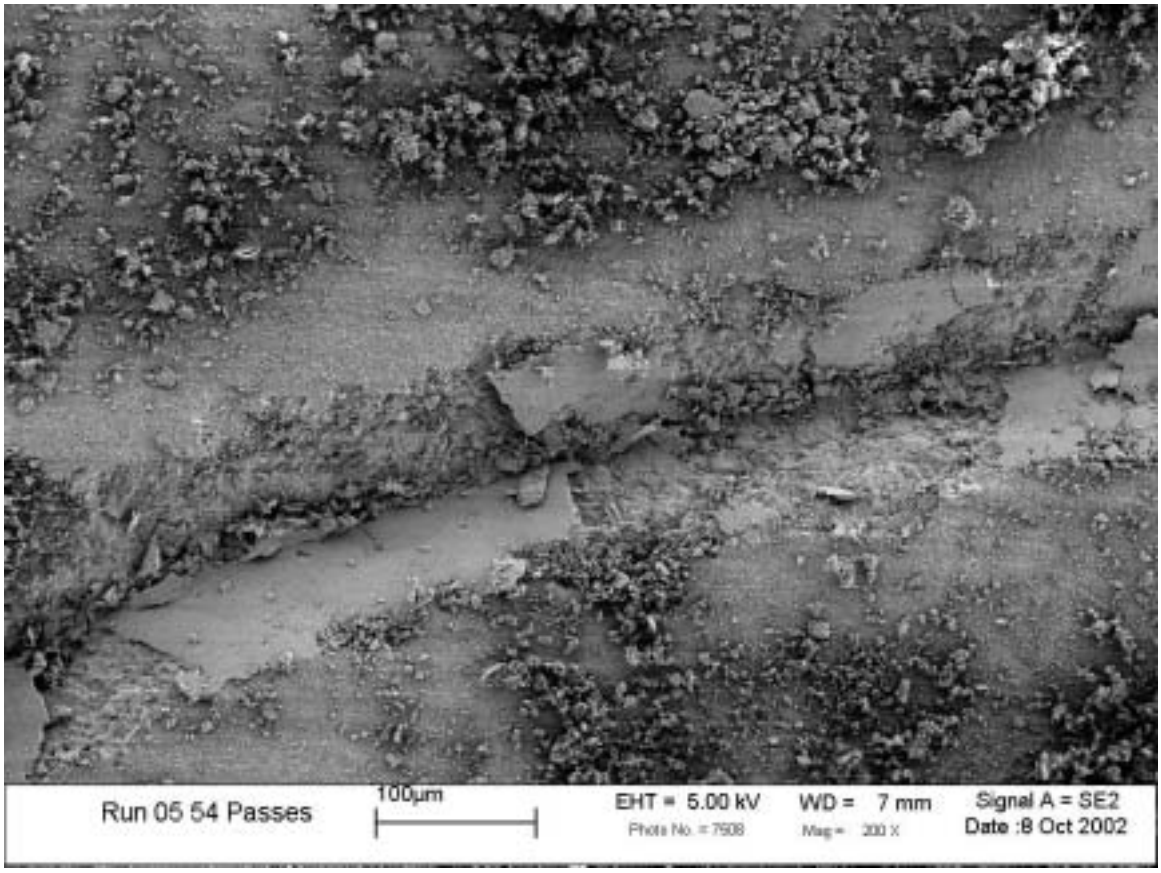

Figure 2.10p. The same wear scar as in Figure 2.10o, at 200x magnification.

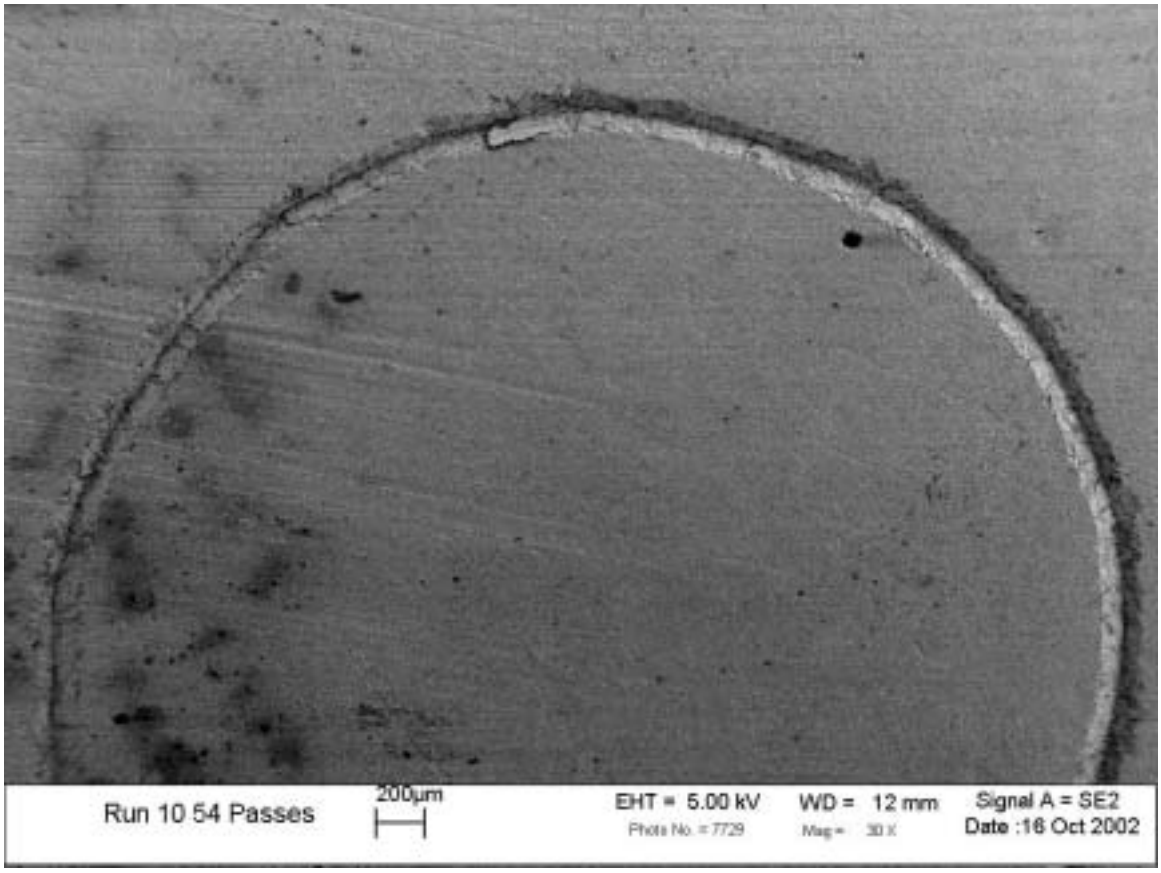

Figure 2.10q. The wear scar after 54 passes consists of a mixture of fractured and plastic flow surfaces.

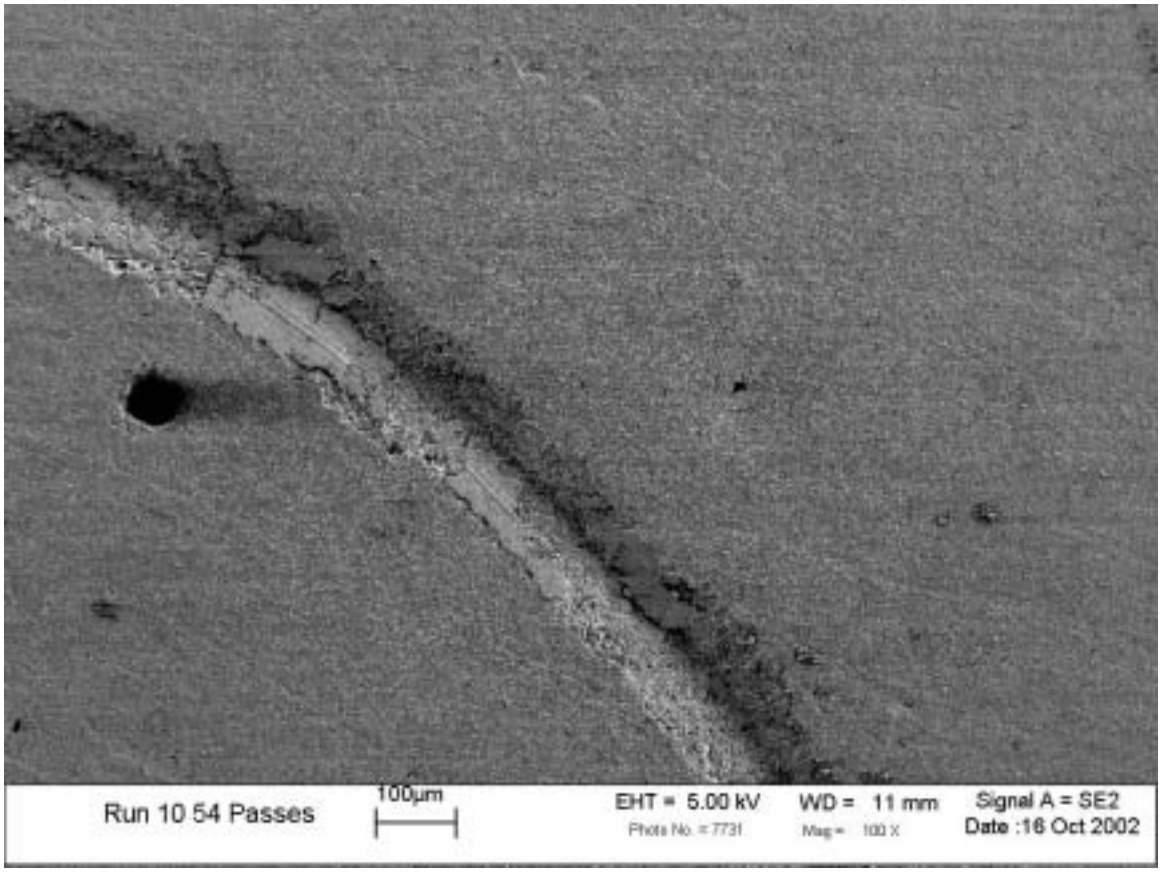

Figure 2.10r. The same wear scar as in Figure 2.10q, at 100x magnification.

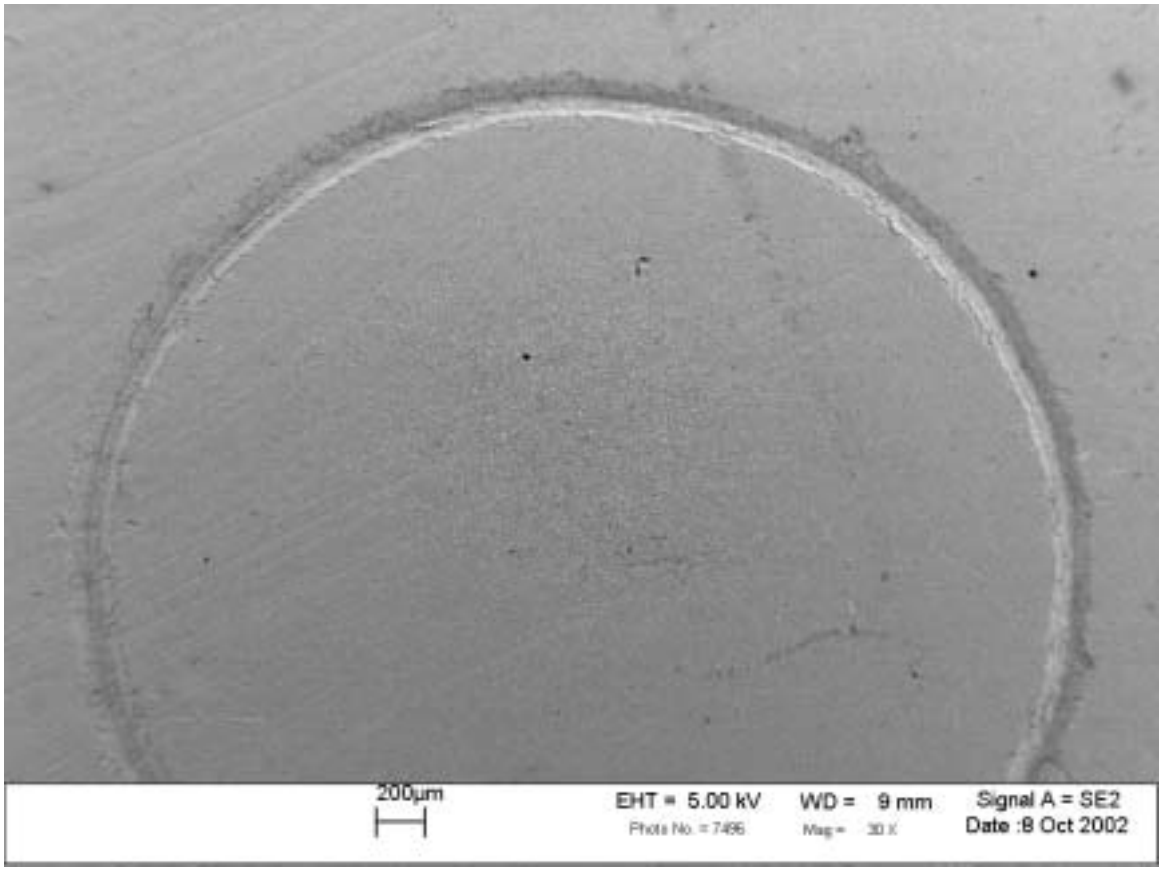

Figure 2.10s. The wear scar after 148 passes consists of a mixture of fractured and plastic flow surfaces.

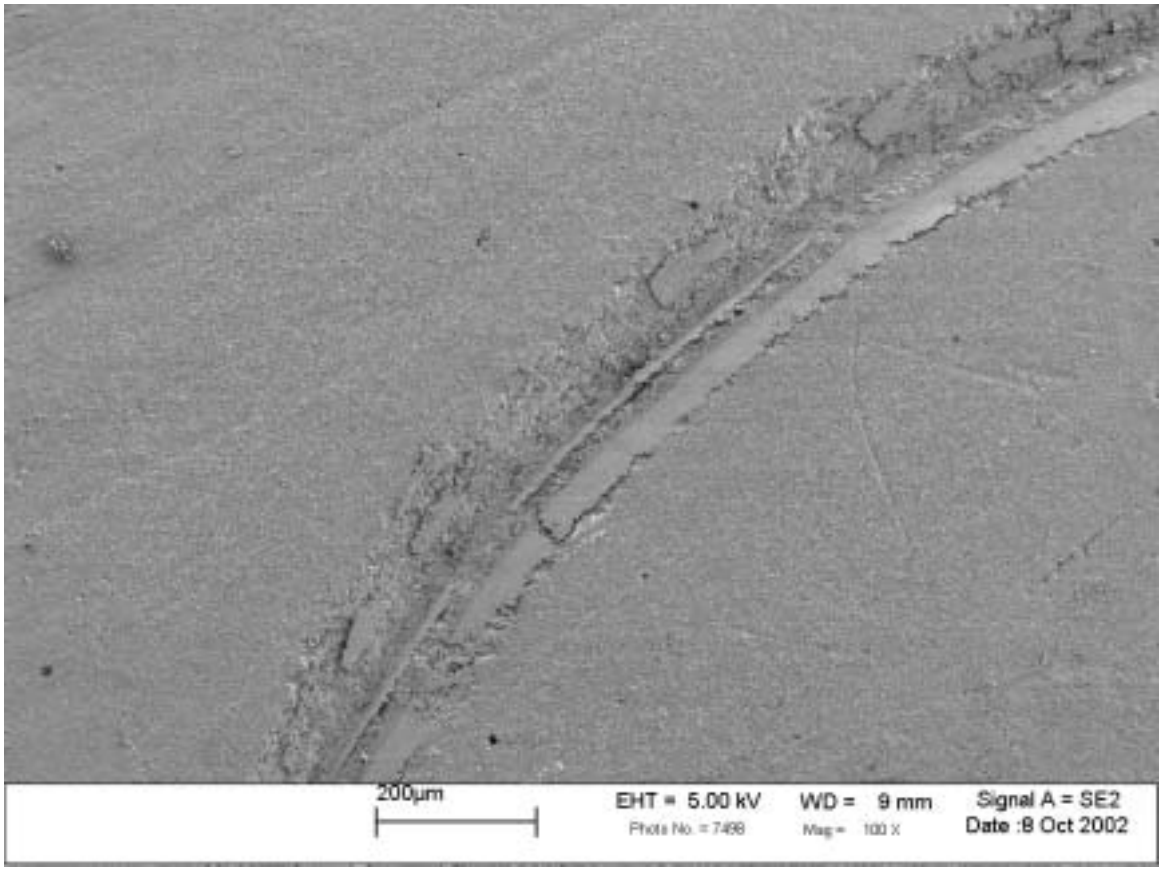

Figure 2.10t. The same wear scar as in Figure 2.10s, at 100x magnification.

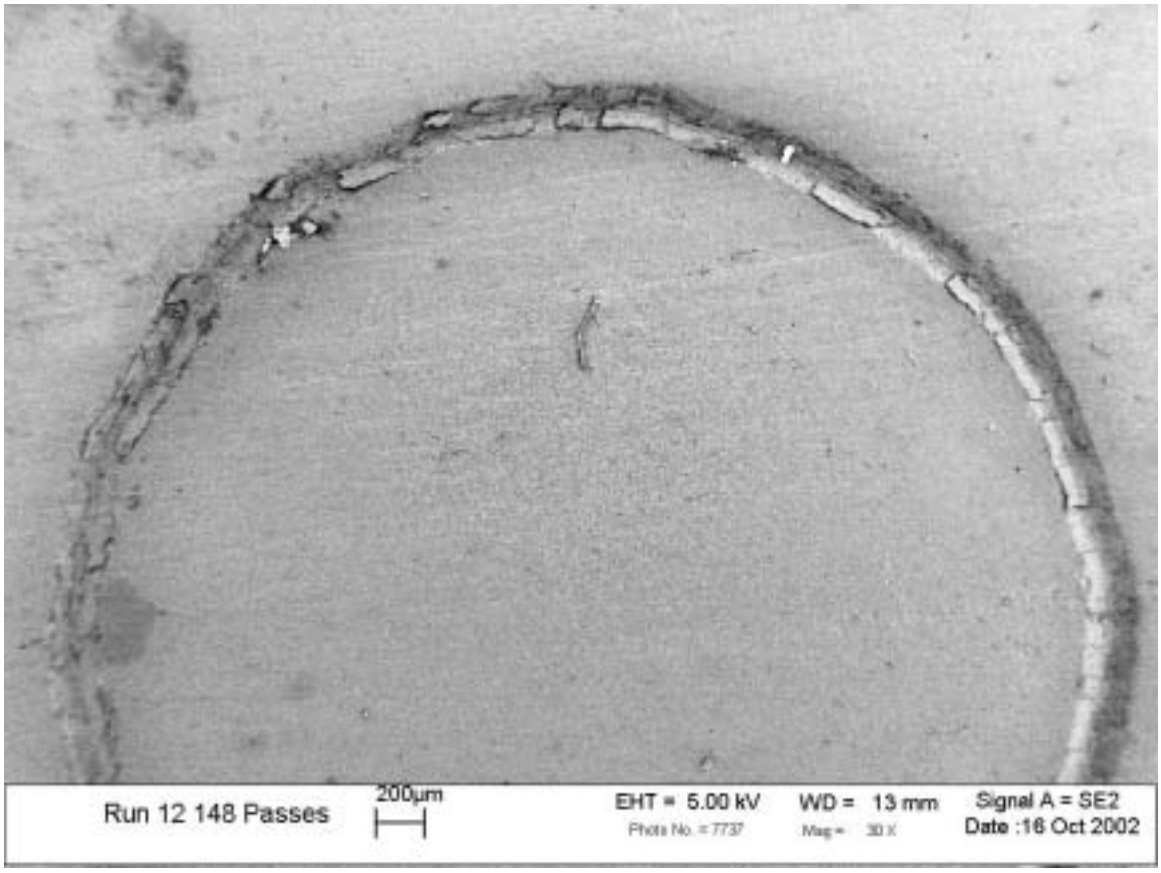

Figure 2.10u. The wear scar after 148 passes consists of a mixture of fractured and plastic flow surfaces.

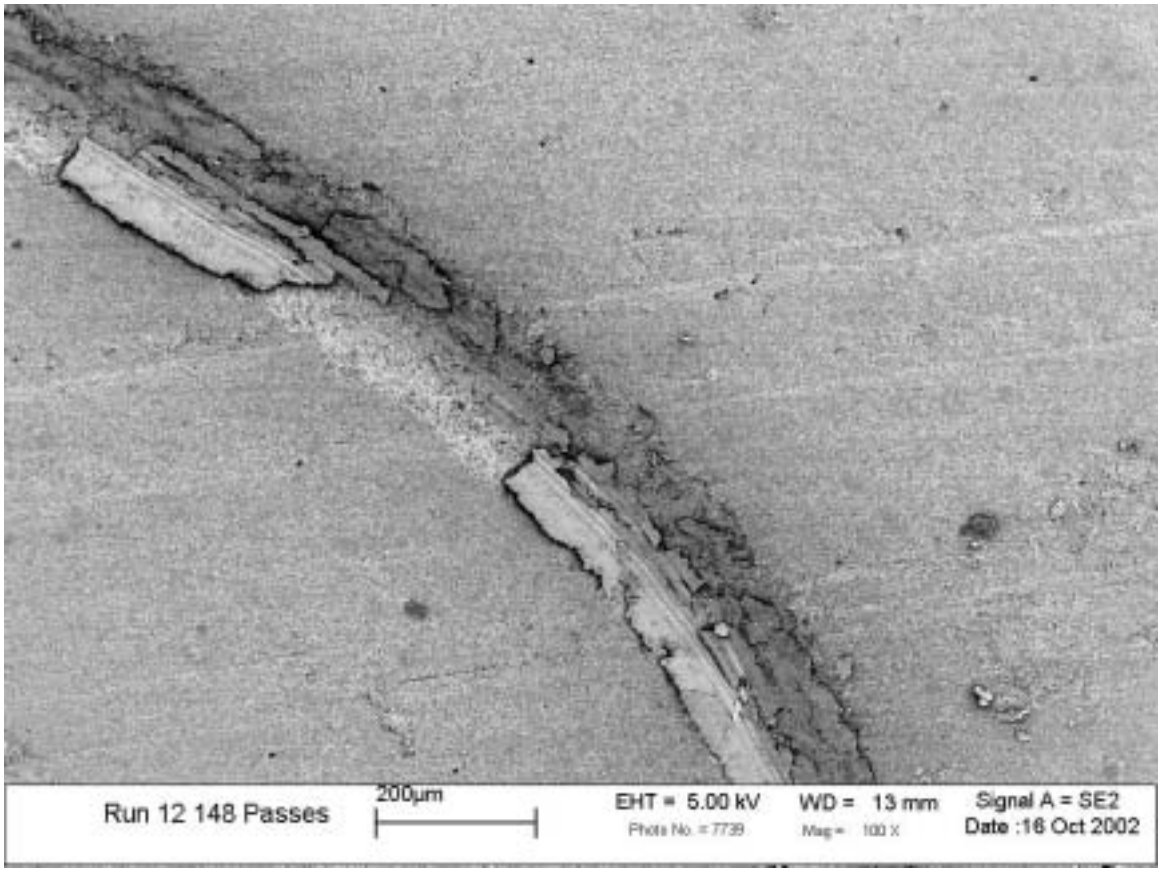

Figure 2.10v. The same wear scar as in Figure 2.10u, at 100x magnification.

the 3 and 7 pass samples, while the wear scar surface of sample 2 (Figures 2.10m and 2.10n) is almost covered by plastic flow debris. We suggest that these two samples are on the boundary of a wear transition; the transition has not occurred in sample 6 (plastic flow is not evident) but has occurred in sample 2 where the surface is covered with plastic flow. Then in the succeeding samples, 54 passes (Figures 2.10o to 2.10r) and 148 passes (Figures 2.10s to 2.10v), the wear scars are mixtures of fractured and plastic flow surfaces. We hypothesize that after the putative wear transition at approximately 20 passes, a steady state process occurs in which the delamination of the plastic material is balanced by re-formation of plastic film from the wear debris. The SEM pictures capture a particular moment of this balancing process.

In order to quantify the visual features in the SEM pictures that were discussed above, we estimated the relative area in the scar track covered by plastic flow material at several different magnifications of the same sample. The results from the different pictures were weighted by the length of the wear scar in the picture to the circumference of the wear scar. The fraction of plastic flow versus the natural logarithm of the number of passes is shown in Figure 2.11. After the first pass, one sample had 92% plastic flow while the other was a mixture of 58% plastic flow and 42% fractured surface. The fraction of plastic flow in the wear scar after 3 and 7 pases was less than 15%. Then, a putative transition occurs after 20 passes with one sample having 12% plastic film and the other 91%. The fraction of plastic film varies between 30% and 80% in the two samples with 148 passes and the two samples with 54 passes. Conceivably other patterns of plastic flow production and film delamination might exist between 20 and 154 passes since we have SEM pictures only for 48 passes between these two limits. But the triboemission measurements, to be discussed in sections 2.4.2 and 2.5.2, provide a continuous probe of the wear process and these measurements provide clear evidence for two, and only two,

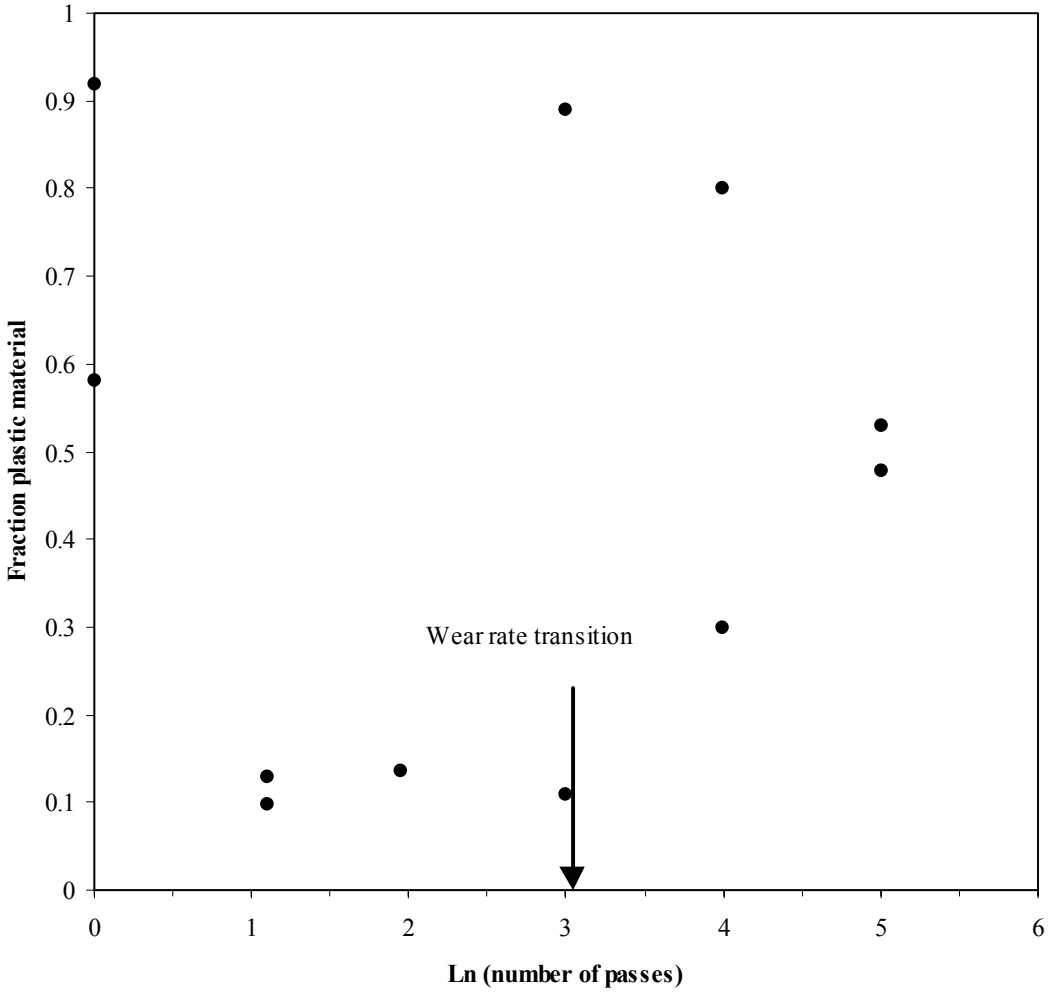

Figure 2.11. Fraction of plastic material versus the natural logarithm of the number of passes.

transitions at 2 and 20 passes. A natural interpretation of the triboemission data, that is consistent with the SEM pictures, is that the triboemission rate is low when the scar surface is free of plastic film, between 2 and 20 passes, and high when the plastic film is cracking and delaminating from the wear scar during the remaining pass periods.

The wear tracks as a function of pass number for 30 N load (Figures 2.12a to 2.12h) display similar transitions from a mixture of fractured surface and plastic flow material on the initial pass (Figures 2.12a and 2.12b), to delamination of the plastic flakes on pass 2 and 3 leaving predominantly fractured material (Figures 2.12c and 2.12d), back to a mixture of fractured surface interspersed with plastic flow debris for 6, 9, 13, and 18 passes (Figures 2.12e to 2.12h). But the transition is not as clear at 30 N load as it is at 10 N load. Rather, the creation of plastic flow material from the wear debris appears to occur concurrently with delamination of plastic flakes created in a previous pass. We were limited to approximately 20 passes at 30 N load because of the tendency of the diamond tip to crack at this high frictional stress. The triboemission rate also displays a transition as a function of pass number that is similar to the transition observed at 10 N load, but the transition is more diffuse at 30 N load compared to the transition at 10 N load. The triboemission data will be discussed in sections 2.4.2 and 2.5.2.

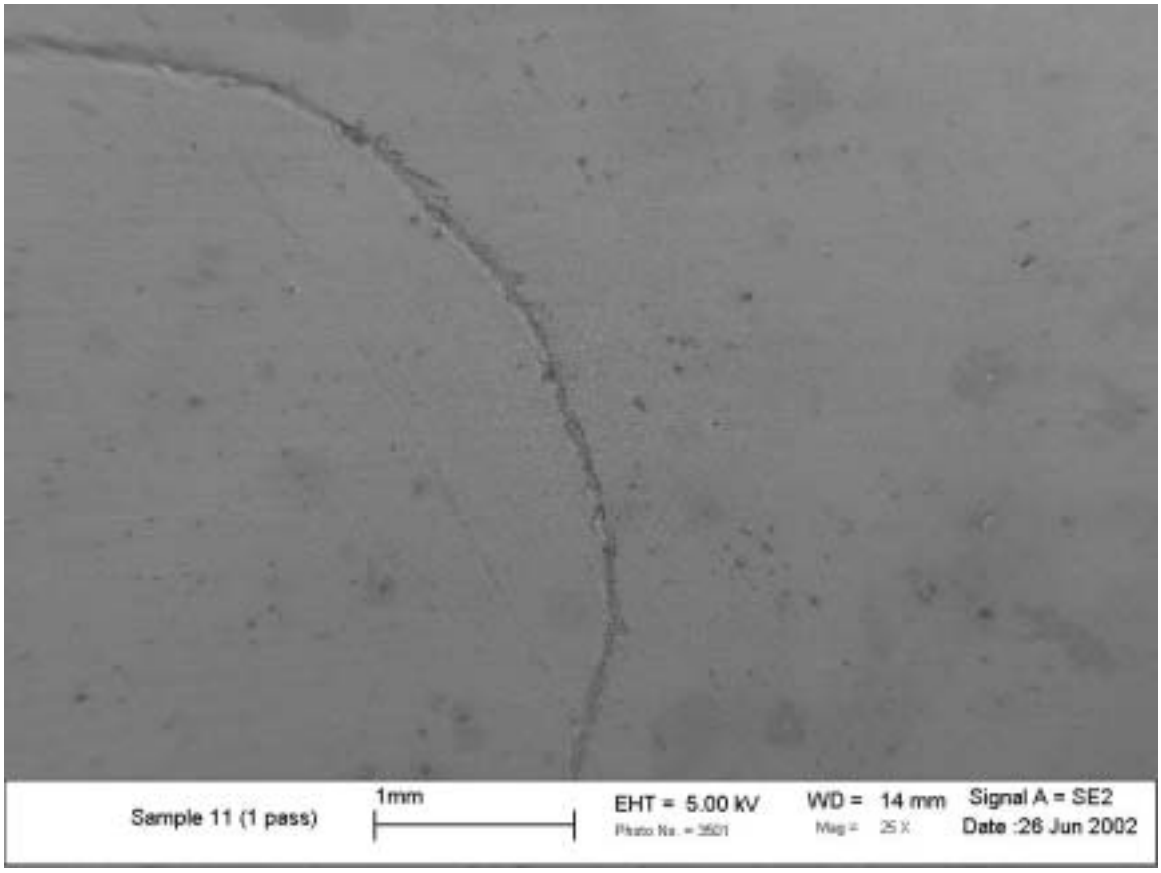

Figure 2.12a. Wear scar after 1 pass at 30 N. The wear track is covered by a mixture of plastic flow material and fractured surface.

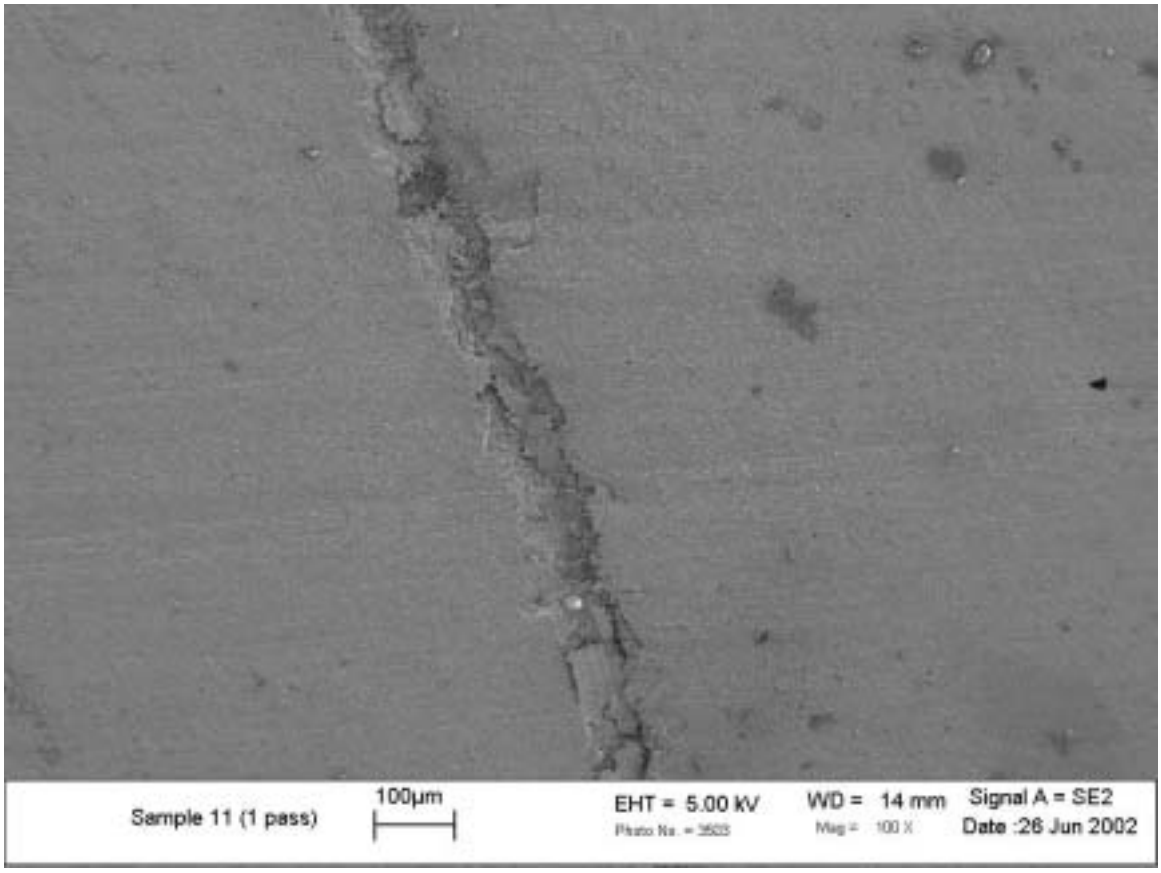

Figure 2.12b. The same wear scar as in Figure 2.12a, at 100x magnification.

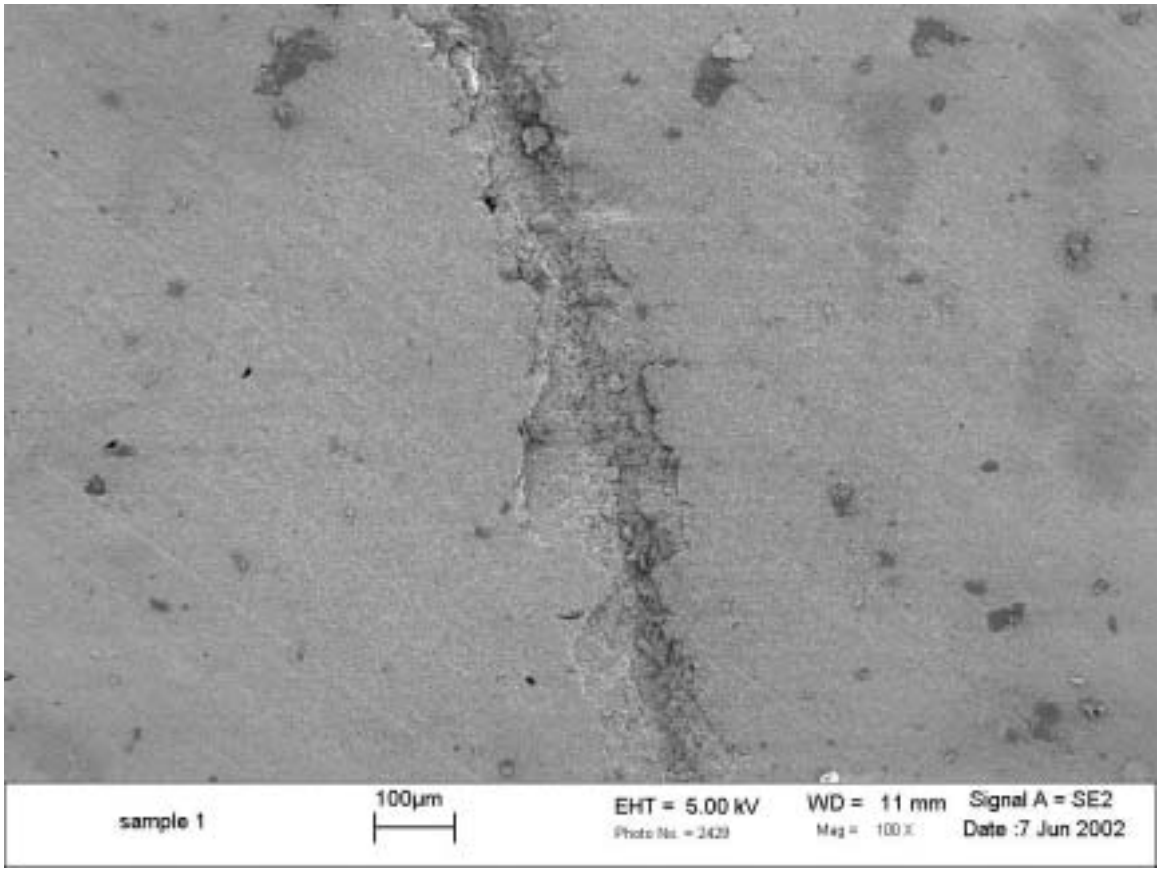

Figure 2.12c. Wear scar after 2 passes at 30 N. The plastic flow material has delaminated, leaving predominantly fractured material on the surface of the wear track.

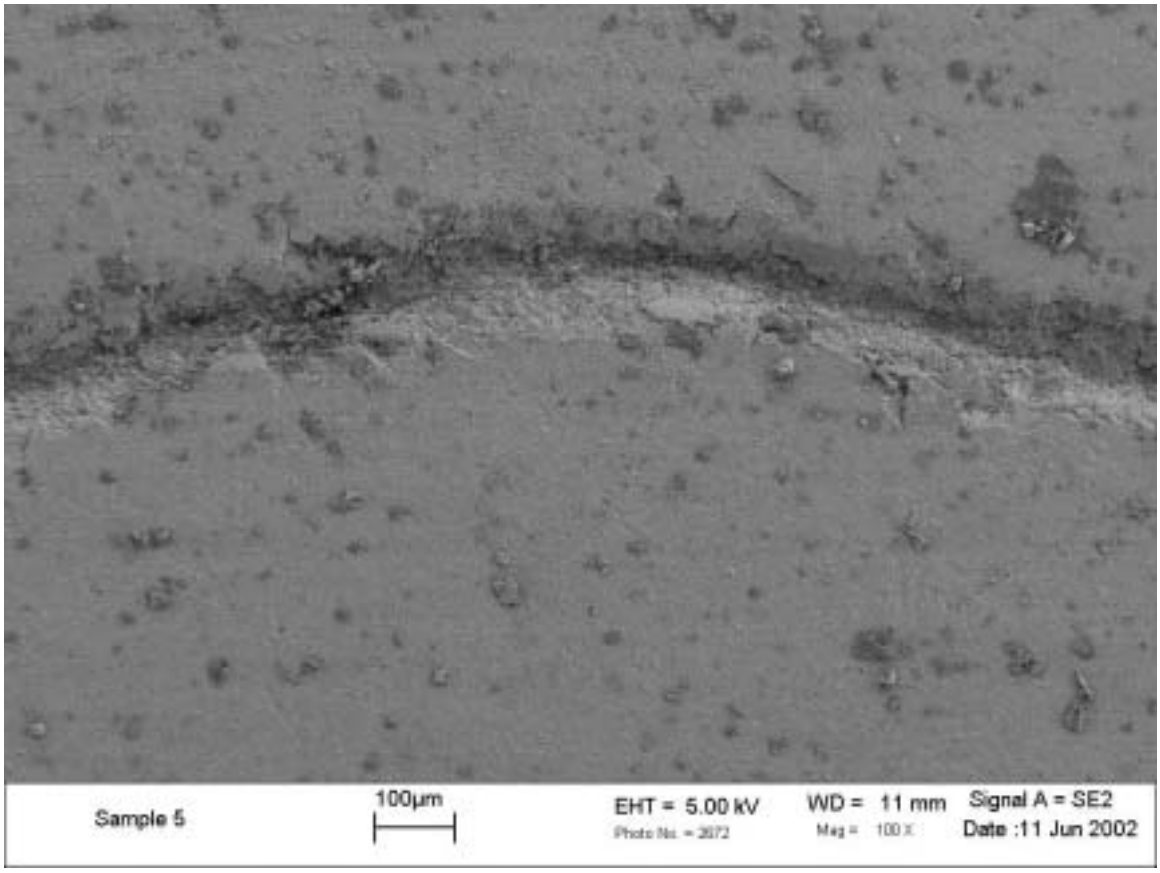

Figure 2.12d. Wear scar after 3 passes at 30 N. The plastic flow material has delaminated, leaving predominantly fractured material on the surface of the wear track.

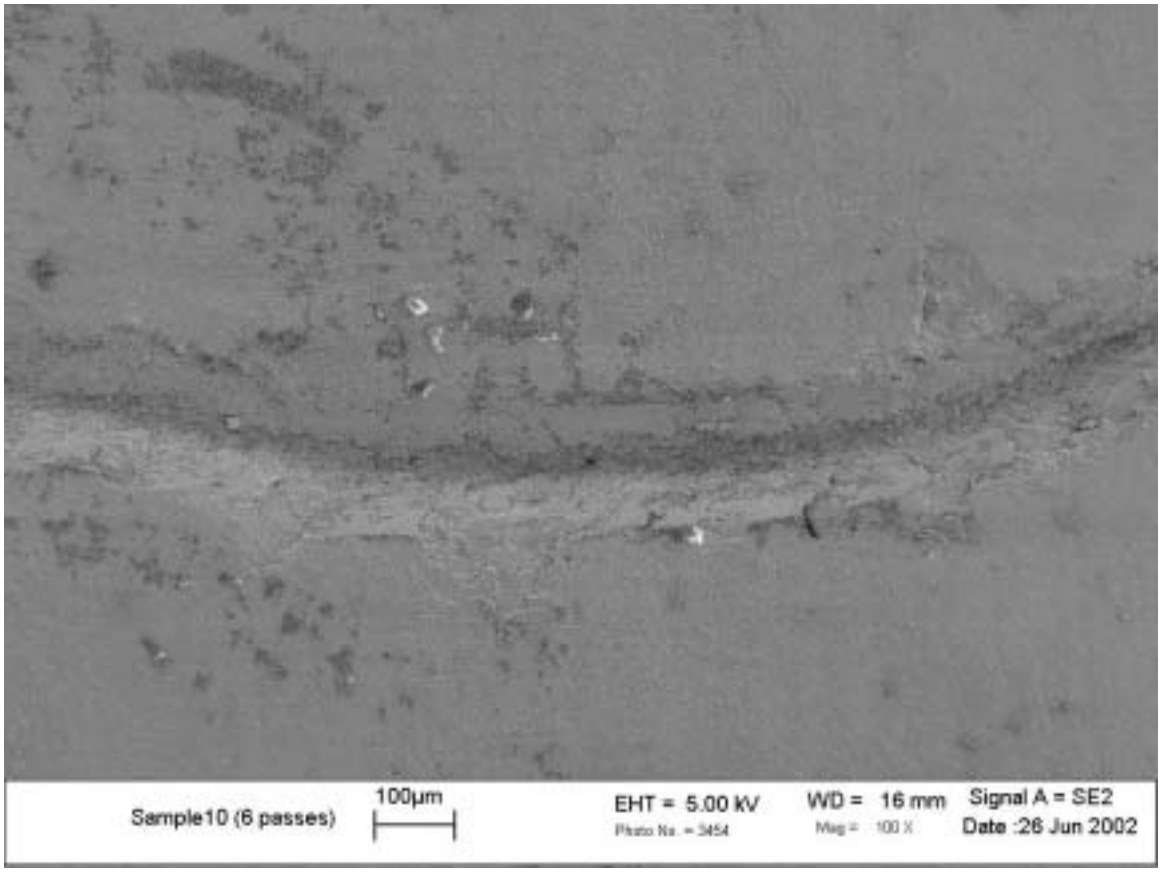

Figure 2.12e. Wear scar after 6 passes at 30 N. The surface of the track consists again of a mixture of fractured material interspersed with plastic flow debris.

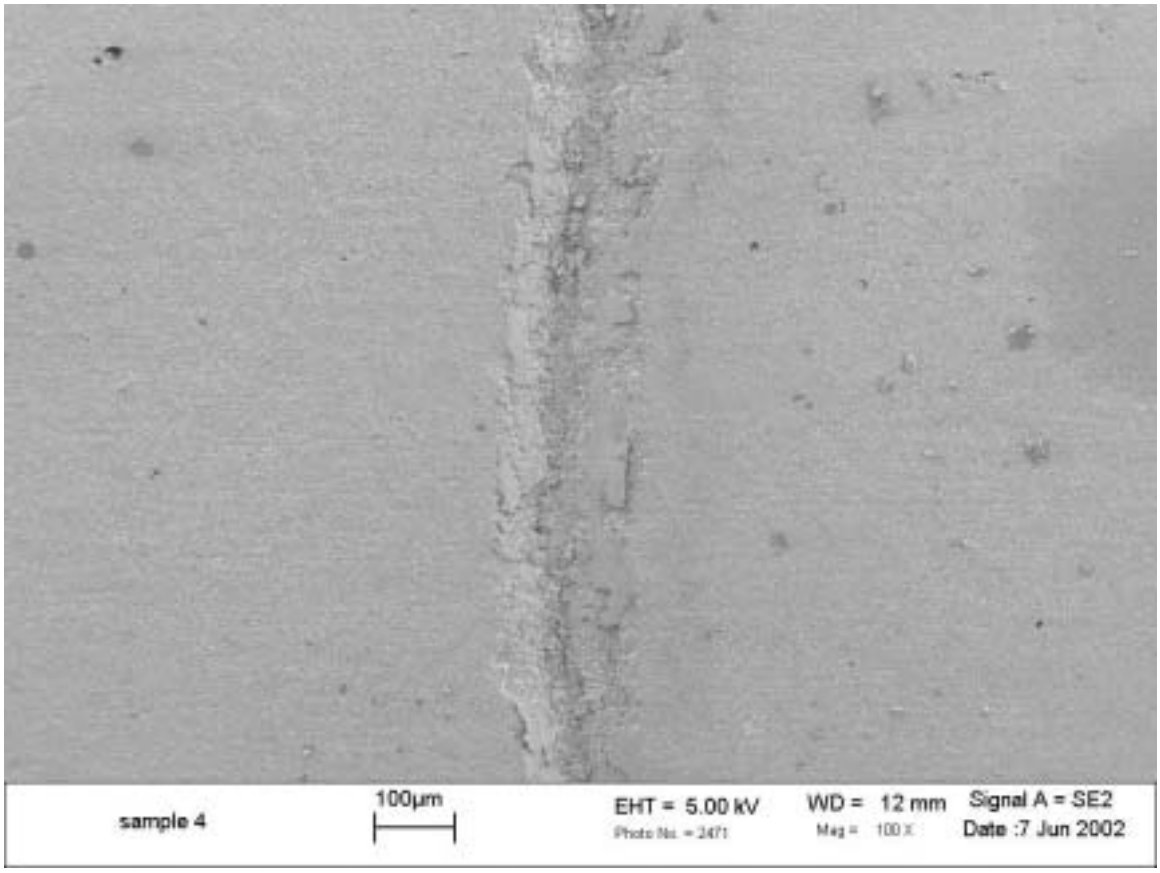

Figure 2.12f. Wear scar after 9 passes at 30 N. The surface of the track consists of a mixture of fractured material interspersed with plastic flow debris.

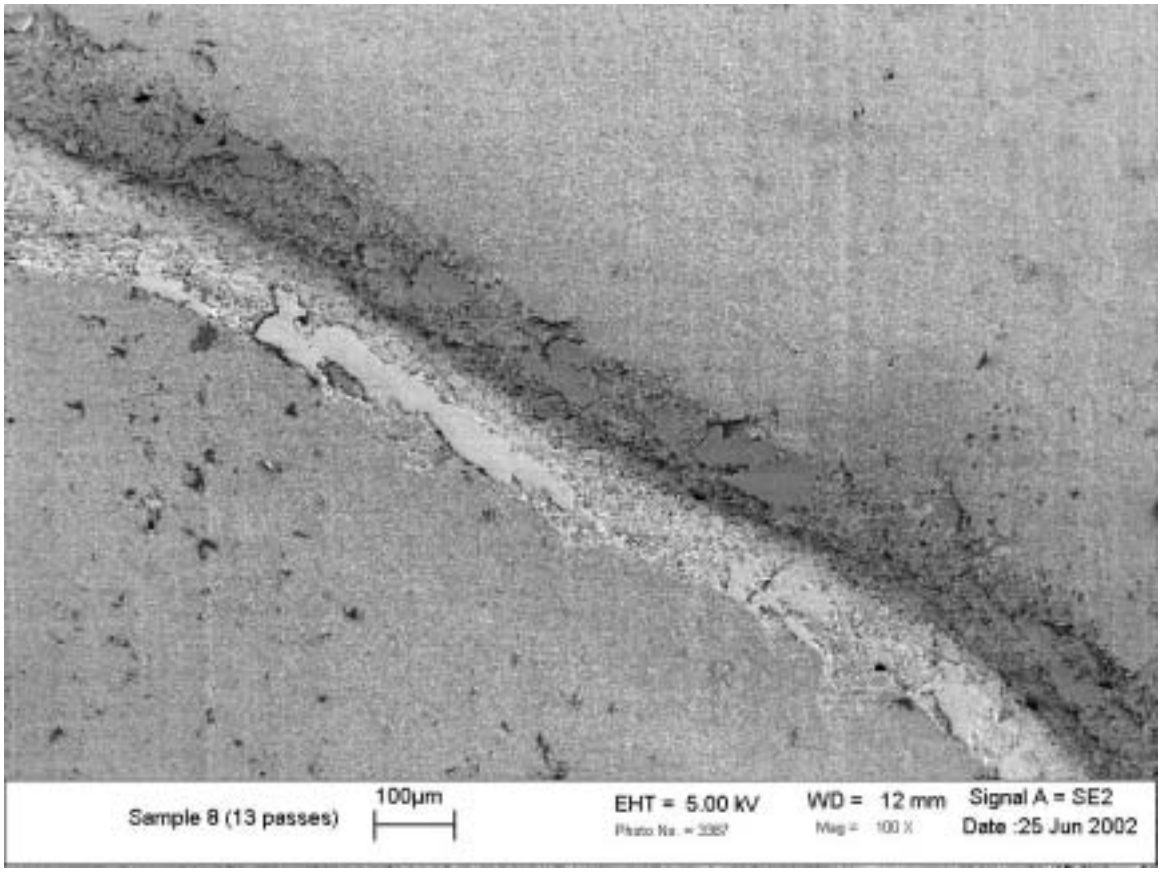

Figure 2.12g. Wear scar after 13 passes at 30 N. The surface of the track consists of a mixture of fractured material interspersed with plastic flow debris.

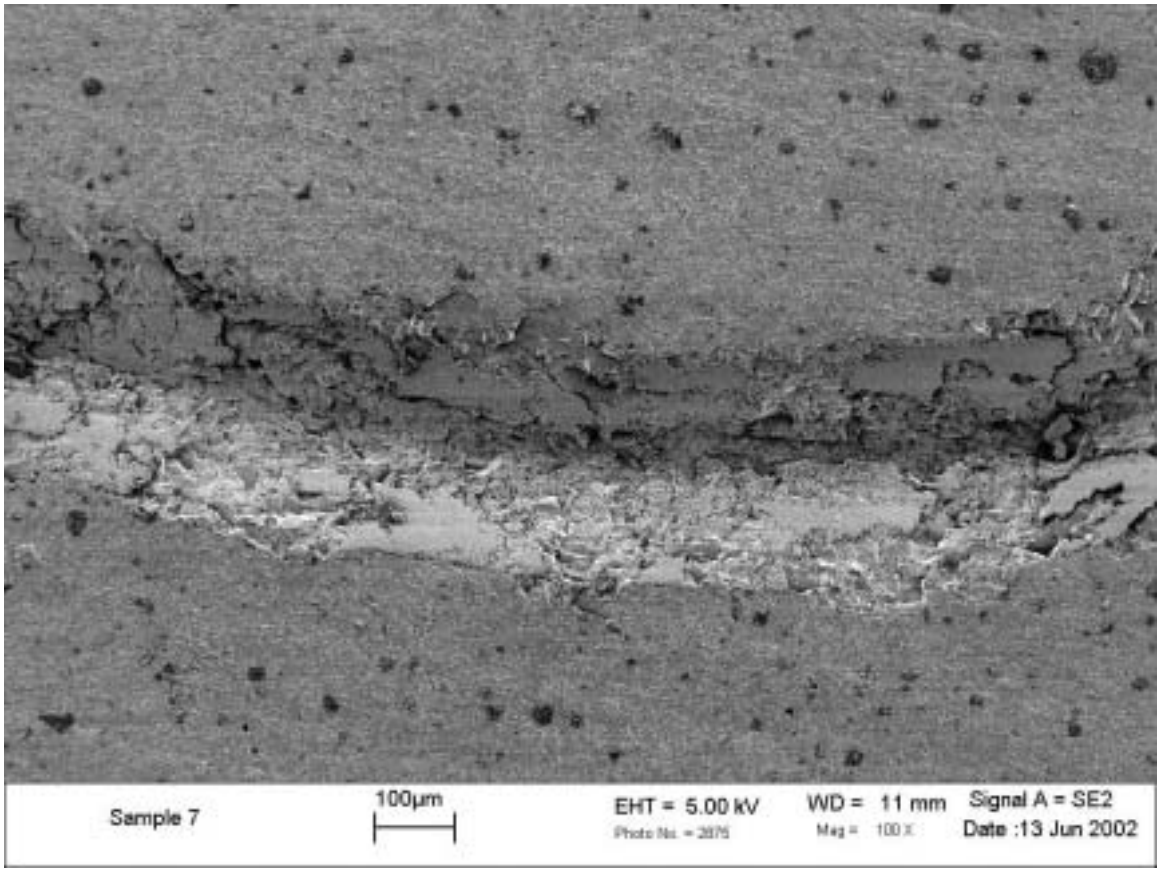

Figure 2.12h. Wear scar after 18 passes at 30 N. The surface of the track consists of a mixture of fractured material interspersed with plastic flow debris.

2.4.2 Emission Data

The differential and cumulative number of electrons emitted while abrading an alumina sample with a 30 N load for 18 passes are shown in Figure 2.13. The period for one pass of the sample under the diamond indenter is 52 seconds. Two characteristics of the emission are displayed in the figure. The first characteristic is the presence of emission bursts at random times. These bursts can be several orders of magnitude higher than the average emission and are seen in Figure 2.13 as spikes in the differential rate and discontinuities in the cumulative rate. This characteristic burst-type behavior of emission has been noted by others [24], [31], [32]. The second characteristic of the emission is a component with approximately constant rate over several passes (for example, from 0 to ~ 600 seconds in Figure 2.13) that results in a nearly linear cumulative emission. This emission rate may change, sometimes in conjunction with a burst and sometimes not, and the slope of the cumulative emission will change. The rate may increase or decrease.

Figure 2.14 shows a plot of the cumulative electron count versus the number of passes from Table 2.1 for the 10 N and 30 N applied loads. It is evident that for both loads, there is very low correlation between the cumulative count and the number of passes. The data plotted in Figure 2.14 is the total cumulative count after abrading the sample for a given number of passes. But our data for a given sample includes the cumulative count for any number of passes, including fractions of a pass, that is less than the total number of passes for that sample. So, for example, at 10 N load and for one pass of the diamond indenter, we have the cumulative emission from all 12 samples listed in Table 2.1 for that load. At 10 N load and for 100 hundred passes, we have the cumulative emission only from the last 2 samples for that load. In Figure 2.15 is shown the cumulative emission as a function of pass number for the different samples abraded with a 10 N load. In the discussion section, we will argue that the emission should be treated as a random variable with a lognormal distribution. A correlation does exist between the population mean of the logarithm of the emission and the logarithm of the number of passes.

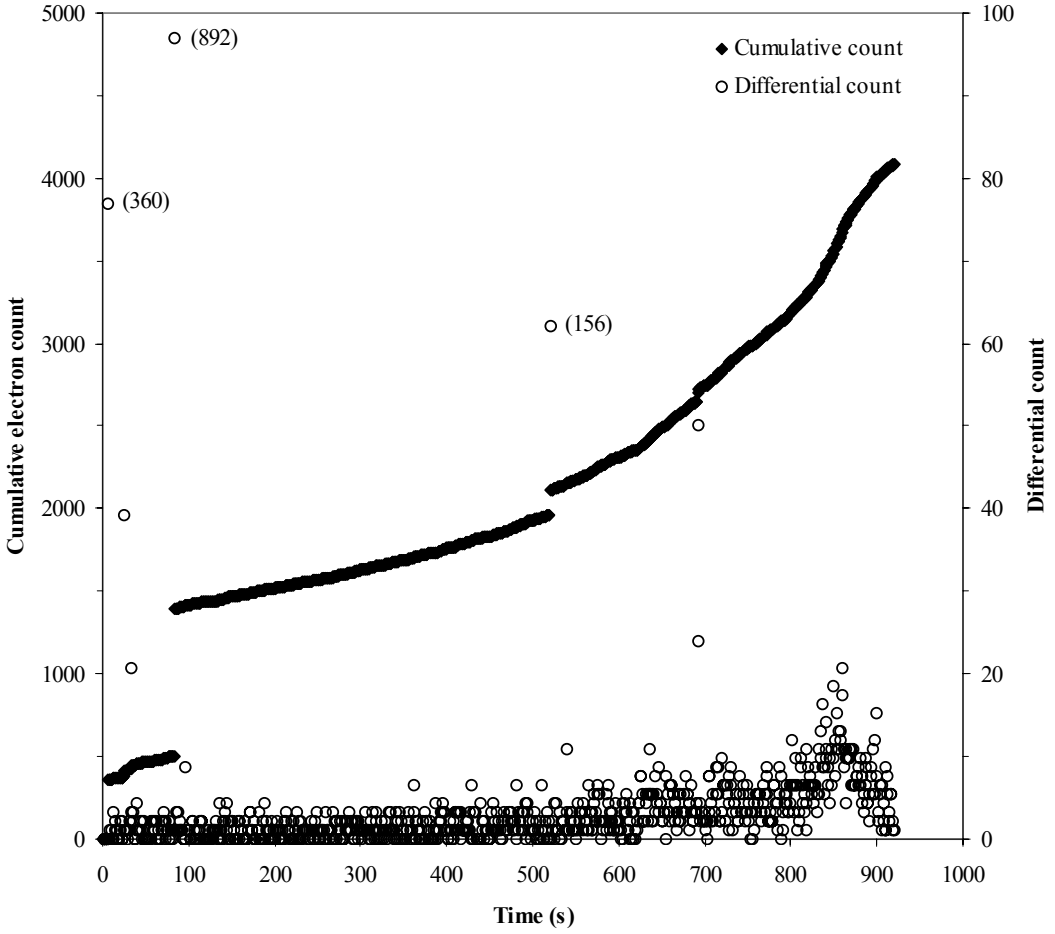

Figure 2.13. Cumulative and differential electron count versus time for a typical alumina sample at the 30 N load. It can be seen that the emission occurs often in bursts.

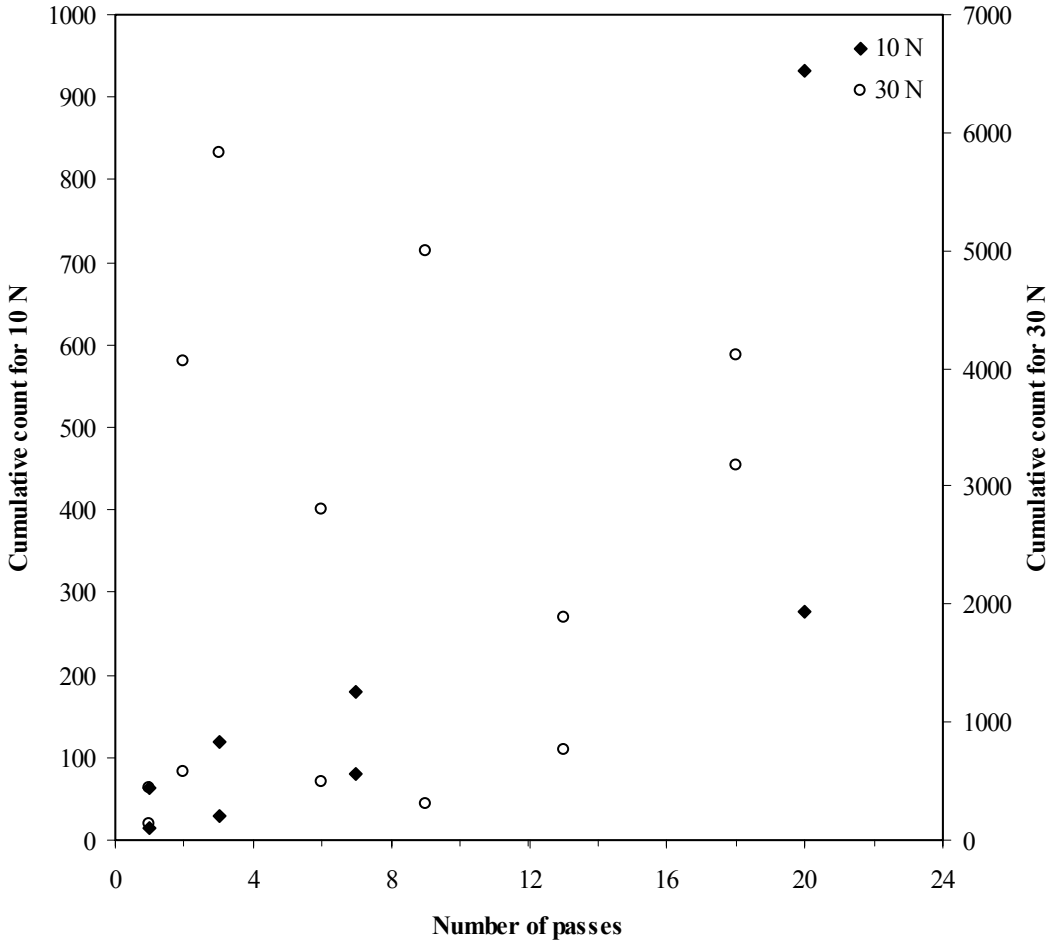

Figure 2.14. Cumulative electron count versus the number of passes for the two applied loads, 10 N and 30 N respectively. The data for the two loads are plotted on different axes.

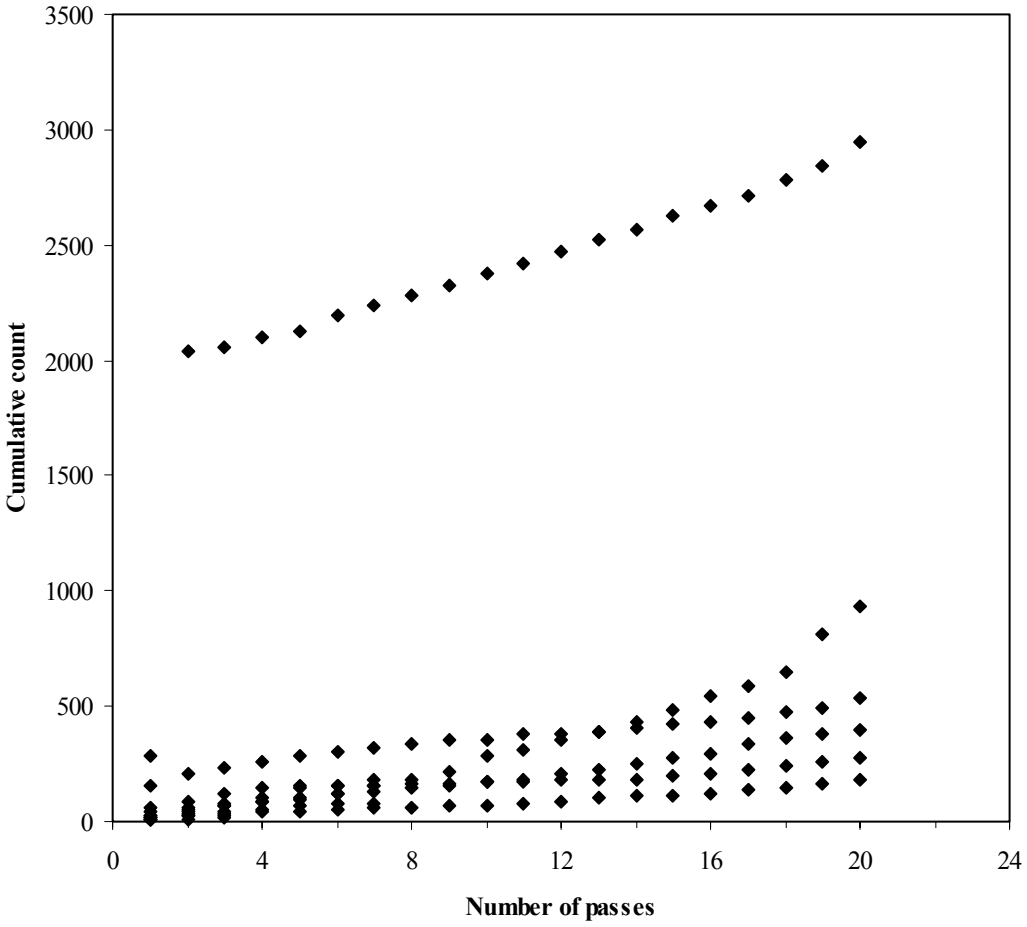

Figure 2.15. The cumulative emission as a function of pass number for the first 20 passes, for the different samples abraded with a 10 N load.

2.5. Discussion

2.5.1 Wear Data

The wear volume for 10 N load increases at a rate of 0.087 mm^3/m per pass up to 20 passes and then decreases to an immeasurably small rate from 20 passes to 148 passes. This dramatic decrease in wear coincides with the wear scar changing from a surface that is predominately fractured grains for 3 and 7 passes, to a surface covered with a mixture of fractured grains and plastic flow film for 54 and 148 passes. The transition in the characteristics of the surface coverage occurs at about 20 passes where one sample had very little coverage of plastic film while the other sample was over 90% covered with plastic flow film. The surface mixture at larger pass number appears to arise from a steady state process of film delamination followed by re-formation of the film from the wear debris. The wear volume for the 30 N load increases at a constant rate of 0.41 mm^3/m per pass up to 20 passes with no evidence of a wear transition. The SEM pictures at 30 N load did not display the contrast between granular and film coated surface evident in pictures taken of surfaces abraded at 10 N load. Rather, the surfaces at all measured pass numbers were a homogeneous mixture of fractured surface and cracked plastic flow film. We discuss our results now in terms of two competing models for describing the abrasion of alumina.

The original question addressed by this thesis was whether the cumulative triboemission from abrasion of alumina correlated with the volume of material removed and, in particular, whether transitions in the rate of material removal were mirrored in the cumulative triboemission rate. The experiment was patterned after research by Xu and Jahanmir [4] who scratched an alumina sample at different loads with a diamond indenter in repeat-pass reciprocating sliding. Their sliding speed, 0.3 mm/sec, was chosen to minimize local heating of the wear track. They observed two or three wear regimes for alumina depending on the normal load applied and on the number of passes. Their results

are plotted in Figure 2.16 as volume removed per pass at 20 N and 40 N load. For both low and high loads (20 and 40 N), the first wear regime consisted of damage accumulation in the material beneath the contact area. The damage within this plastic zone was observed from SEM pictures to occur in the form of intragrain twin/slip bands and intergranular microcracks. After a critical number of passes (8 passes at 20 N and 3 at 40 N), Xu and Jahanmir observed a transition from a damage accumulation process to a material removal process that involved mainly grain dislodgement. They described this as "mild wear", as opposed to the first wear regime when very little material was actually removed. As they increased the number of passes at high load (40 N), the wear process exhibited a second transition from grain dislodgement to a more severe regime characterized by lateral crack chipping. They described this third regime as "severe wear". They also noted that beside the load and the number of passes, the dominating wear mechanism depends as well on the ceramic microstructure, i.e. grain size and strength of grain boundaries.

In our experiment, we duplicated the material, indenter and indenter geometry, and sliding speed used Xu and Jahanmir. We chose loads of 10 N and 30 N to straddle the loads that they studied. Based on their results, we expected to see damage accumulation and possibly a transition with increasing pass number to the mild wear regime at 10 N load. We did not expect to see at this load a transition to severe wear with concomitant lateral crack chipping. At 30 N load, we expected to see the transition to mild wear and possibly a transition with increasing pass number to severe wear. What we saw for both 10 N and 30 N load was evidence in the SEM pictures for lateral crack chipping on the first pass; that is, our samples appeared to start immediately in the severe wear regime. Further evidence that the wear behavior skipped the mild wear regime for both the 10 N and 30 N load in our experiment is shown in Figure 2.17. This is a plot of the natural logarithm of the wear volume versus natural logarithm of pass number for both loads. A linear regression fit to the data from one to 20 passes for 10 N load is shown on the figure. The initial slope of the 10 N data is 0.8 and the intercept at one pass (equal to the

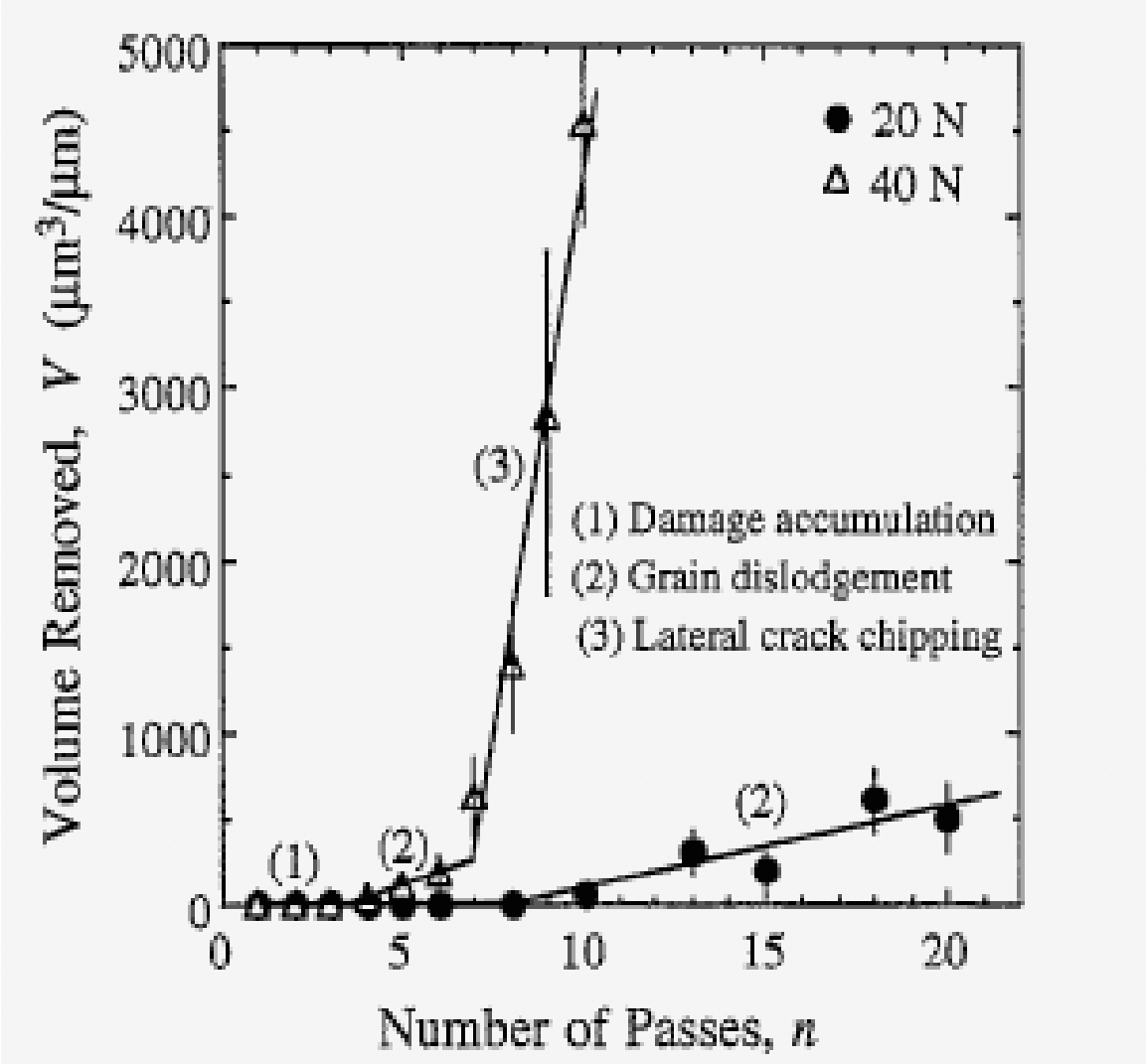

Figure 2.16. Xu and Jahanmir's results for the wear of alumina abraded by a conical diamond indenter in repeated pass sliding. They observed either one or two transitions as a function of load and pass number. The wear rate always increased with the pass number. (H.H.K. Xu and Said Jahanmir, Ref. [4]).

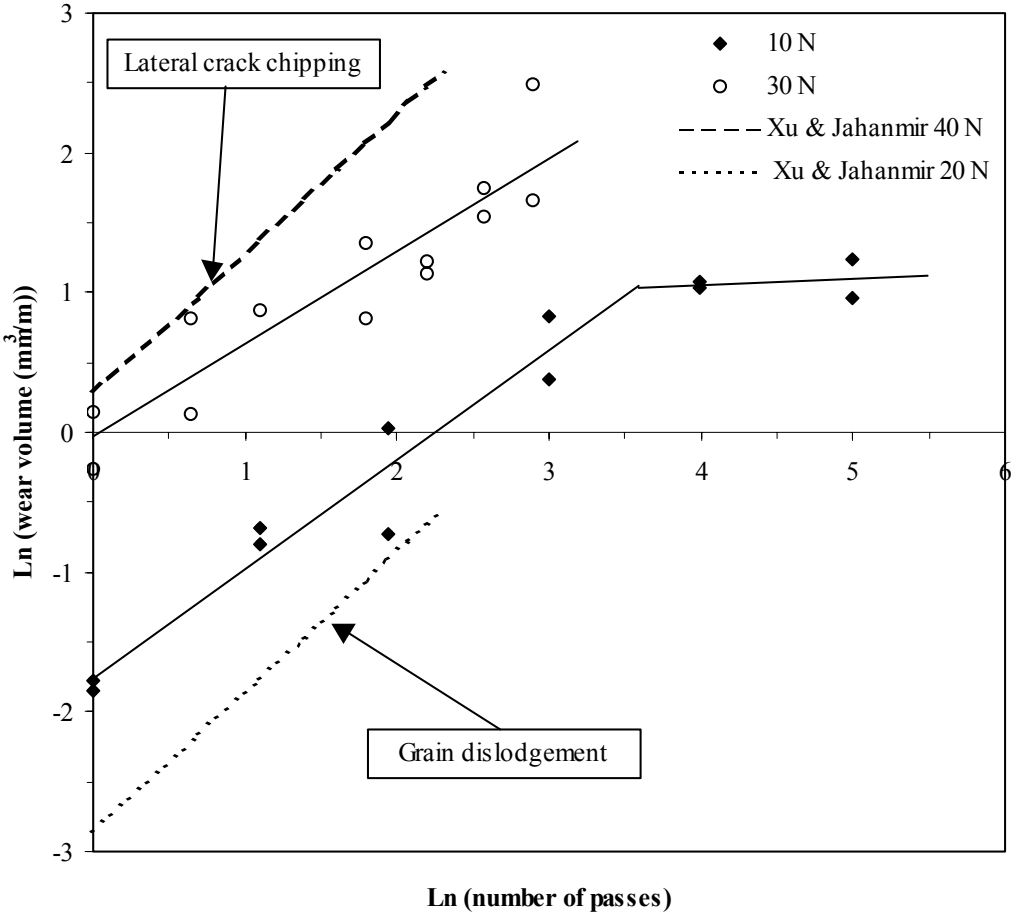

Figure 2.17. Natural logarithm of the wear volume versus the natural logarithm of the number of passes for all the samples, at the two loads. Xu and Jahanmir's results are indicated by dashed lines on the plot.

natural logarithm of the slope in the linear plot) is -1.8. After 20 passes, the wear rate for the 10 N load is nearly independent of pass number. The wear rate for 30 N load does not exhibit a transition from one to 20 passes. The linear regression fit to the 30 N data has a slope of 0.7 and an intercept of zero at one pass. We have estimated the volume removal rate from region 2 (mild wear from grain dislodgement) and region 3 (severe wear from lateral crack chipping) of the measurements from Xu and Jahanmir. Their wear rates are linear in pass number and have slopes (in the linear plot) of 0.05 mm^3/m per pass (mild wear) and 1.3 mm^3/m per pass (severe wear), respectively. We have indicated these two rates on Figure 2.17 by dashed lines.

The most striking difference between our data and the measurements of Xu and Jahanmir is the wear behavior for 10 N load. The initial wear rate (intercept at one pass) is greater than the mild wear and less than the severe wear rate measured by Xu and Jahanmir. But of more significance than the quantitative differences in wear rate is the qualitative difference in the functional dependence of the wear rate on pass number. We observe a transition in the wear behavior at approximately 20 passes. If the linear wear rate were proportional to the number of passes and the linear slope increased after the transition, as Xu and Jahanmir observe in their wear transitions, then on our log-log plot, the wear volume would increase rapidly after the transition, shifting up to a slope equal to one and with larger intercept. Instead, the wear rate becomes nearly independent of the number of passes after the transition. The difference is less striking between the behavior we observe for the wear at 30 N load and the model suggested by Xu and Jahanmir for abrasive wear. The linear rate of wear that we measure at 30 N load is close to the severe wear rate that Xu and Jahanmir measure. Where we differ is that they observe a region of mild wear at 40 N load and then a transition to severe wear after 7 passes. In our case, there is no evidence of a mild wear region, the wear is severe on the first pass, even though our load is 10 N less than theirs. As a consequence of these significant differences in the wear behavior that we observe and the model of abrasive wear proposed by Xu and

Jahanmir, we consider next a model of wear suggested by Ajayi and Ludema [18] and expanded by Berthier et al [39], [40].

Ajayi and Ludema [18] performed a seminal study of the wear of alumina by different materials (silicon carbide, silicon nitride, zirconia and alumina). They noted that when two ceramic materials are brought into contact and tribological stress is applied, material is usually removed from both surfaces as wear debris. The formation of debris occurs by two wear processes. One process involves fracture on the scale of the asperity size, but this process only accounts for a small fraction of the volume of material removed from the surfaces in contact.

The bulk of the removed material is generated by a process that occurs on a larger scale, which varies from material to material. In the case of alumina, the wear mechanism starts with plastic deformation, followed by the initiation of cracks and subsequent formation of flake-like wear debris that separates from the surface. Some of the wear debris is lost from the system, but some of it is recycled at the interfaces and is further fragmented in repeat pass sliding. The wear debris that is trapped at the interface between the surfaces in contact is ground into very fine wear debris particles (authors estimated particle sizes of 10-50 nm). Eventually, these fine debris particles reattach to the surface by a mechanism similar to powder agglomeration forming the so-called transfer film. The authors proposed that the forces responsible for the film's strong adhesion to the surface are van der Waals and electrostatic forces. These forces are strong enough that the transfer film is not removed from the surface by subsequent passes of the slider and they resist ultrasonic cleaning methods. The film is considered to have a protecting role and is responsible for a reduction of the observed wear rates in some situations. Ajayi and Ludema observed that the characteristics of this transfer film depend strongly on the nature of the two materials in contact. They did not study the abrasion of alumina by diamond, but they did note that in the case of a couple consisting of a covalent and an

ionic material, the film that forms often consists of “islands” that adhere to the wear track.

Xu and Jahanmir [4] observe a wear process consisting of a series of distinct processes beginning with damage accumulation and progressing (the extent of the progression depending on load) to grain dislodgement and then lateral crack chipping. Their model does not go beyond the severe wear stage and does not take into account the effect of wear debris in the wear scar. Ajayi and Ludema observe a progression of material removal beginning with plastic deformation and followed by crack initiation. But then another stage occurs in which flake-shaped particles delaminate from the surface as wear debris and subsequent wear is controlled primarily by the extent to which debris is ejected from the wear scar versus being recycled and re-forming plastic film. Our observations are more in line with the observations of Ajayi and Ludema [18] rather than to those of Xu and Jahanmir [4]. We see no evidence of a period of damage accumulation followed by mild wear associated with grain dislodgement. Instead, we observe in the SEM pictures (Figures 2.12a, 2.12b and 2.10a to 2.10d) plastic deformation and severe cracking after the first pass. There is a sharp reduction in the wear rate for 10 N load after 20 passes that is consistent, again from the SEM pictures (Figures 2.10m to 2.10v), with the formation of a protective transfer film on the wear track. The wear rate for 30 N is constant as a function of pass number; there is no evidence of a wear transition up to 18 passes.

Our experimental design was based on the test conditions used by Xu and Jahanmir and yet our results are closer to the observations of Ajayi and Ludema. In order to understand this puzzling result, we summarize in Table 2.2 the experimental parameters of the three experiments. Our material system, diamond indenter on alumina, was identical to the system of Xu and Jahanmir and different from the system of Ajayi and Ludema, alumina cylinder on alumina disk. Our average grain size is comparable to the grain size of Xu and Jahanmir’s sample and smaller than the grain size in the samples of Ajayi and

Ludema. The dispersion in grain size was considerably larger in our sample than in the samples of Xu and Jahanmir. Ajayi and Ludema did not provide information on the dispersion of grain size in their samples. The range of loads was comparable for all three experiments, but a significant difference, factor of 1000, exists between the sliding speed used by Ajayi and Ludema and the identical speeds used in our experiment and by Xu and Jahanmir. A significant difference also exists between the total number of repeat passes Ajayi and Ludema used versus the comparable number of passes in our experiment and the experiments of Xu and Jahanmir. However, we expect that the differences and similarities between our results and the other two experiments are due primarily to the interaction between three factors: the sample atmosphere, the surface roughness, and the type of motion (reciprocating versus repeat pass).

The first factor is the ambient atmosphere in which the experiments are performed. Both Xu and Jahanmir as well as Ajayi and Ludema conducted their tests in laboratory air with a relative humidity of 40-50%, while ours were conducted inside a vacuum chamber at pressures smaller than 10^{-4} Pa. The presence of water on the surface of alumina reduces the friction due to the formation of stable aluminum hydroxides, which in turn form a layered structure (trihydroxide-bayerite) that reduces the frictional shear stress [41]. We hypothesize that, unlike in Xu and Jahanmir's experiment, only trace quantities of water vapor existed on our sample surfaces during the wear process and, therefore, the frictional shear stress was higher on our samples.

The second factor, surface roughness, also contributed to a higher shear stress because the real area of contact for rough surfaces is smaller than for smooth surfaces and, consequently, the microcontact pressures are higher. The high contact pressure and the absence of hydroxide lubrication in our samples is probably responsible for the absence of the mild wear regime observed by Xu and Jahanmir.

	Xu and Jahanmir [4]	Ajayi and Ludema [18]	Our study
Material System	Diamond indenter abrading high purity alumina samples	Silicon carbide, silicon nitride, zirconia and alumina on alumina	Diamond indenter abrading high purity alumina samples
Surface Roughness	< 1 μm	0.217 μm	1.8 ± 0.8 μm
Grain Size	3 μm	10.0 μm	3.8 ± 3.4 μm
Contact Geometry	Conical indenter (120° apex angle) on flat	Cylinder-on-flat	Conical indenter (120° apex angle) on disk
Atmosphere	Laboratory air with relative humidity of 40-50%	Laboratory air with relative humidity of about 45%	Vacuum better than 10^{-4} Pa
Load	20 N and 40 N	13.7 N and 25.5 N	10 N and 30 N
Sliding Speed	0.3 mm/s	0.25 m/s	≈ 0.3 mm/s
Sliding Distance	Repeat pass reciprocating sliding up to 20 passes	Repeat pass sliding up to ≈ 2000 passes	Repeat pass sliding up to 148 passes
Observations	Either one or two transitions as a function of load and pass number. Wear rate always increased with pass number. Mild wear rate = 0.05 mm^3/m per pass Severe wear rate = 1.3 mm^3/m per pass	Wear rate increased or decreased depending on the pin material. Wear rate for alumina-on-alumina approximately = 0.02 mm^3/m per pass	Measurable wear occurred as early as the first pass. The wear rate decreased from 0.087 mm^3/m per pass to approximately zero after 20 passes at 10 N. The wear rate was constant, 0.41 mm^3/m per pass, up to 18 passes for 30 N load.

Table 2.2. Experimental parameters of the three experiments.

The third major difference between our experiment and work of Xu and Jahanmir is the type of repeat contact between the diamond indenter and the alumina sample. In our experiment, the disk-shaped sample rotated under the diamond indenter while being pressed against it. Ajayi and Ludema used a similar experimental geometry. In contrast, the experimental geometry used by Xu and Jahanmir consisted of reciprocal motion of the indenter across the sample. Ajayi and Ludema [18] suggest that in the case of reciprocating sliding, the formation of the transfer film may not occur because its formation is contingent upon fine debris material being trapped at the interface between the two materials. The debris will be pushed out of the wear scar at the ends of the stroke by the reciprocating indenter. This may explain why Xu and Jahanmir did not observe a transfer film in their experiment and why their wear rate never decreased in contrast to our results at 10 N load.

2.5.2 Triboemission Data

Cumulative triboemission as a random variable: the sample-to-sample distribution

The cumulative electron count as a function of load and the number of passes exhibited significant variability from sample-to-sample under ostensibly identical testing conditions, emphasizing the necessity of treating it as a random variable with an underlying population characterized by population parameters. The determination of the population distribution is critical in order to draw statistically valid inferences regarding the population parameters and their dependence on experimental variables [1]. The sample-to-sample variability in the cumulative emission can be seen in Figure 2.15 where we plotted the cumulative emission as a function of pass number for different samples. These measurements were taken with 10 N load. As an example of the variability, the cumulative emission varies from 6 to 287 counts after one pass and from 178 to 2,943 counts after 20 passes. The population distribution is clearly skewed with respect to the

mean for any given pass number and it has an extremely long tail for cumulative counts greater than the mean. The distribution is clearly not a normal (Gaussian) distribution. We next analyze the data in terms of four distributions: the normal, lognormal, exponential, and the Weibull distribution.

In order to identify the population distribution, we compare the data for a given pass number to the predicted distribution using the probability plot. The probability plot for a given distribution scales the ordinate and abscissa of the graph such that if the data is distributed as hypothesized, then the plotted data will be linear on the graph and the population parameters can be determined [42]. In Figure 2.18 are plots of the data for one pass at 30 N, based on the normal, lognormal, exponential, and Weibull probability plots using the Minitab statistical software application. As expected, the data fits the normal probability plot very poorly. The fit on the exponential probability plot also is very poor. The fits on both the lognormal and Weibull probability plots are both good, but looking at plots for several different pass numbers, the lognormal probability plot consistently fit the tails of the data distribution better than did the Weibull probability plot. If we apply standard statistical tests to the hypothesis that the distribution is lognormal (the null hypothesis), we obtain large P-values indicating that we can not rule out the possibility that the distribution is lognormal. We can not, of course, rule out the possibility that the data is characterized better by another distribution.

A random variable is lognormal if the logarithm of the variate is normally distributed. A normal distribution arises from the additive effect of many causes that are themselves independent random variables, while the lognormal distribution arises from the multiplicative effect of many causes that are independent random variables. The median of a lognormal population is estimated from the geometric mean of the data. If μ and μ^* are the means of normal and lognormal distributions, respectively, and σ and σ^* are their

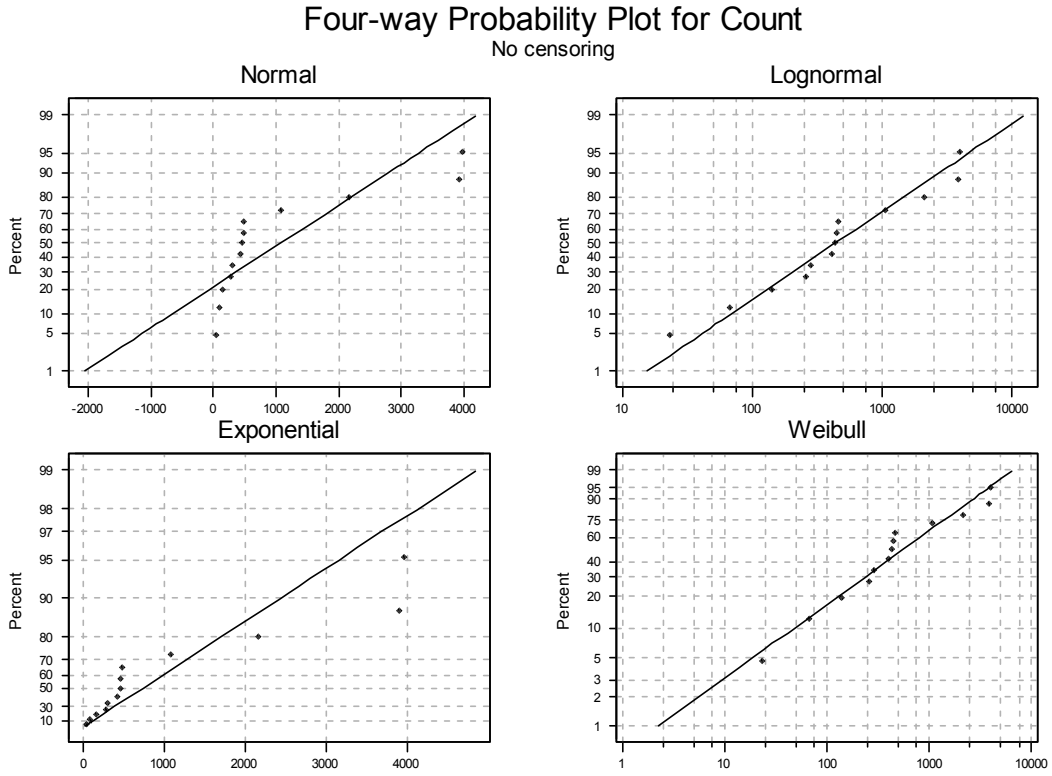

Figure 2.18. Probability plots for normal, lognormal, exponential and Weibull distributions.

respective standard deviations, then the interval $\mu - \sigma$ to $\mu + \sigma$ for the normal distribution is equivalent to the interval μ^*/σ^* to $\mu^**\sigma^*$ for the lognormal distribution in the sense that both intervals contain 68.3% of the probability weight. The lognormal distribution is skewed except in the limit $\sigma^* \rightarrow 1$ when it becomes equivalent to a normal distribution. Limpert et al. [1] review the lognormal distribution and provide examples of its application from many areas of science.

Possible origin of the lognormal distribution for triboemission

The abrasion of alumina by the diamond indenter breaks off material on the wear scar surface and grinds the wear debris during multiple passes. Some of the broken material is pushed out of the wear track by the indenter and contributes to the cumulative wear of the surface and some is recycled in the wear scar and contributes to the transfer, or third body, film discussed in section 2.5.1. The predominant source of triboemission is from cracks that are created during this breakage process as discussed in section 2.5.1. In the next section, we show that the cumulative wear correlates well with the cumulative triboemission, except under conditions when most of the wear debris is recycled rather than ejected from the wear scar. Given this correlation, the question arises why the distribution of the cumulative wear from sample-to-sample is normal, or close to normal, while the distribution of the cumulative triboemission is lognormal.

We hypothesize that the cumulative triboemission for a given load and number of passes is proportional to the number of debris particles that are created during the abrasion process. The cumulative wear volume from sample-to-sample for specified load and number of passes is a random variable with normal, or near normal, distribution. But for a given cumulative wear volume, the number of debris particles can vary and, in fact, we argue that this number is a random variable with lognormal distribution. The mean cumulative wear volume correlates with the mean cumulative triboemission, but the distributions of these two quantities are different. Our argument that the number of debris particles is a random variable with lognormal distribution goes as follows.

In 1940, Rasumovsky [43] discovered that the size distribution of ore deposits that have been crushed was lognormal. Kolmogoroff [44] then put forward a model of breakage, based on Rasumovsky's empirical findings, that explained the lognormal distribution. Aitchison and Brown [45] summarize the details of Rasumovsky's arguments, but the basic concept is that crushing ore is a multiplicative, rather than additive, process. If X_j is the size of a piece of ore after it has been broken j times, then its size after being broken again can be written

$$X_{j+1} = X_j - \varepsilon_j * X_j \tag{2.1}$$

where $0 \leq \varepsilon_j < 1$ is an independent random variable that can be normally distributed. The size of the ore after being broken j times relative to its initial size X_0 is the multiplicative consequence of all the breakage steps

$$X_j = X_0 \Pi(1 - \varepsilon_j) \tag{2.2}$$

and it follows that the distribution of X_j is lognormal. We make the connection that crushing ore is analogous to crushing the alumina surface by the diamond indenter and, therefore, the size of wear particle debris will be a random variable with lognormal distribution.

We now make a parallel argument that the number of wear debris particles is also a random variable with lognormal distribution. If $N_j = \text{Int}(n_j)$ is the number of debris particles after the wear volume has been broken j times, then a possible model for the distribution of N_j is the recursion relation

$$n_{j+1} = n_j + (1 + \delta_j)(n_j - n_{j-1}) \tag{2.3}$$

where $0 \leq \delta_j$ is an independent random variable that can be normally distributed. We've placed no upper limit on δ_j since particles existing after step j can, in principle, break into more than two particles. Thus, starting with $n_1 = 1$ representing all the material that ultimately is broken into wear debris and assuming $n_0 = 0$, then the number of particles after j process steps is the multiplicative consequence of all the breakage steps

$$N_j = \text{Int}\ \{\Pi(1 + \delta_j)\} \tag{2.4}$$

and it follows that the distribution of the total number of debris particles is lognormal. Given our assumption that the cumulative triboemission is proportional to the number of debris particles, it follows that the distribution of the cumulative triboemission is lognormal.

The preceding arguments provide a heuristic basis for understanding our observation that the cumulative triboemission is a random variable with lognormal distribution. The lognormal distribution of crushed ore sizes is well established, but as far as we know, no one has extended those arguments to infer that the number of ore fragments after crushing also is a random variable with lognormal distribution. The distributions of particle size and particle number are strongly correlated by the conditions

$$\text{initial ore volume before crushing} = \Sigma_i \, n_i \, v_I \tag{2.5}$$

$$\text{number of fragments after crushing} = \Sigma_i \, n_i \tag{2.6}$$

where n_i is the number of fragments of size v_i after crushing and v_i is the fragment volume. The distribution of n_i as a function of v_i is lognormal for a given initial ore volume. For an ensemble of the same initial ore volume, we have argued that the total number of ore fragments, the sum over n_i, is a random variable with lognormal distribution. We are unable at this time to prove that the conservation of wear volume (the first condition above) and the condition that the fragment size is a random variable with lognormal distribution, necessarily implies that the sum of fragments (the second condition above) is a random variable with lognormal distribution.

Population parameters

We have established that the cumulative electron count is a random variable with a lognormal distribution. If X_i is the variate of this distribution, then the variate for the logarithm of the cumulative electron count, $Y_i = \ln(X_i)$, is also a random variable but is normally distributed. The lognormal and normal distributions are characterized by the means μ^* and μ and the standard deviations σ^* and σ, respectively, where $\mu^* = \exp(\mu)$ and $\sigma^* = \exp(\sigma)$. The population parameters μ^* and σ^* depend on experimental

parameters such as sliding speed, load, surface roughness, number of passes, and so forth. Our goal is to understand these macroscopic dependencies and ultimately to relate them to the underlying microscopic interactions between two surfaces sliding across each other. We first consider the dependence of μ^* on load and pass number and then the dependence σ^* on the same two experimental parameters.

There are several ways to estimate the population parameters, μ^* and σ^*, from the experimental data. The most transparent approach is to take the logarithm of the cumulative triboemission and since the resulting distribution is normal, the unbiased estimators of μ and σ are

$$\text{estimate of } \mu = \Sigma \ln(\text{cumulative emission})/N \tag{2.7}$$

$$\text{estimate of } \sigma = \Sigma \{\ln(\text{cumulative emission}) - \text{estimate of } \mu\}^2/(N-1) \tag{2.8}$$

where N is the number of measurements taken with the same experimental parameters. If the context is clear, we will not explicitly distinguish between the population parameters and estimates of the parameters.

The natural logarithm of the cumulative emission versus the natural logarithm of the pass number is plotted in Figure 2.19 and Figure 2.20. The estimated population mean of the cumulative triboemission is, of course, expected to increase with increasing pass number and this is visually evident in the figures. Also evident in these two figures is that the dispersion in the cumulative triboemission from sample-to-sample is considerably larger at 30 N than at 10 N. It is important to note that the uncertainty in the estimated mean is given by this dispersion, but divided by the square root of the number of samples. We now analyze in more detail the estimated population parameters as a function of load and pass number.

The mean of the cumulative triboemission as a function of load and pass number

The natural logarithm of the cumulative count versus the natural logarithm of number of passes is shown in Figure 2.21 for 10 N and 30 N load. The error bars on the plot were calculated using a 68 % confidence interval based on the t-distribution. The number of data points in the average varied from 12 for 10 N and one pass (13 for 30 N and one pass) to two data points for both 10 N (at 148 passes) and 30 N (at 18 passes). The t-distribution was used to calculate the confidence intervals since the number of data points was relatively low. A linear regression fit to both the 10 N and 30 N data also is shown on the figure. The correlation coefficients for 10 N and 30 N are $R^2 = 0.986$ and $R^2 = 0.957$, respectively, confirming a strong linear correlation for both loads between the average logarithm of the cumulative emission and the logarithm of the pass number. The linear fits for 10 N and 30 N are

10 N: Average {ln (cumulative emission)} = 1.29*ln (pass number) + 3.025 (2.9)

30 N: Average {ln (cumulative emission)} = 0.719* ln (pass number) + 5.99 (2.10)

The linear log-log relationship between the cumulative triboemission and the pass number implies a power law relationship between the population means and pass number for both 10 N and 30 N. The exponents are 1.29 and 0.719 for 10 N and 30 N, respectively. The prefactors are 20.6 and 399 counts per pass for 10 N and 30 N, respectively.

The relation between the average natural logarithm of the cumulative electron count and the natural logarithm of the number of passes, shown in Figure 2.21, appears to have an oscillatory component superimposed on the linear dependence. This oscillatory component is more evident for 10 N load than for 30 N and though its amplitude is close

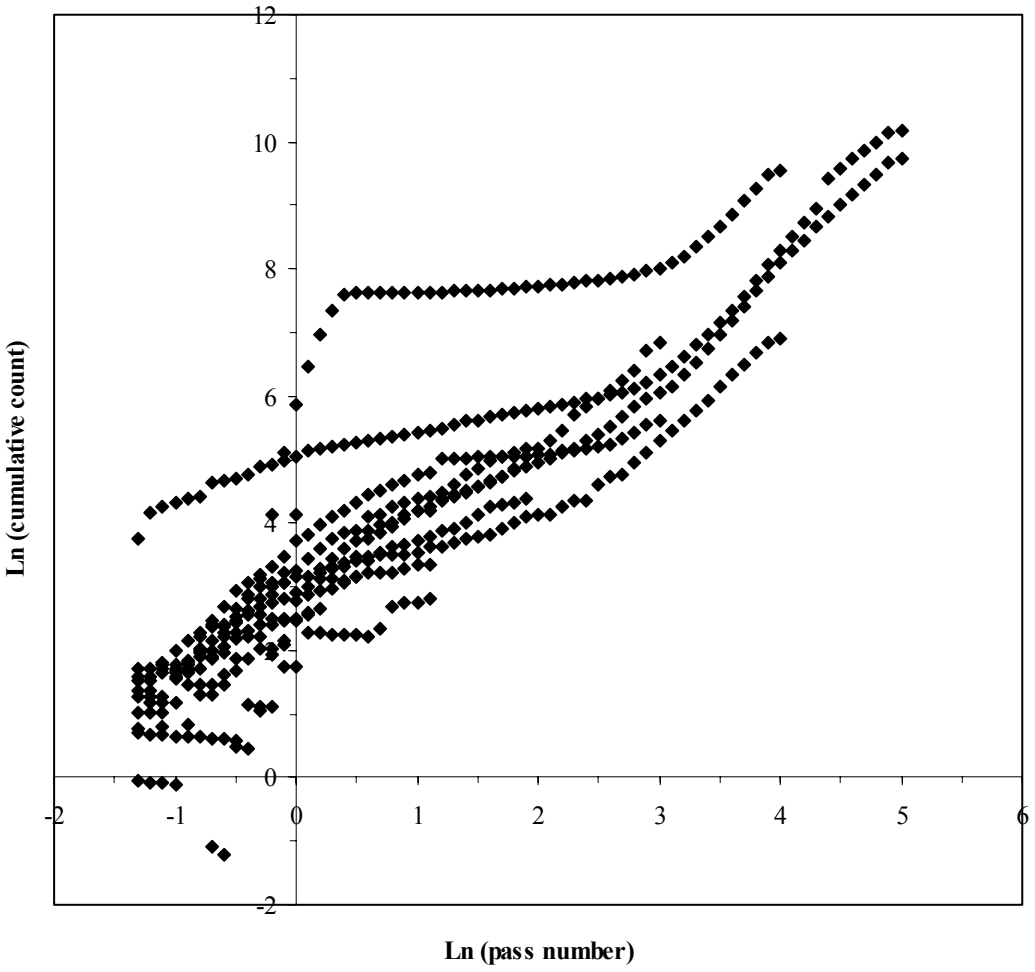

Figure 2.19. The natural logarithm of the pass number versus the natural logarithm of the cumulative emission for 10 N.

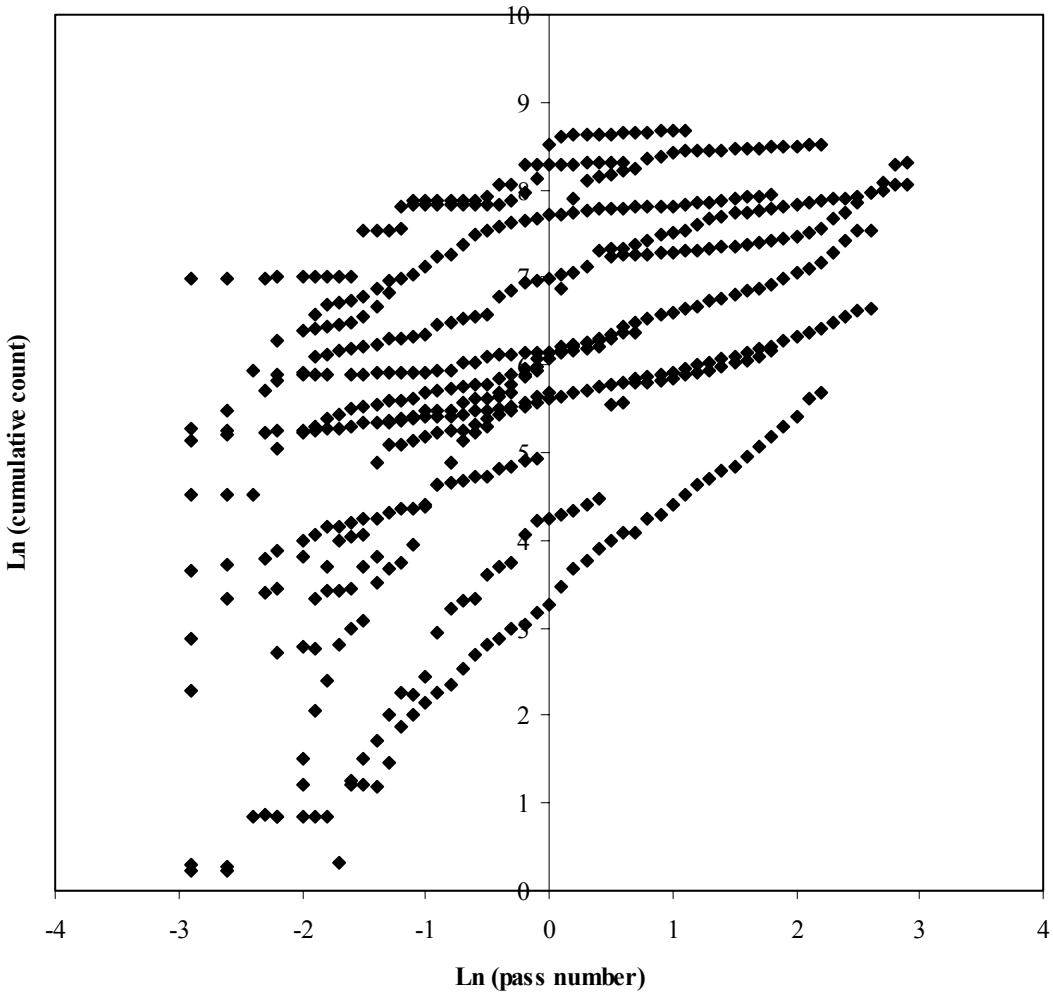

Figure 2.20. The natural logarithm of the pass number versus the natural logarithm of the cumulative emission for 30 N.

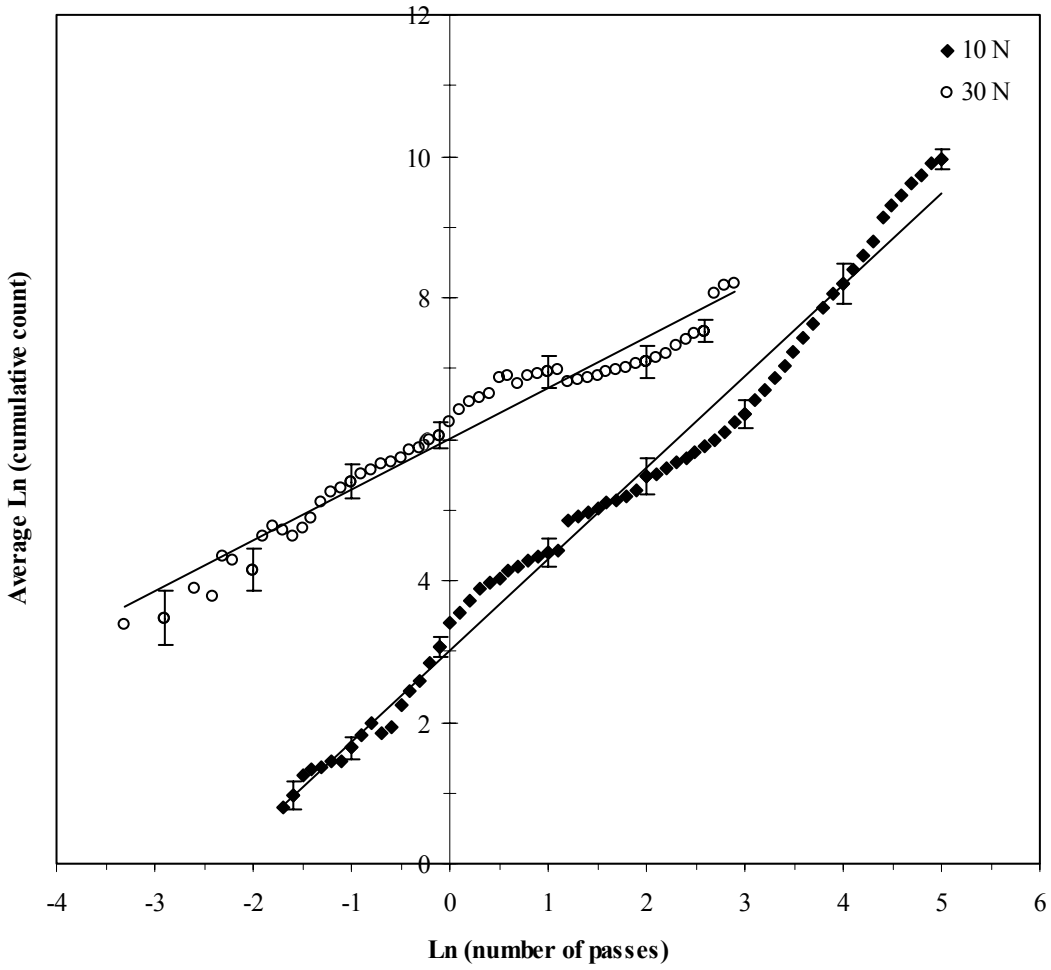

Figure 2.21. Average natural logarithm of the cumulative electron count versus the natural logarithm of the number of passes. For any given number of passes, the natural logarithm of the cumulative electron count is averaged over all samples.

to the uncertainty in the data, indicated by the error bars, we believe it is a real systematic effect. In Figure 2.22, we amplified the oscillatory component of the data for 10 N load by subtracting the linear regression fit from the data and plotting the difference versus the logarithm of pass number. Instead of being sinusoidal, the oscillatory component consists, instead, of four linear regions (labeled A, B, C, and D in Figure 2.22) punctuated by three abrupt changes in slope. Regions A and B are the first pass of the indenter over the surface while regions C and D are from multiple passes of the indenter. Again, the linear dependence of the log-log plot in the separate regions implies a power law dependence of cumulative emission on pass number with different exponents in the regions. We find that the four exponents are 0.317, 2.21, 0.907, and 1.91 for regions A, B, C, and D, respectively. We argue in the next section, based on SEM pictures of the wear scars, that the wear processes in region C and D are qualitatively different and that these differences in wear are reflected in the power law behavior of the cumulative triboemission. We have no SEM pictures taken from regions A and B and can only speculate that similar differences in the wear processes occur in these two regions.

The data points in Figure 2.22 are an average over measurements from different samples. The number of samples in the average changes at different pass numbers; there are 12 samples contributing to the average after one pass and two samples contributing to the average after 148 passes. One might be concerned that the observed abrupt changes in slope are associated with changes in the number of samples contributing to the average. The cumulative emission for one of the two samples that went 148 passes (10 N load) was relative smooth, it did not display the bursts of emission that are generally seen in the triboemission. We took this data and subtracted the linear trend to extract the oscillatory component of a single sample. This component is plotted in Figure 2.23. The oscillatory components for a single sample and for the mean from a variable number of samples are nearly identical in regions C and D (differences do exist in regions A and B) demonstrating that at least in regions C and D the changes in slope as a function of pass number are not due to changes in the number of samples contributing to the average.

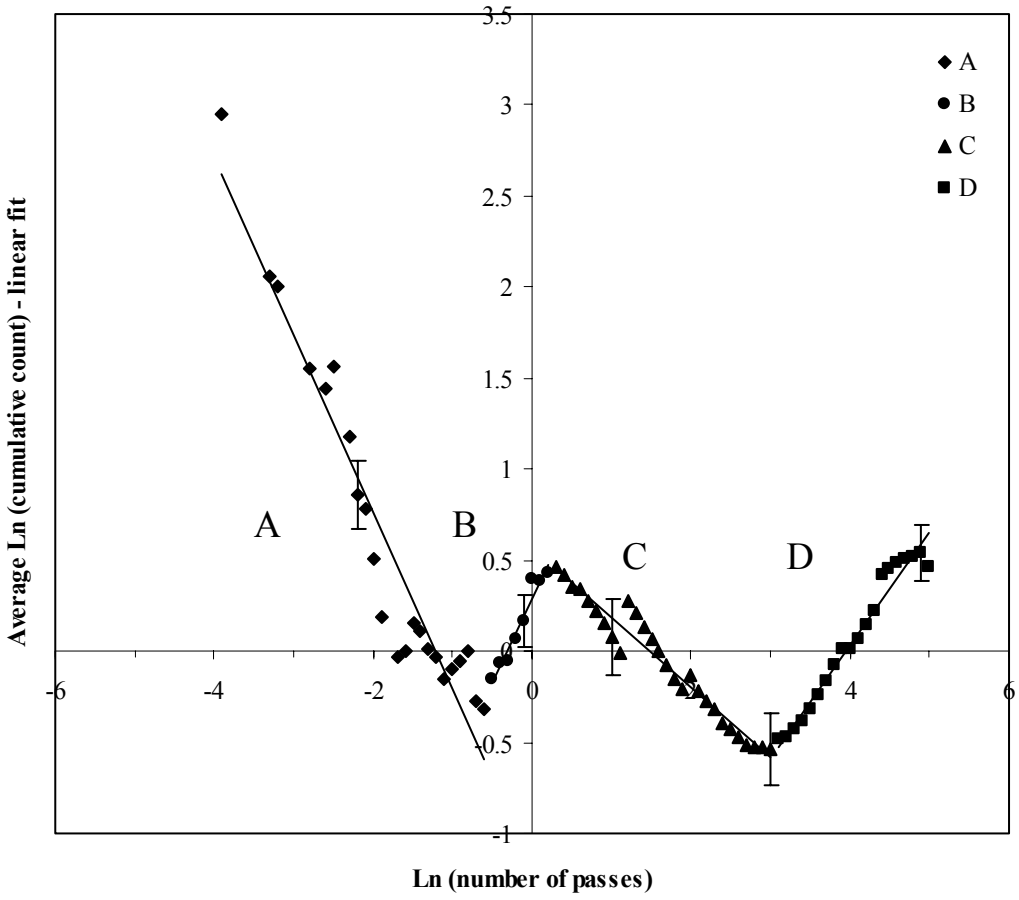

Figure 2.22. The oscillatory component of the data for 10 N load was amplified by subtraction of the linear regression fit from the data. The difference is plotted versus the logarithm of pass number.

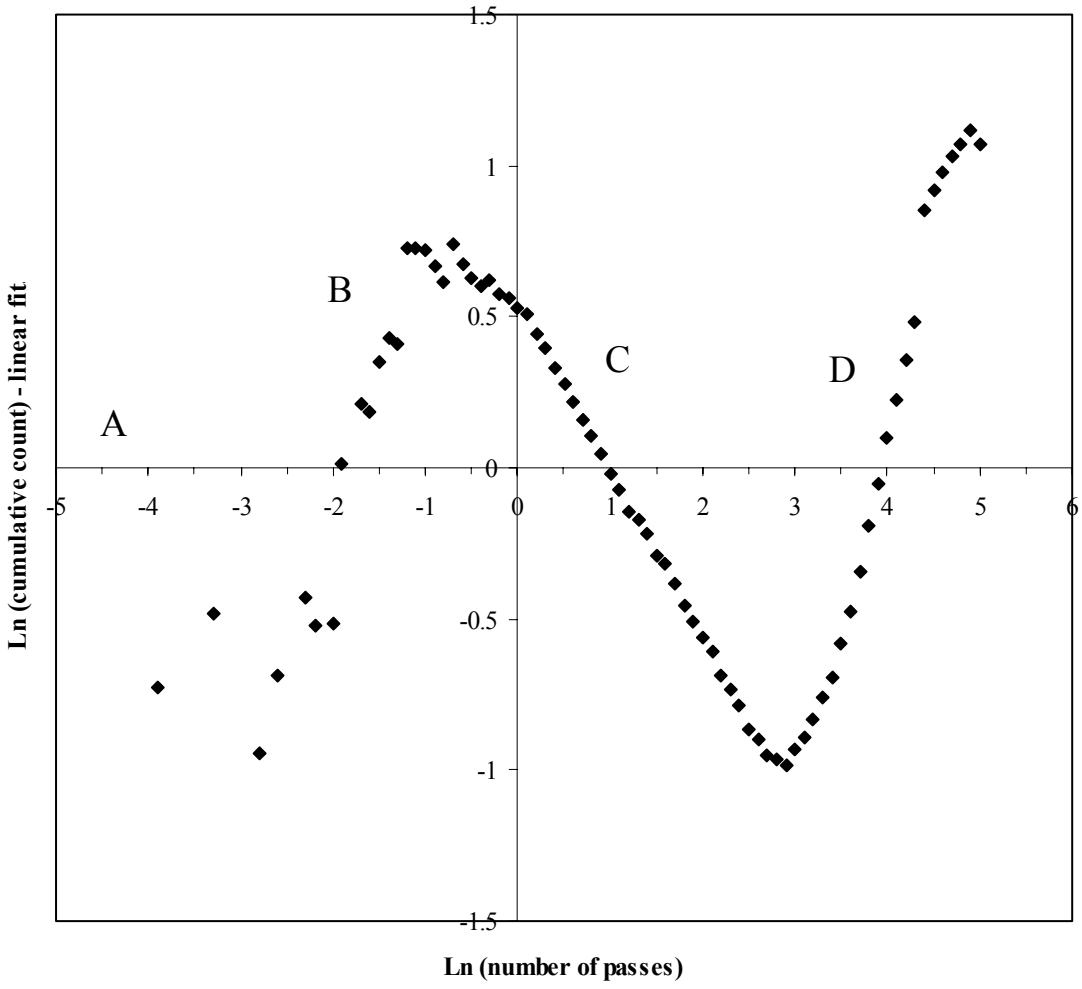

Figure 2.23. The oscillatory component of the data for a single sample at the 10 N load was amplified by subtraction of the linear regression fit from the data. The difference is plotted versus the logarithm of pass number. The four regions, A, B, C and D are still present in the case of a single sample, as well as for the average data from all the samples.

The standard deviation of cumulative emission as a function of load and pass number

The second parameter describing the lognormal distribution of the cumulative triboemission is the standard deviation of the population. Again, it is convenient to focus on the, $\text{Ln}(\sigma^*) = \sigma$, that can be estimated from the normally distributed natural logarithm of the cumulative triboemission. A plot of the natural logarithm of the lognormal standard deviation $\text{Ln}(\sigma^*) = \sigma$ versus the logarithm of the number of passes is shown in Figure 2.24. Confidence intervals (plus/minus one standard deviation) for representative data points on the figure have been calculated assuming a Chi-square distribution of the estimated variance. There exists significant uncertainty in the standard deviation, particularly at high pass number where only two data points were available for the estimate, but a trend is evident for 30 N load (correlation coefficient = – 0.95) that the standard deviation of the logarithm of cumulative emission decreases steadily with the logarithm of the number of passes. Again, it is important to emphasize that this is the sample-to-sample variability at constant pass number and constant load. For the low load (10 N), the correlation between the standard deviation of the logarithm of cumulative emission and the logarithm of the number of passes is much weaker (correlation coefficient = -0.59). This lack of correlation is clearly evident in the plot.

Since the logarithm of the cumulative triboemission is increasing with the logarithm of the number of passes, the coefficient of variation, $\sigma/|\mu|$, is decreasing for both 10 N and 30 N load as shown in Figure 2.25. As will be discussed in the next section, the coefficient of variation for the wear volume also decreases with increasing pass number reinforcing the correlation between wear volume and cumulative emission.

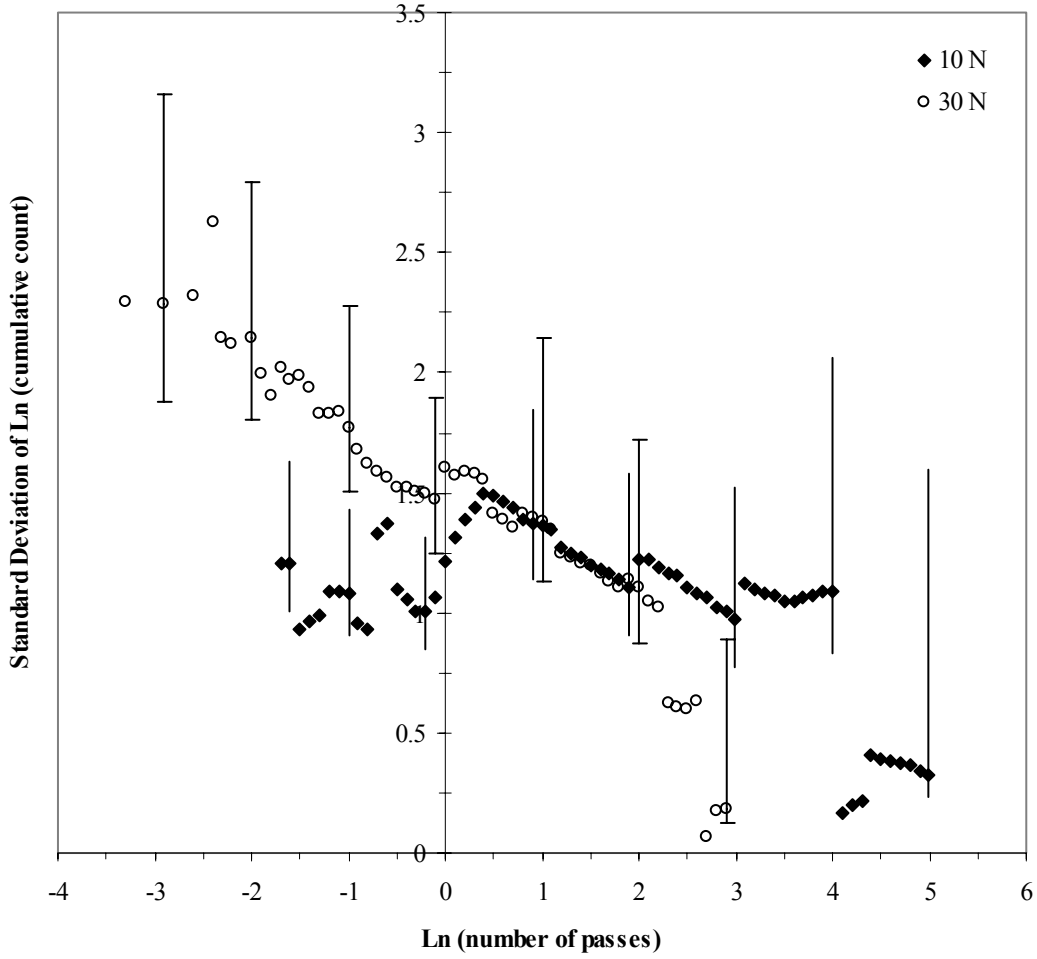

Figure 2.24. Standard deviation of the logarithm of the cumulative electron count versus the logarithm of the number of passes.

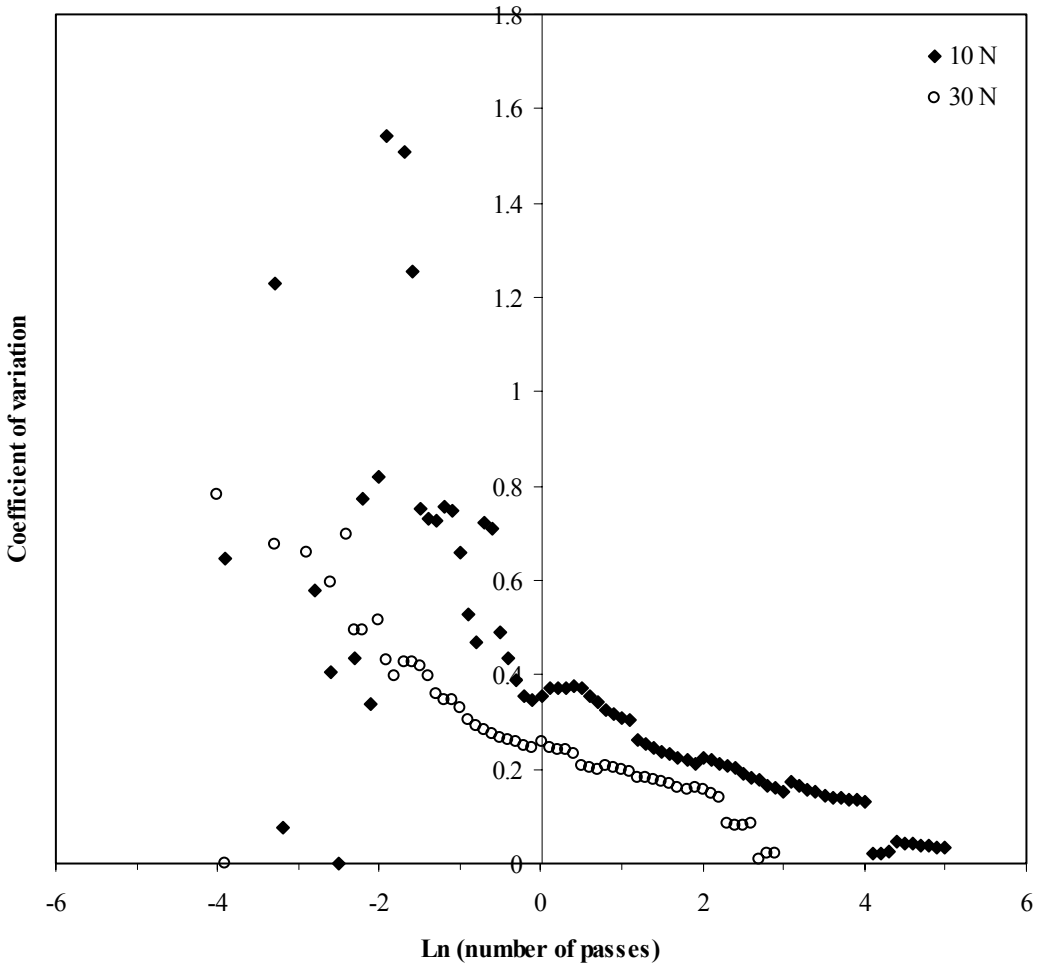

Figure 2.25. Coefficient of variation of the logarithm of emission versus the logarithm of pass number.

2.5.3 Correlation between triboemission and wear

As far as we know, this is the first study to address the question: does the cumulative triboemission correlate with the wear volume using pass number and load as implicit variables. We argued in section 2.5.2 that the cumulative triboemission is a random variable with lognormal distribution. This observation expands our initial question to a coupled pair of questions: does the cumulative triboemission correlate with the wear volume in each sample individually and, if not, does the population mean of the cumulative triboemission correlate with the population mean of the wear volume as an implicit function of load and pass number? We first address the question of whether a correlation exists for individual samples.

Remember that the wear volume only can be measured at the end of a triboemission measurement. So for each sample, characterized by the load and total number of passes, we have the total cumulative emission and the total cumulative wear volume. The cumulative emission is plotted versus wear volume in Figure 2.26 for each sample with solid and open symbols for 10 N and 30 N load, respectively. Visually, we see poor correlation between the two quantities and our assessment is confirmed by a low correlation coefficient $R^2 = 0.033$. Three of the data points (54 and 148 passes with 10 N load) with cumulative triboemission greater than 5000 and wear volume of approximately 3 mm^3/m are significantly off the general trend displayed by the other data points. If we exclude those points (we explain why they are atypical below) then the correlation coefficient is still very low ($R^2 = 0.28$).

Since the cumulative triboemission and wear volume do not correlate well for individual samples, we consider next the degree of correlation between the population means for cumulative emission and wear. The cumulative triboemission is a random variable with lognormal distribution. As a consequence, the logarithm of the mean cumulative triboemission is normally distributed. The wear volume also is random variable with

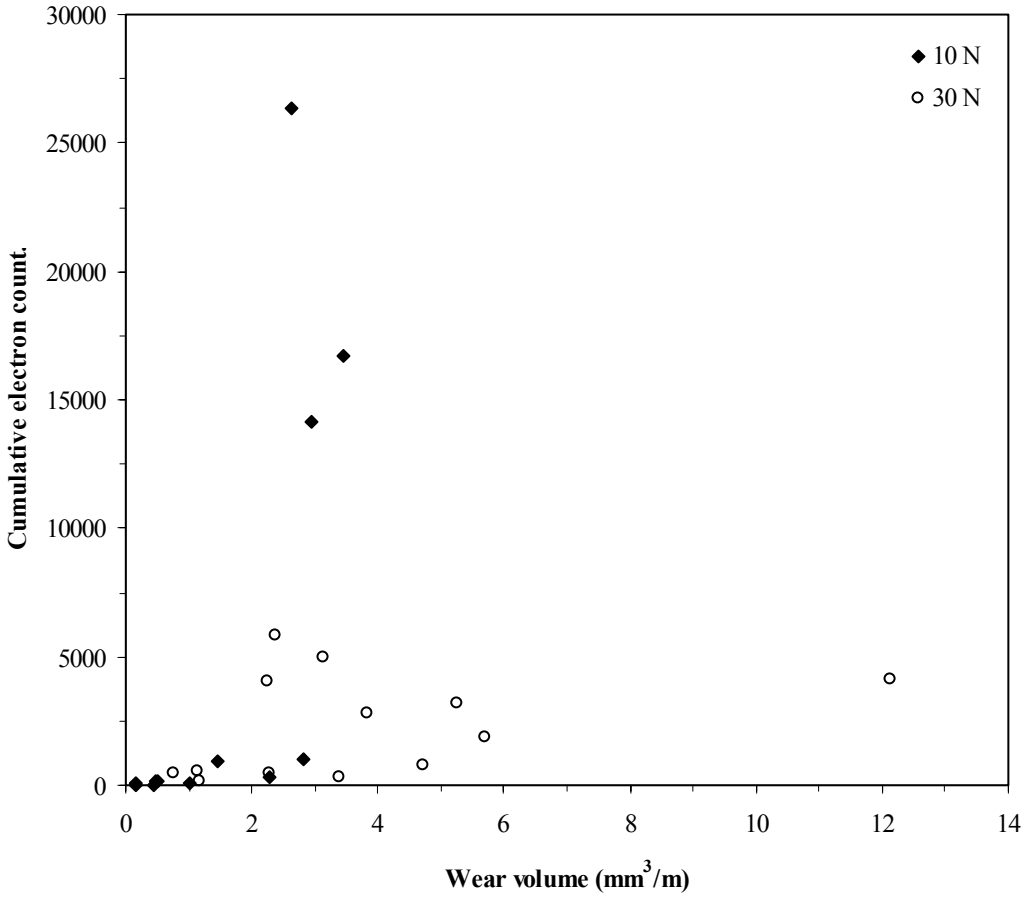

Figure 2.26. Cumulative electron count versus the wear volume for the 10 N and 30 N loads.

normal distribution. If the ratio of the wear volume standard deviation to the wear volume mean is small, then the logarithm of wear volume mean will be normally distributed. We plot in Figure 2.27 the mean logarithm of the cumulative triboemission versus the logarithm of the wear volume using a log-log plot so that each quantity is normally distributed and to identify whether a power law dependence exists between the mean cumulative triboemission and the mean wear volume. The correlation coefficient between these two quantities is $R^2 = 0.72$ if all data points are included and $R^2 = 0.91$ if the data points for 48 and 154 passes with 10 N load are excluded. The correlation is quite strong, if those data points are excluded, and is independent of load. We now argue that the data points that do not correlate well with the rest of the data are associated with a wear regime in which debris in the wear scar is being cracked and broken, creating significant triboemission, but the debris is not being pushed out of the wear scar by the indenter. As a consequence of recycling, but not ejecting the debris, the cumulative triboemission rate is high but the wear volume rate is very low and the data in this wear regime does not correlate well with the remainder of the data.

We infer the special nature of the wear regime represented by the data points for 54 and 148 passes with 10 N load from an analysis of the SEM pictures (Figures 2.10o to 2.10v) and the cumulative triboemission for these particular samples. In section 2.5.2, Figure 2.21, we plotted the logarithm of the mean cumulative triboemission versus logarithm of the pass number for 10 N and 30 N loads. The data for both loads is represented well by a low amplitude oscillation superimposed on a linear trend. The linear fit is subtracted from the total and the amplified oscillation for 10 N load is plotted in section 5.2, Figure 2.22. Four emission regimes are observed characterized by different linear slopes labeled A, B, C, and D. The data is replotted in this section, Figure 2.28, for regions B, C, and D. Region A is not included because it occurs during the first pass where there is no measurement of the wear volume, only measurements of the cumulative triboemission data. In this figure, the areal fraction of plastic flow debris from the SEM pictures, discussed in section 2.4.1, is superimposed (abscissa on the right hand axis of the figure)

on the triboemission data. In region B, where the mean cumulative triboemission rate is higher (positive slope) than the overall trend, the wear scar is a mixture of plastic flow debris and fractured surface. In region C, where the mean cumulative triboemission rate is lower (negative slope) than the overall trend, the plastic flow debris is almost entirely absent from the wear scar. In region D, again the mean cumulative triboemission rate is higher (positive slope) than the overall trend and like in region B the wear scar is a mixture of plastic flow debris and fractured surface. We infer from the pattern displayed in Figure 2.28 that in regions B and D, where a significant fraction of plastic flow debris is observed in the SEM pictures, that the cumulative triboemission rate is relatively high because the plastic film is cracking, delaminating, and re-forming due to the tribological stress created by the indenter. The cumulative triboemission rate is relatively low in region C where the plastic flow debris is largely absent.

Returning to our initial question regarding the correlation of the mean cumulative triboemission and the mean wear volume, a high correlation exists for regions A, B, and C for the 10 N load and for the entire data set when the load is 30 N. But the correlation breaks down in region D for 10 N load where the wear scar is a mixture of plastic flow debris and fractured surface. We infer that in both regions B and D the wear debris is alternately forming plastic film and breaking up. But in contrast to region B, the debris is not being ejected from the wear scar in region D during the recycling process. The difference in the wear process between regions B and D is possibly due to the larger width of the wear scar in region D, compared to its width in region B. As a consequence, the ground wear debris is continually re-formed into plastic transfer film on the wear scar surface before it can reach the edge of the scar and be ejected.

Thus, the answer to the question, does a correlation exist between the mean cumulative

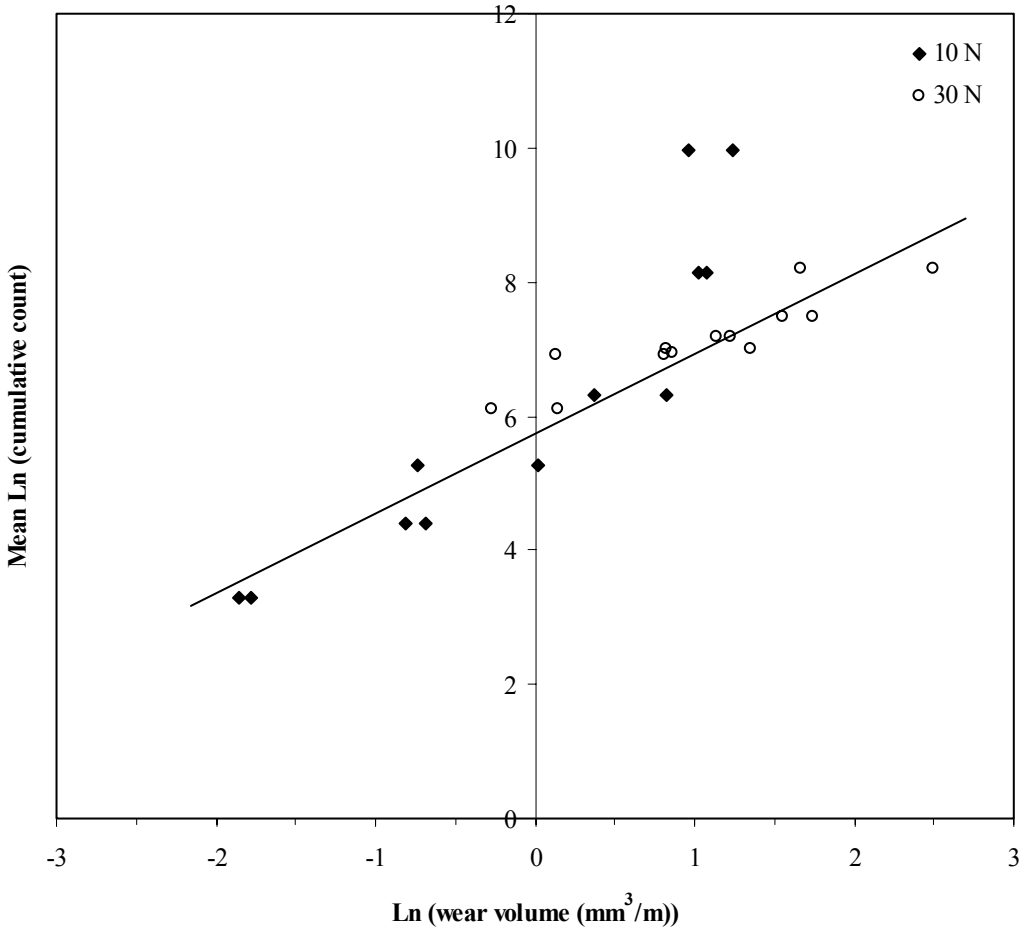

Figure 2.27. Mean natural logarithm of the cumulative electron count versus the natural logarithm of the wear volume for 10 N and 30 N.

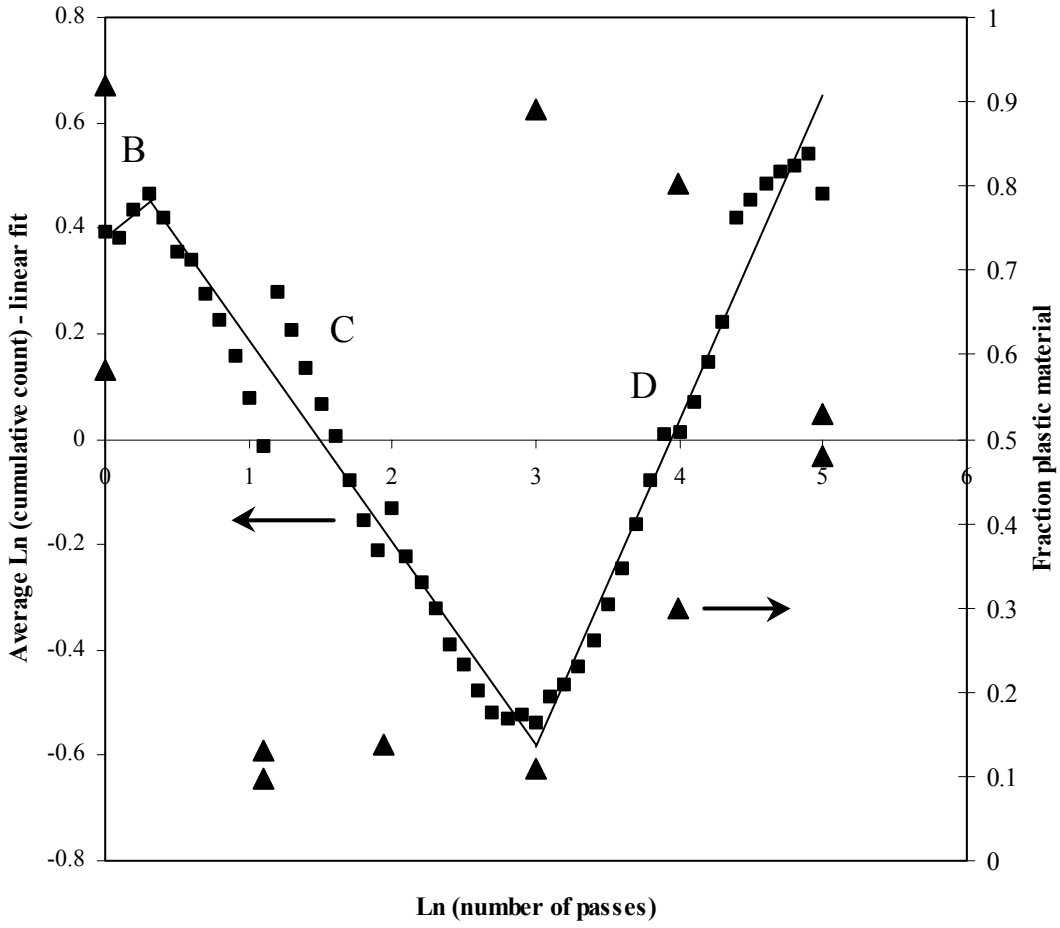

Figure 2.28. Variation with respect to a linear trend of the logarithm of the mean cumulative triboemission versus the logarithm of the number of passes (squares - left abscissa). Fraction of plastic flow debris in the wear scar versus logarithm of the number of passes (triangles – right abscissa).

triboemission and the mean wear volume, is a qualified yes. Only after many passes at low load does the correlation break down because the triboemission rate remains high but the wear rate is low. Excluding this nonconforming wear regime, a linear regression fit of the logarithm of the mean cumulative triboemission versus the logarithm of the mean wear volume gives

$$\text{Ln (mean cumulative triboemission)} = 1.19*\text{Ln(mean wear volume)} + 5.74 \quad (2.11)$$

The linear log-log relation implies a power law dependence

$$\text{Mean cumulative triboemission} = 311(\text{mean wear volume})^{1.19} \quad (2.12)$$

We do not have a model at this time for the observed power law relationship, but suspect it may reflect the conservation principle discussed in section 5.2. That is

$$\text{Volume of wear debris} = \Sigma n_i v_I \quad (2.13)$$

$$\text{Cumulative triboemission} \propto \Sigma n_I \quad (2.14)$$

where n_i is the number of debris particles with volume v_i.

The existence of a significant correlation between the cumulative triboemission and the wear of alumina provides an important real time probe of the wear process in this material. In particular, the wear transitions observed in this material can now be studied on a much finer time scale, through observation of the triboemission spectra, than is possible from direct measurements of the wear volume. An important goal of future research is to make connection between the largely phenomenological models of wear that now exist and the more fundamental theoretical studies that presently are exploring the statistical mechanics of non-equilibrium driven systems.

2.6 Summary and Conclusions

This study addressed the question whether the cumulative triboemission from the abrasion of alumina correlates with the volume of material removed and, in particular, whether transitions in the rate of material removal are mirrored in the cumulative triboemission rate. This correlation between the wear of alumina and triboemission has not been attempted before, despite the fact that it may provide an important real-time probe of the wear process and give insight into its evolution.

We studied this correlation by abrading the alumina samples with diamond in a conical indenter-on-disk contact geometry and measuring the electron triboemission from the surfaces in contact using a channel electron multiplier (CEM). The tests were carried out inside a vacuum chamber at pressures lower than 10^{-4} Pa and at room temperature. The alumina samples were scratched by the diamond indenter under two different loads (10 N and 30 N) and for different numbers of passes. After the tests, the surface profiles of the scratched specimens were measured by stylus profilometry and the volume of material removed from the samples was calculated from the surface profiles of the wear tracks. The samples were finally examined by scanning electron microscopy (SEM).

For both loads, the wear volume increased at first linearly as a function of pass number, but the rate of material removal decreased dramatically, to an immeasurably small value, after approximately 20 passes for the 10 N load. This dramatic decrease in wear coincides with the wear scar changing from a surface that is predominately fractured grains, to a surface covered with a mixture of fractured grains and plastic flow film, as revealed by examination of the SEM micrographs of the samples. For one pass, the wear track consists almost entirely of plastic flow material in one sample or areas of plastic flow interspersed with smaller areas of intergranular and intragranular fracture in the second sample. Then, after 3 and 7 passes, the plastic flow material has delaminated from all four

samples and the wear scar is made up almost entirely of fractured surface. The two samples that went through 20 passes are qualitatively different. One of these two samples has almost no plastic flow material in the wear scar, similar in appearance to the 3 and 7 pass samples, while the wear scar surface of the other one is almost covered by plastic flow debris. We suggest that these two samples straddle a wear transition. The transition has not occurred in the first sample, but has occurred in the second one where the surface is covered with plastic flow material. Then in the succeeding samples, 54 passes and 148 passes, the wear scars are mixtures of fractured and plastic flow surfaces. We hypothesize that after the putative wear transition at approximately 20 passes, a steady state process occurs in which the delamination of the plastic material is balanced by re-formation of plastic film from the wear debris. The SEM pictures represent snapshots of this continual balancing process. The wear tracks as a function of pass number for 30 N load display similar transitions from a mixture of fractured surface and plastic flow material on the initial pass to delamination of the plastic flakes on pass 2 and 3 leaving predominantly fractured material, back to a mixture of fractured surface interspersed with plastic flow debris for 6, 9, 13, and 18 passes. The transition, however, is not as clear at 30 N load as it is at 10 N load. Rather, the creation of plastic flow material from the wear debris appears to occur concurrently with delamination of plastic flakes created in a previous pass.

These results were surprising in light of an experiment similar to our own performed by Xu and Jahanmir [4]. Based on their results, we expected to see damage accumulation during the initial passes of the diamond indenter and then possibly a transition to the mild wear regime at 10 N load. We did not expect to see at this load a transition to severe wear with concomitant lateral crack chipping. At 30 N load, we expected to see the transition from damage accumulation to mild wear and then possibly a transition with increasing pass number to severe wear. What we saw for both 10 N and 30 N load was evidence in the SEM pictures for lateral crack chipping on the first pass; that is, our samples appeared to start immediately in the severe wear regime. In addition, a transition we observed at 10

N load at approximately 20 passes had no analogue in the wear behavior observed by Xu and Jahanmir. The difference is less striking between the behavior we observe for the wear at 30 N load and the model suggested by Xu and Jahanmir for abrasive wear.

Our experimental design was based on the test conditions used by Xu and Jahanmir and yet our results are closer to the observations of Ajayi and Ludema [18] who performed a similar experiment. They noted a progression of material removal beginning with plastic deformation and followed by crack initiation. After which flake-shaped particles delaminate from the surface as wear debris and subsequent wear is controlled primarily by the extent to which debris is ejected from the wear scar versus being recycled to form fresh plastic film. We ascribe these significant differences between Xu & Jahanmir's results and ours to differences in the experimental parameters, the most important in order of priority being the type of repeat contact between indenter and sample (repeat pass sliding in ours versus reciprocating sliding in theirs), the surface roughness and the ambient atmosphere (vacuum in ours, laboratory air in theirs).

The triboemission measured in our experiment is characterized by the same burst-type behavior at random times that was observed by others [24], [31], [32]. A second important characteristic of the triboemission is the presence of a component with approximately constant rate over several passes that results in a nearly linear cumulative emission. This emission rate varies, sometimes in conjunction with a burst and sometimes not, with concomitant changes in the slope of the cumulative emission. For 10 N and 30 N, there was poor correlation between the cumulative count and the number of passes. But we provided evidence that the cumulative emission is a random variable with a lognormal distribution and that a correlation does exist between the population mean of the logarithm of the emission and the logarithm of the number of passes. In addition to this correlation, we found a striking correlation at 10 N load between the slope of the mean cumulative emission with pass number and the relative fraction of plastic flow debris in the wear scar.

In order to explain the possible origin of the lognormal distribution of the triboemission, we hypothesized that the cumulative triboemission for a given load and number of passes is proportional to the number of debris particles that are created during the abrasion process. The cumulative wear volume from sample-to-sample for specified load and number of passes is a random variable with normal, or near normal, distribution. But for a given cumulative wear volume, the number of debris particles can vary and, in fact, we argue that this number is a random variable with lognormal distribution. The mean cumulative wear volume correlates with the mean cumulative triboemission, but the distributions of these two quantities are different. Our argument that the number of debris particles is a random variable with lognormal distribution parallels the discovery by Rasumovsky [43] that the size distribution of ore deposits that have been crushed is lognormal.

The cumulative emission and the cumulative wear volume for each individual sample are poorly correlated. But a significant correlation (R^2 = 0.91) does exist the mean cumulative triboemission and the mean cumulative wear volume for most of the wear regimes observed in our experiments. Our interpretation of the wear and emission processes in these regimes, based on SEM micrographs, is that the wear and triboemission rates are low when the wear scar surface is free of plastic film and high when a significant fraction of plastic film exists on the wear scar and goes through cycles of cracking, delaminating and re-forming. In this wear regime, we find that the mean cumulative emission is proportional to the mean wear volume to the 1.2 power. In one wear regime, after 20 passes with 10 N load, the correlation between cumulative emission and wear volume breaks down. We suggest that plastic film is still being created and broken by tribological stress in this wear regime, but that the wear debris is not being ejected from the wear scar. Consequently, the wear rate is low while the emission rate is high.

The existence of a significant correlation in most wear regimes between the cumulative triboemission and the wear of alumina provides an important real time probe of the wear process in this material. In particular, the wear transitions observed in this material can now be studied on a much finer time scale, through observation of the triboemission spectra, than is possible from direct measurements of the wear volume. An important goal of future research is to make connection between the largely phenomenological models of wear that now exist and the more fundamental theoretical studies that presently are exploring the statistical mechanics of non-equilibrium driven systems.

References

[1] E. Limpert, W.A. Stahel and M. Abbt, *Log-normal Distributions across the Sciences: Keys and Clues*, Bioscience **51** No. 5, 341-352 (2001).

[2] O.O. Ajayi and K.C. Ludema, *Surface damage of structural ceramics: Implications for wear modeling*, Wear **124**, 237-257 (1988).

[3] S. Jahanmir and X. Dong, *Mechanism of mild to severe wear transition in alpha-alumina*, Journal of Tribology, Vol. **114**, 403-411 (1992).

[4] H.H.K. Xu and Said Jahanmir, *Transitions in the mechanism of material removal in abrasive wear of alumina*, Wear **192**, 228-232 (1996).

[5] A.G. Evans, M.E. Gulden and M. Rosenblatt, Proc. R.. Soc. London, Ser. A, **361**, 343 (1968).

[6] A.G. Evans and R. Wilshaw, J. Mater. Sci. **12**, 97 (1976).

[7] M.V. Swaim, in R.C. Bradt (ed.), *Fracture Mechanics of Ceramics*, Vol. 3, 1978, p. 257.

[8] R.L. Agham and R. McPherson, J. Am. Ceram. Soc. **56**, 46-47 (1973).

[9] T. Sugita and A. Hashikawa, Wear **72** 295-303, (1981).

[10] P.H. Mehortra, in K.C. Ludema (ed.), Proc. Int. Conf. on Wear of Materials, Reston, VA, April 11-14, 1983, American Society of Mechanical Engineers, New York, 1983, pp. 194-201.

[11] J.E. Hines, R.C. Bradt and J.V. Biggers, in K.C. Ludema, W.A. Glaesser and S.K. Rhee (eds.), Proc. Int. Conf. on Wear of Materials, Dearborn, MI, April 16-18, 1979, American Society of Mechanical Engineers, New York, 1979, pp. 540-550.

[12] T.F.J. Quinn and W.O. Winer, *Development of a theory of wear of ceramics*, Q. Prog. Rep., Tribology Project,, DOE-ECUT, p. 37. (1985).

[13] I.M. Hutchings, *Tribology: Friction and Wear of Engineering Materials*, CRC Press, pp. 116 (1992).

[14] T.E. Fischer and W.M. Mullins, *Chemical aspects of ceramic tribology*, J. Phys. Chem **96**, 5690-5701 (1992).

[15] T.E. Fischer and H. Tomizawa, *Interaction of tribochemistry and microfracture in the friction and wear of silicon nitride*, Wear **105**, 29-45 (1985).

[16] A. Blomberg, M. Olsson and S. Hogmark*, Wear mechanisms and tribo mapping of Al2O3 and SiC in dry sliding*, Wear **171**, 77-89 (1994).

[17] S.J. Cho, H. Moon, B.J. Hockey and S.M. Hsu*, The transition from mild to severe wear in alumina during sliding*, Acta Metall. Matter. Vol. **40**, No. 1, pp. 185-192 (1992).

[18] O.O. Ajayi and K.C. Ludema, *Mechanism of transfer film formation during repeat pass sliding of ceramic materials*, Wear **140**, 191-206 (1990).

[19] Y.S.Wang, C. He, B. J. Hockey, P. I. Lacey and S. M. Hsu, *Wear transitions in monolithic alumina and zirconia-alumina composites*, Wear **181**, 156-164, Part 1 (1995).

[20] O.O. Ajayi, S.C. Kang and K.C. Ludema, in F.A. Smidt and P.J. Blau (eds.), *Engineered Materials for Advanced Friction and Wear Applications*, American Society for Metals, Metals Park, OH, 1988, pp. 13-22.

[21] J. Kramer, Der metallische Zustand, Vanderhoek and Ruprecht, Goettingen, Germany (1950).

[22] N. Ohmae, K. Nakayama and S. Mori, *Exoelectrons and Tribology*, Japanese J. of Tribology **40**, No. 5, pp. 355-362 (1995).

[23] J.T. Dickinson et al*., Emission of electrons and positive ions upon fracture of oxide films*, J. Vac. Sci. Technol., **12** (2) (1981).

[24] J.T. Dickinson, L. Scudiero, K. Yasuda, M.W. Kim and S.C. Langford*, Dynamic tribological probes: particle emission and transient electrical measurements*, Tribology Letters **3**, 53-67 (1997).

[25] M.W. Kim, S.C. Langford and J.T. Dickinson, *Electron and photon emission accompanying the abrasion of MgO with diamond*, Tribol. Lett. **1**, 147 (1995).

[26] J.A. Ramsey*, Exoelectron emission from abraded metal surfaces at high and ultrahigh vacuums*, J. Appl. Phys. **37**, pp. 452-453 (1966).

[27] K. Nakayama, H. Hashimoto and T. Susuki, *Triboemission of charged particles and photons from solid surfaces during frictional damage*, J. of Physics D **25**, pp. 303-308 (1992).

[28] J.T. Dickinson, D.L. Doering and S.C. Langford*, Electron emission and free charge carrier production due to fracture of single crystal silicon*, in *Atomic and molecular processing of electronic and ceramic materials: preparation, characterization and properties*, MRS, Pittsburg, Pennsylvania, I.A. Aksay et al. eds., 39-45 (1987).

[29] C.J. Kaalund and D. Haneman*, Positive ion and electron emission from cleaved Si and Ge*, Physical Review Letters **80**, 16, 3642-3645 (1998).

[30] G.J. Molina, D.A. Mazilu, A.L. Ritter, M.J. Furey, C. Kajdas*, A study of triboemission from the sliding contact of Si and Ge*, submitted to The Society of Tribologists and Lubrication Engineers (STLE), 2003 Annual Meeting.

[31] G.J. Molina, *Triboemission from ceramics: Charge intensity and energy distribution characterizations*, Ph.D. Thesis, Virginia Tech (2000).

[32] G.J. Molina, M.J. Furey, A.L. Ritter and C. Kajdas*, Triboemission from alumina, single crystal sapphire, and aluminum*, Wear **249**, 214-219 (2001).

[33] B. Sujak and A. Gieroszynski, Acta Phys. Polon. **28**, 311 (1965).

[34] B. Sujak and A. Gieroszynski, Acta Phys. Polon. **A37**, 733 (1970).

[35] D.R. Arnott and J.A. Ramsey, Surface Sci. **28**, 1 (1971).

[36] J.T. Dickinson, P.F. Braunlich and L.A. Larson*, Characteristic emission of negatively charged particles during tensile deformation of oxide-covered aluminum alloys*, Applications of Surface Science **1** 515-537 (1978).

[37] J.T. Dickinson, D.B. Snyder and E.E. Donaldson, *Acoustic emission and electron emission during deformation of anodized aluminum*, J. Vac. Sci. Technol. **17** (1) (1980).

[38] L.L. Lapin, *Probability and Statistics for Modern Engineering*, Second Edition, PWS-Kent Publishing Co., Boston, MA, 1990, pp. 168-175.

[39] Y. Sun, Y. Berthier, B. Fantino and M. Godet, A quantitative investigation of displacement accomodation in 3rd-body contact, Wear **165** (2), 123-131 (1993).

[40] S. Descartes and Y. Berthier, *Rheology and flows of solid third bodies: background and application to an MoS1.6 coating*, Wear **252** (7-8), 546-556 (2002).

[41] R.S. Gates, S.M. Hsu, and E.E. Klaus, Tribol. Trans. **32**, 357 (1989).

[42] Minitab online help, Release 12.1 (1998).

[43] N.K. Rasumovsky, C.R. Acad. Sci. U.R.S.S. **28,** 814 (1940).

[44] A.N. Kolmogoroff, C.R. Acad. Sci. U.R.S.S. **31,** 99 (1941).

[45] J. Aitchison and J.A.C. Brown*, The Lognormal Distribution with special reference to its use in economics*, (Cambridge Press, Cambridge, 1957), p. 26.

Chapter 3. Friction and Wear of Alumina in the Presence of the Chemical Vapor Aluminum Tri-Sec-Butoxide

3.1 Introduction

Ceramic materials are desirable for applications involving high loads and high temperatures or systems in corrosive atmospheres because they have large compressive strength, low density, and resist corrosion and chemical attack. However, the very properties that could make ceramics the material of choice in numerous practical applications make them difficult to machine and finish into high precision components. The original motivation of this research was to explore the feasibility of coating ceramic-on-ceramic and ceramic-on-metals by tribochemistry. The primary goal was to develop a new approach for finishing high precision ceramic components. Normally, these components are made oversize and then ground and polished to the final tolerance. High precision metal components are finished in the same way, by machining the rough stock down to the final specifications. But ceramics, because they are hard and brittle, do not machine very well and this step in the manufacturing process adds significantly more cost to the product than the analogous step in making precision metal components. Furthermore, the process of grinding the ceramic introduces subsurface cracks and defects, which weaken the component and reduce its reliability. The first part of this experiment tried to explore another approach to making precision ceramic components, that is, make the rough component undersize and grow ceramic on ceramic (or ceramic on metal) to the final tolerance. This method of modifying a ceramic surface generates much less stress, and the thickness of the ceramic deposit can be precisely controlled.

Figure 3.1 shows a schematic view of these two approaches to making precision ceramic components.

The experiment described here involved studying the wear of alumina on alumina in the presence of the chemical vapor aluminum tri-sec-butoxide (ATSB). The motivation was to determine whether fresh ceramic can be grown on the contacting surfaces from an appropriate chemical vapor, using tribological stress as a source of energy for decomposing the vapor. This technique is known as tribochemical vapor deposition (TCVD) and is similar to the ordinary chemical vapor deposition (CVD) in that heat created by friction is an important source of energy for driving the chemical reaction. Since the growth of fresh ceramic may occur at a slower rate than the loss of material due to wear, we were looking for a reduction in the wear rate as evidence that the concept of tribochemical vapor deposition is feasible. We performed a split-plot factorial design experiment to test whether TCVD was a viable approach to reduce wear. The plot variable was surface roughness and the sub-plot variables were the presence or absence of ATSB in the atmosphere, normal load and sliding speed. We found that ATSB did not have a statistically significant effect on wear. This negative result may be due to several reasons including: (1) insufficient ATSB in the boundary region, (2) insufficient energy to initiate the necessary reactions, (3) one or more slow reaction rates that created bottlenecks for creation of fresh material, and (4) poor adherence of fresh material on the contact surfaces. Further research will be required to understand why some condensation reactions occur under boundary lubrication conditions while others do not.

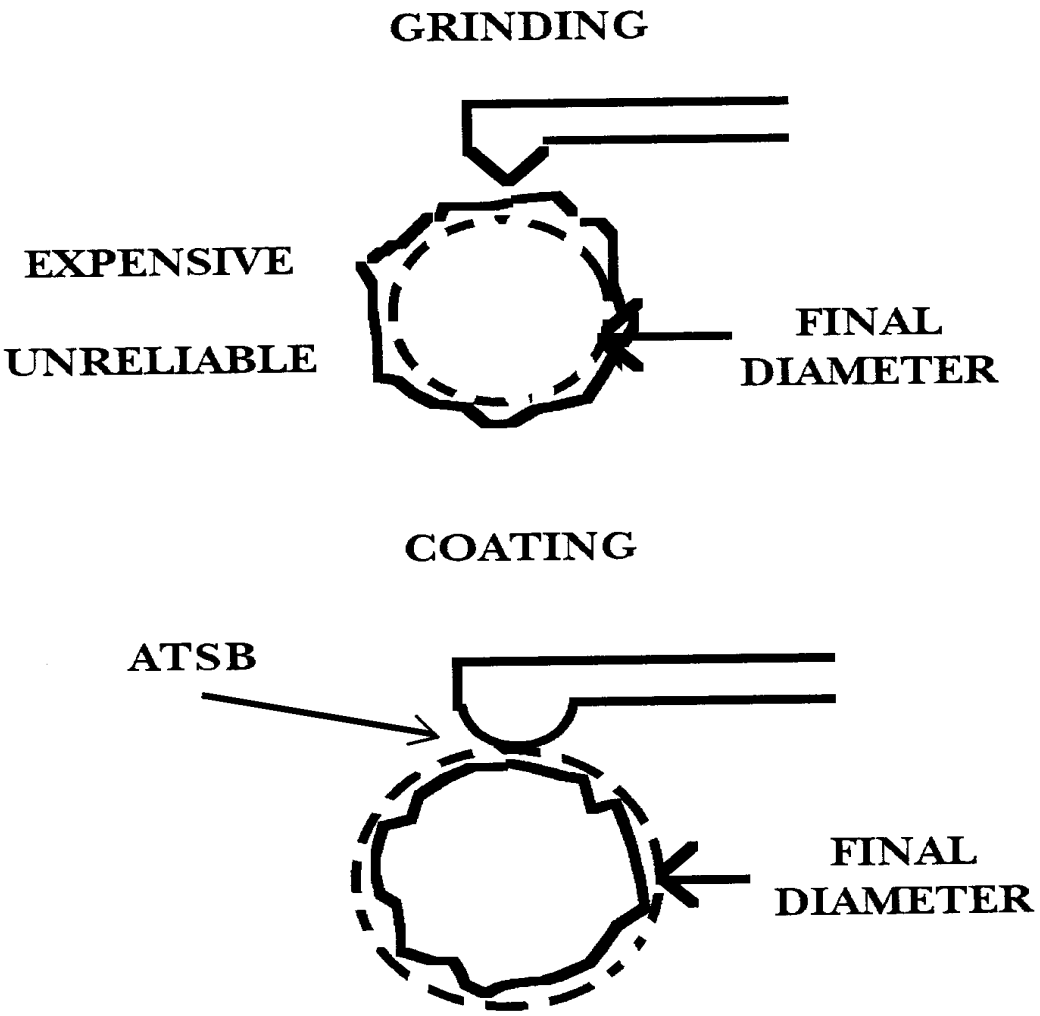

Figure 3.1. Schematic view of grinding versus coating for making precision ceramic components.

3.2 Background

In this study we explored whether the wear and friction of two alumina surfaces in sliding contact can be reduced by introducing the chemical vapor aluminum tri-sec butoxide, $[C_2H_5CH(CH_3)O]_3Al \equiv$ ATSB, from the environment into the boundary layer where it may break down and form alumina or possibly a mixture of alumina and aluminum hydroxide. This organometallic vapor was chosen because it has been used to grow films of alumina by metal organic chemical vapor deposition (MOCVD) at temperatures ranging from 300 - 400 °C [1].

The initiation of surface chemical reactions by tribomechanical energy in the boundary layer between two contacting surfaces has been studied extensively [2, 3, 4]. The Magma-Plasma model was an early attempt by Thiessen and his coworkers to explain their experimental results [5]. The model postulated that a plasma of energetic electrons and ions existed in the boundary region between two impacting bodies and that moving dislocations were being created on the two surfaces by the collision. The model originally applied to a projectile incident on a surface but might equally well describe the initiation of chemical reactions by the collision of asperities in the boundary layer between two moving surfaces. It is postulated that the plasma and surface excitations provide the energy necessary to initiate the reactions. Gilman [4] has argued that the existence of shear strain in the boundary region can reduce the symmetry of molecules adsorbed on the contacting region resulting in the destabilization of the electronic bonds and promotion of chemical reactions.

Reduction of wear and friction under dry sliding conditions by introduction of appropriate chemicals from the environment into the boundary layer has been demonstrated by Furey et al. [6], Tripathy et al. [7] and Singer [8, 9]. Furey et al. demonstrated that the concept of tribopolymerization is an effective approach to

designing specific molecular structures for boundary lubrication of ceramics under high contact stress conditions. They defined tribopolymerization as the planned and continuous formation of protective polymeric films directly on rubbing surfaces by the use of selected compounds capable of forming polymeric films "in situ". Tripathy et al., using this technique, obtained wear and friction reductions of 47% for a monoester (condensation type monomer) in hexadecane and up to 80% for Diallyl Phthalate (addition type monomer) in the same solvent.

Singer et al. [10] demonstrated the tribochemical creation of lubricative boundary layer compounds in a study of the metal-ceramic tribocouple Mo/SiC. This system achieved low, steady-state friction values ($\mu = 0.01$) when exposed to H_2S gas, but the friction coefficient immediately rose to $\mu = 1$ when the gas was cut off.

We hypothesized that the tribomechanical energy generated at the interface between two contacting surfaces might create fresh material from an appropriate chemical vapor by reaction mechanisms that are similar to chemical vapor deposition (CVD) and plasma chemical vapor deposition (PCVD). In the case of CVD, the chemical vapor decomposes on contact with a hot surface to deposit the coating material. The chemical vapor can be deposited on a cooler surface by PCVD because energy is supplied to the molecular constituents by the dc or rf plasma. Extensive literature exists on coating surfaces with ceramics by these two techniques [11, 12, 13, 14]. The most common precursors for depositing alumina are aluminum chloride ($AlCl_3$), trimethylaluminum ($AlMe_3$), alkoxides (aluminum tri-sec butoxide and others) and aluminum β-diketonates ($Al(acac)_3$). Deposition of alumina from aluminum chloride by CVD requires that the temperature of the substrate be in the range 700 - 900 °C. Trimethylaluminum can be used to deposit alumina at lower temperature, but it is pyrophoric. The alkoxides, on the other hand, are stable, have relatively low toxicity, and decompose on substrates in the temperature range 300 - 400 °C.

The formation of alumina by the decomposition of aluminum tri-sec butoxide vapor adsorbed on a surface proceeds by the condensation reaction

$$2\,[C_2H_5CH(CH_3)O]_3Al + \text{tribomechanical energy} \rightarrow Al_2O_3 + \text{products} \qquad (3.1)$$

where the products may be water, 2 - butanol, or butene. The ATSB molecule has sufficient oxygen that alumina or aluminum hydroxide may form in the boundary region without additional oxygen from the atmosphere.

The boundary layer between sliding surfaces is an extremely complex environment. In order to provide initial guidance in untangling the relationship between the dependent response variables friction and wear and the independent factors presence of ATSB, surface roughness, sliding speed, and the normal load, we did four replications of a split-plot factorial experiment [15]. The surface roughness could not be randomized with the other variables and, therefore, was treated as the plot variable. The sub-plot variables were the presence of ATSB, sliding speed and normal load. The normal load and sliding speed combinations were chosen to sample the different wear regimes of alumina [16, 17].

3.2 Experimental

3.2.1 Procedures and measurements

The experiment consisted of pressing two alumina balls against the opposite sides of a rotating alumina tube and measuring the friction coefficient and specific wear as a function of the four factors (presence of ATSB, surface roughness, sliding speed and normal load). Figure 3.2 shows the tubular alumina sample and one of the alumina balls that was pressed against it. The cylindrical alumina sample was mounted on a mandrel in a reaction chamber and was rotated at different speeds and for different distances by a precision stepper motor. Figure 3.3 shows a general view of the experimental setup with the reaction chamber and the precision stepper motor. Figure 3.4 is a close-up of the sample mounted on the mandrel inside the chamber. In these two pictures, the alumina balls are not yet pressed against the cylinder.

The alumina tube was 3.8 cm long and the nominal O.D was 2.54 cm. The two alumina balls were pressed against the opposite sides of the alumina cylinder by adjustable dead weights creating a single wear track around the cylinder. The alumina tube could be moved longitudinally with respect to the alumina balls so that wear and friction measurements for eight different treatment combinations could be made on one alumina sample tube.

The eight alumina sample tubes were cut from 99.8% purity alumina tubing from McDanel [Beaver Falls, PA]. One set of four samples, the rough surface, was ground with a diamond wheel to minimize the eccentricity of the tube. The second set of four samples, the smooth surface, was ground with a diamond wheel and then polished. The alumina balls that were pressed against the alumina tubing were 1.27 cm diameter, precision alumina balls (grade 50) from Sapphire Engineering [North Falmouth, MA].

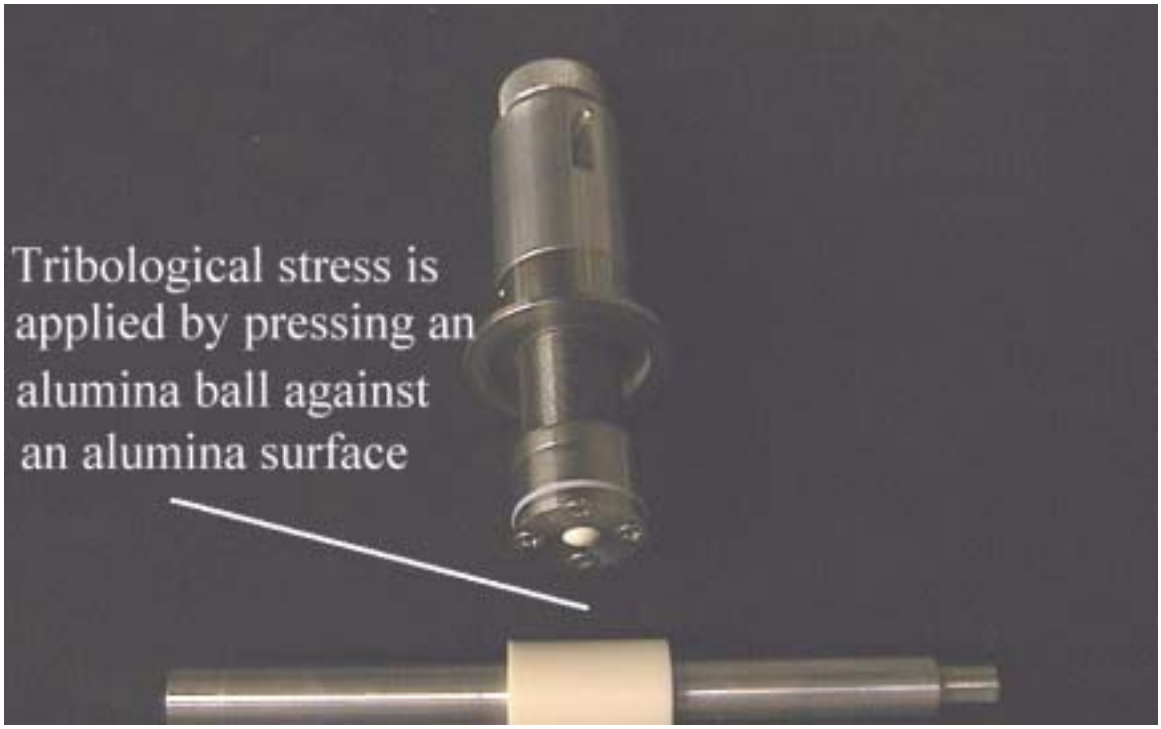

Figure 3.2. Tribological stress is applied by pressing an alumina ball against the cylindrical alumina sample.

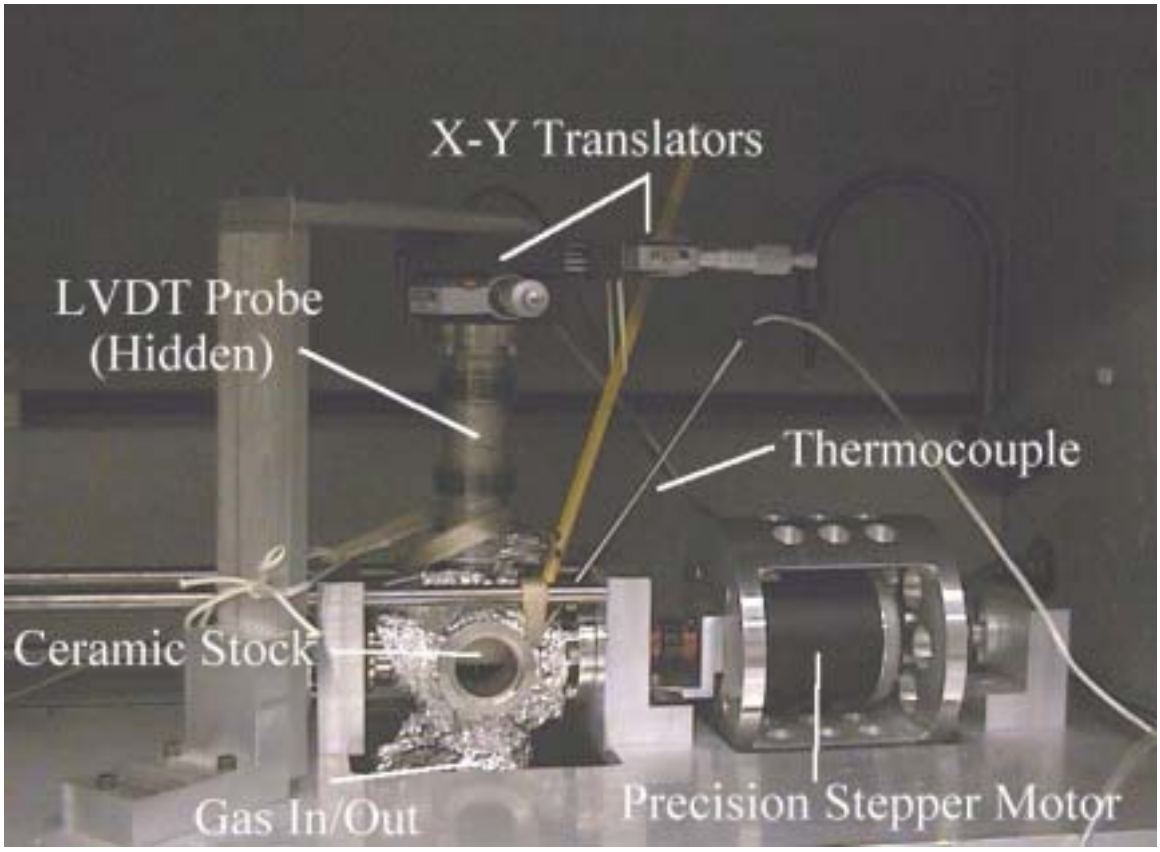

Figure 3.3. General view of the experimental setup. The ceramic sample is inside the reaction chamber. The alumina balls are not yet pressed against the sample. The precision stepper motor to the right of the reaction chamber rotated the sample for predetermined distances at different speeds.

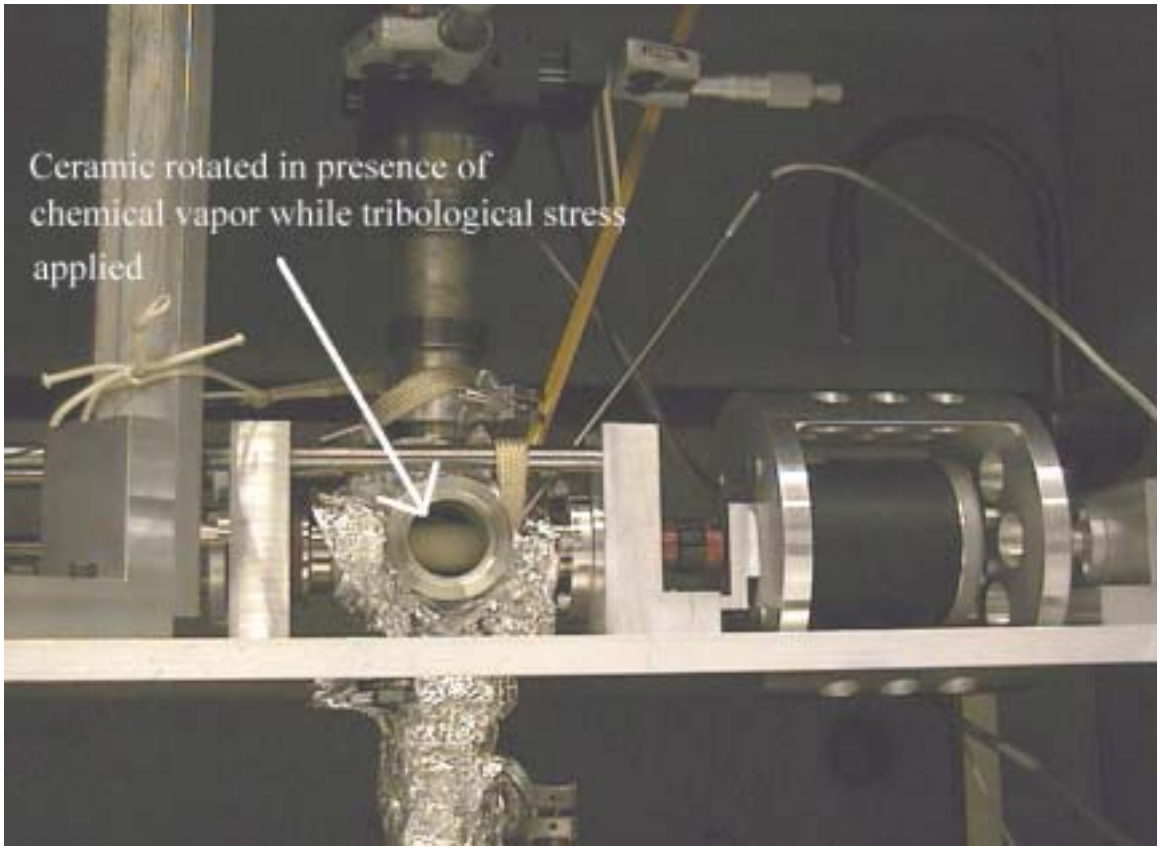

Figure 3.4. Close-up of the ceramic sample inside the reaction chamber. Heating tape was wrapped around the chamber and covered by aluminum foil. The open front port of the chamber is where the alumina ball is pressed against the sample.

The factor of primary interest in this experiment was the influence of the chemical vapor aluminum-tri-sec-butoxide on the specific wear and coefficient of friction. The ATSB was 97% purity from Aldrich Chemical [Milwaukee, WI]. The ATSB was generated in a bubbler heated to 145°C and was carried by purified nitrogen through the reaction chamber at a flow rate of 1000 cm^3/s. Figure 3.5 shows a schematic view of the rotating alumina sample inside the reaction chamber and of the flow path of the ATSB. The equilibrium vapor pressure of ATSB at 145° C is 0.27 kPa (2.1 mm Hg). All the gas lines and the reaction chamber were wrapped in heating tape and maintained at a temperature above the condensation temperature of ATSB.

In order to measure the friction coefficient, the stepper motor driving the alumina sample was mounted on a reaction torque gauge. The kinetic friction was determined from the torque at the beginning, middle, and end of a wear measurement. We did not observe any significant time dependence for the coefficient of friction and, therefore, conclude that within our statistical uncertainty, the coefficient of friction does not depend on sliding distance.

After the treatments, the surface profiles of the wear tracks were measured using a high precision linear variable differential transformer (LVDT) probe. Figure 3.6 is a schematic view of the LVDT probe and the eight circular wear tracks on the alumina sample.

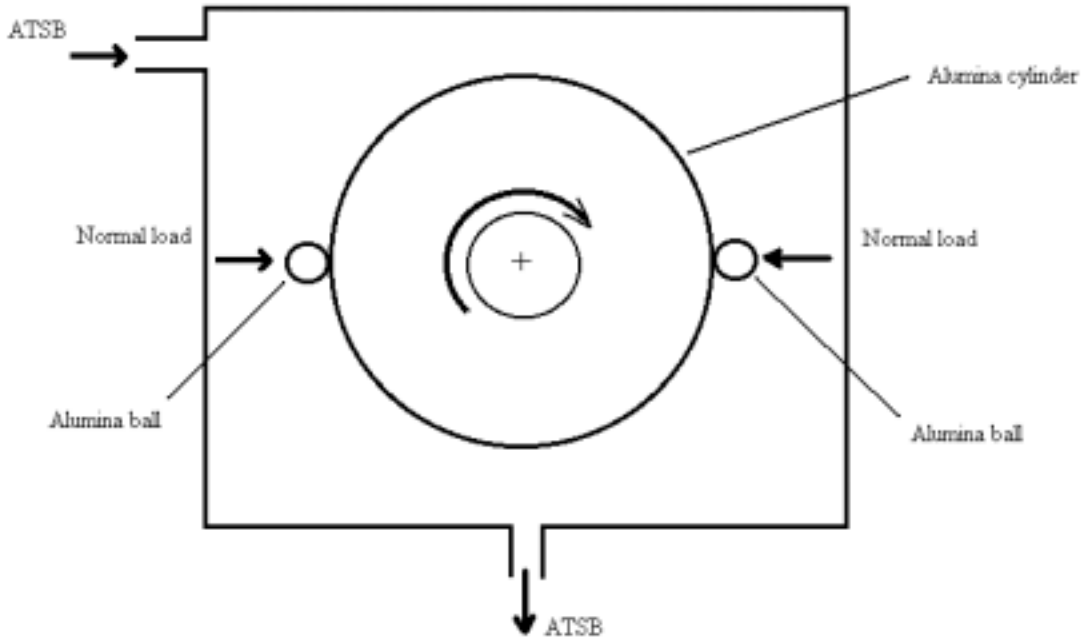

Figure 3.5. Schematic view of the cylindrical alumina sample rotating under tribological stress from the alumina balls inside the reaction chamber. The flow path of the ATSB is indicated by arrows.

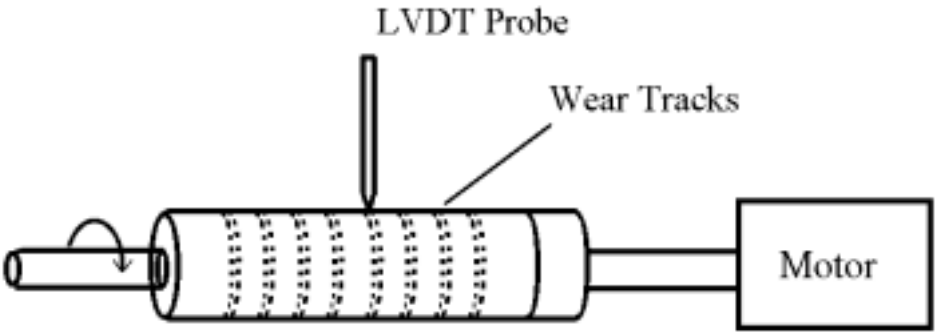

Figure 3.6. Schematic view of the LVDT probe and the eight circular wear tracks on the alumina sample. The profiles of the wear tracks were measured after the treatments.

3.2.2 Split-plot factorial design

One approach for examining the effects of two or more factors on a response is the one-at-a-time approach. To examine the effect of a single variable, an experimenter varies the levels of this variable while holding the levels of the other independent variables fixed. This process is continued until the effect of each variable on the response has been examined. However, the one-at-a-time approach is suitable only for situations in which the factors do not interact. We say that there is interaction between two factors when the effect of one factor on the response does not remain the same for different levels of the second factor. In other words, t*wo* factors A and B are said to interact if the difference in mean responses for two levels of one factor is not constant across levels of the second factor. A three-way interaction between factors A, B and C might indicate that the difference in mean response for levels of C changes across combinations of levels for factors A and B. In such a case, the information obtained from the one-at-a-time approach would lead to a faulty prediction.

Factorial experiments are useful for examining the effects of two or more factors on a response, whether or not interaction exists. In a factorial experiment, each factor has a certain number of levels; when the factor-level combinations are assigned to experimental units at random, we have a completely randomized design with treatments being the factor-level combinations. By definition, a factorial experiment is an experiment in which the response is observed at all factor-level combinations of the independent variables. The advantage of this technique over the one at a time approach is that it can be used to determine the response of some process to simultaneous changes in factors and, more important, it allows one to determine the existence of possible interactions between the factors in question.

The statistical design used for this experiment was a special kind of factorial design, know as split plot. The split-plot design consisted of four rough and four smooth alumina

tubes that comprised four replications and two levels of the plot variable surface roughness. Eight wear tracks were generated on each tube corresponding to eight random treatment combinations of the three sub-plot factors with two levels per factor. Each alumina tube with eight treatments is considered to be a block [18]. Thus, the complete split-plot factorial experiment consisted of 64 treatments: two surface treatments for the plot variable, 8 sub-plot treatments, and 4 replications. The response functions (dependent variables) were the specific wear and the coefficient of friction. The factors and levels used in these two sets of experiments are shown in Table 3.1. Constant parameters are also shown in the table.

Archard's wear equation (3.2) relates the volume worn per unit sliding distance, Q, to the macroscopic quantities W, the normal load, and H, the hardness of the softer surface.

$$Q = K*W/H \tag{3.2}$$

The constant K is known as the *wear coefficient* and it is dimensionless and always less than unity. The dimensionless wear coefficient K is of fundamental importance, and provides a valuable means of comparing the severity or wear processes in different systems. However, for engineering applications the quantity K/H is often more useful. This is denoted by the symbol k and called the *dimensional wear coefficient*. k is usually quoted in units of mm^3/Nm and represents the volume of material removed by wear (in mm^3) per unit distance slid (in meters), per unit normal load on the contact (in newtons). The measure of wear provided by k is particularly helpful for comparing wear rates in different classes of material. In some materials, elastomers for example, there are basic problems with the use of the dimensionless coefficient K since the plastic indentation hardness H cannot be defined. Archard's wear equation implies that if the dimensional wear coefficient k is a constant for a given sliding system, the volume (or mass) of material lost by wear is proportional to the distance slid and to the normal load W as a zeroth-order approximation.

Volume of material removed = k*W*distance (3.3)

The time interval that the ball was in contact with the rotating alumina tube determined the sliding distance. We chose the time for each treatment combination so that the product of load and distance was constant and equal to 1760 N-m. With the largest influence on wear volume held constant by this choice of time intervals, it was possible to distinguish more accurately the smaller effects of the chemical vapor, sliding speed, and load. A consequence of keeping the product of load and sliding distance constant is that the influence of load and sliding distance on wear can not be distinguished (The two factors are confounded).

The friction was measured at different times (equivalent to different sliding distances) during the experiment and did not vary within our statistical uncertainty. Therefore, any variation in friction with load level can be associated with the load rather than with sliding distance. A further consequence of choosing this product of load and distance was that the longest runs of the experiment (for low load and low speed) took 24 hours while the shortest runs (for high load, high speed) took 2.4 minutes.

Plot variable - surface roughness (μm)			
0.55		7.5	
Sub-plot variables			
Aluminum tri-sec butoxide (ATSB)	Normal Load (N)	Sliding Speed (m/s)	
Present in N_2 carrier gas	1.0	0.02	
Absent from N_2 carrier gas	10	1.2	
Constant Parameters			
Alumina Grain Size	Temperature of Bubbler and Chamber	Gas Flow Rate	Equilibrium vapor pressure of ATSB at 145°C
5 μm	145 °C	1000 cm^3/s	0.27 kPa (2.1 mmHg)

Table 3.1. Factors, levels and constant parameters for the split-plot factorial study.

3.3 Results

3.3.1 Specific wear

Figure 3.7 shows a scanning electron microscope (SEM) micrograph of a characteristic wear track. A typical surface profile (averaged over 10 random angles around the tube) is shown in Figure 3.8a. and 3.8b. Due to the limited travel of the micrometer to which the LVDT probe is attached, it was necessary to cover the length of the alumina tube in two sweeps. The positions of the 8 wear tracks are indicated in the figures. In order to determine the area of worn material (the wear volume is the area times the circumference of the alumina tube), the slow variation in surface height was removed by subtracting from the data (Figure 3.8a) a polynomial function that had been fit to the profile. Each track on the wear profile (Figure 3.8b) was then fit with a quadratic polynomial from which the volume of worn material for that track was calculated. The wear volume was divided by the product of load and distance (1760 N-m) to obtain the specific wear.

The main effects of each factor on the specific wear are shown in Figure 3.9a-d as boxplots [19]. The variation in specific wear between ATSB present and ATSB absent in the carrier gas is not statistically significant as is evident from the boxplots. Further statistical analysis of the data for the effect of ATSB on the specific wear is discussed below. The largest influence on specific wear is surface roughness with the wear of rough samples being significantly larger than the wear of smooth samples. The effect of speed on specific wear is also significant with higher wear occurring at higher speed. The variation in specific wear as a function of load is not statistically significant.

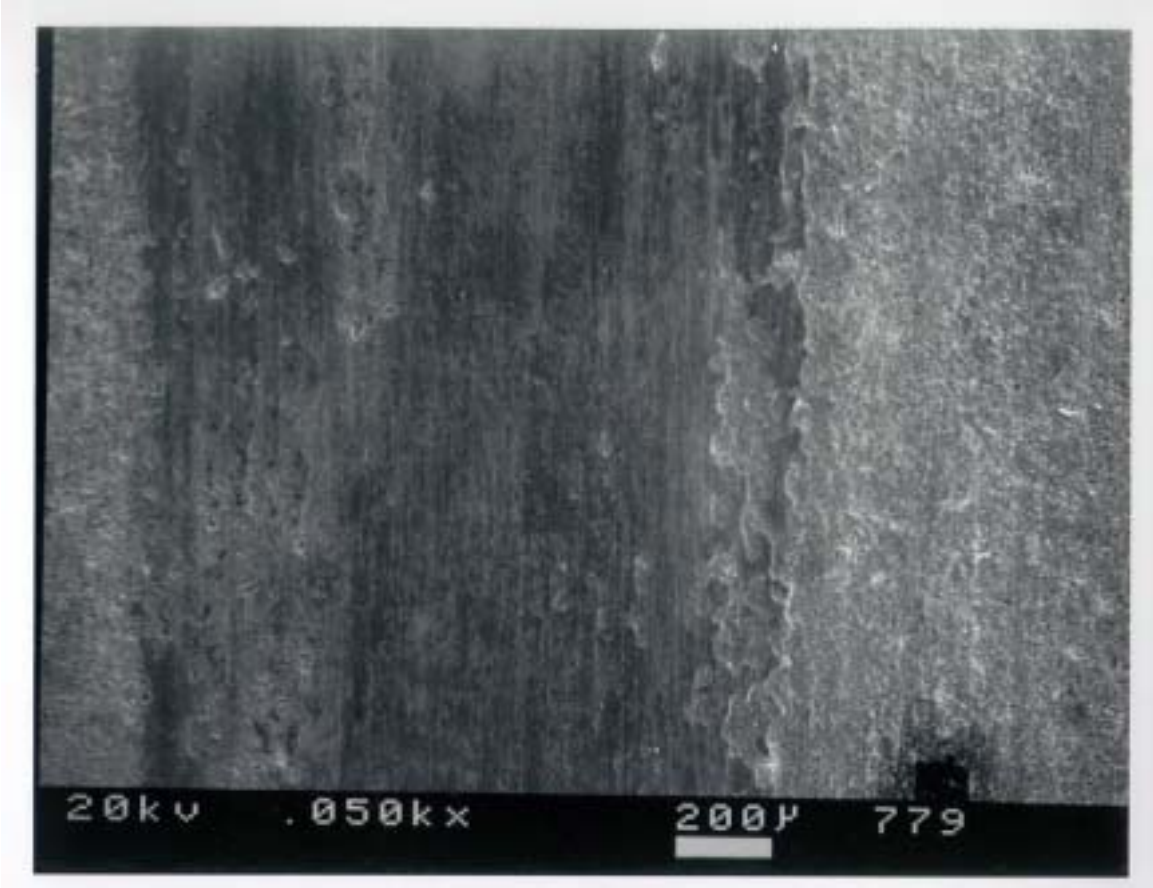

Figure 3.7. Typical SEM micrograph of the wear track created by the alumina balls sliding over the cylindrical surface of the alumina sample.

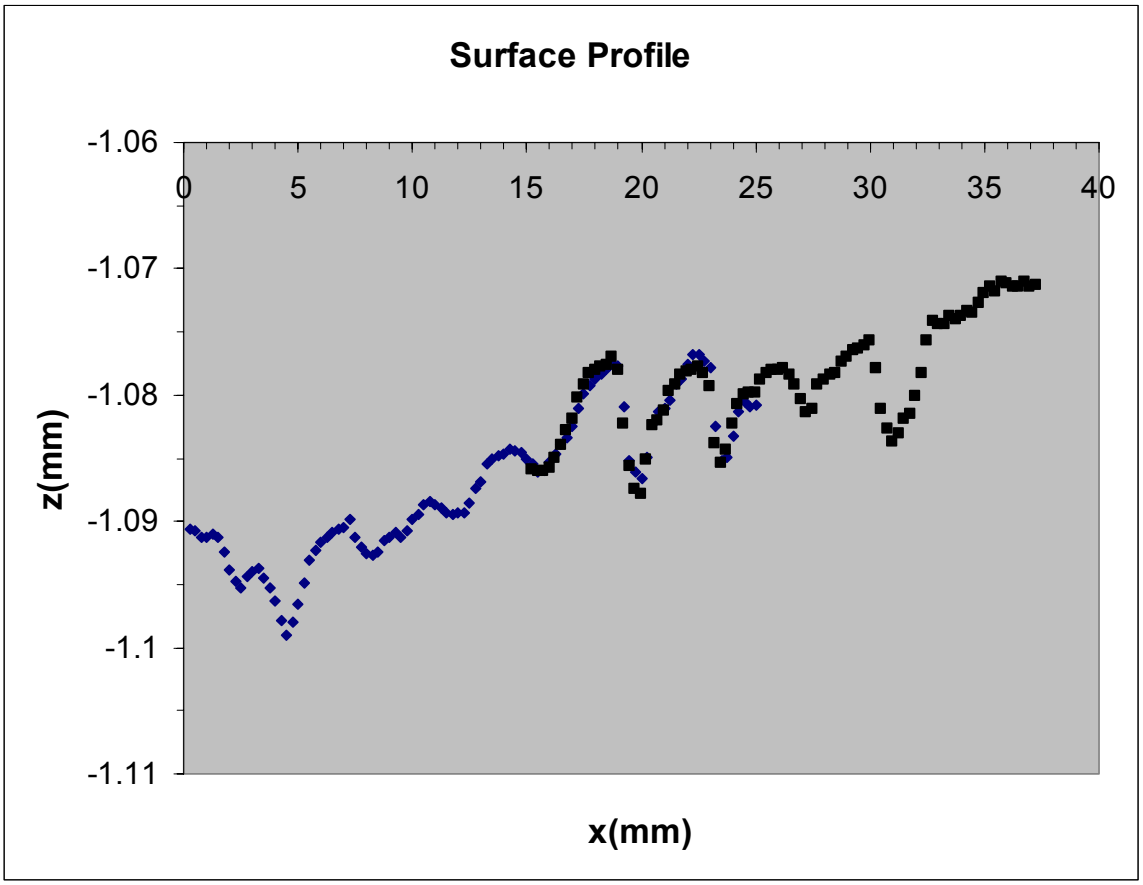

Figure 3.8a. Typical surface profile averaged for 10 random angles around the tubular sample. Due to the limited travel of the micrometer to which the LVDT probe is attached, it was necessary to cover the length of the alumina tube in two sweeps, which is reflected in the two different symbols used for the points on the graph. The positions of the wear tracks are indicated by vertical dashed lines.

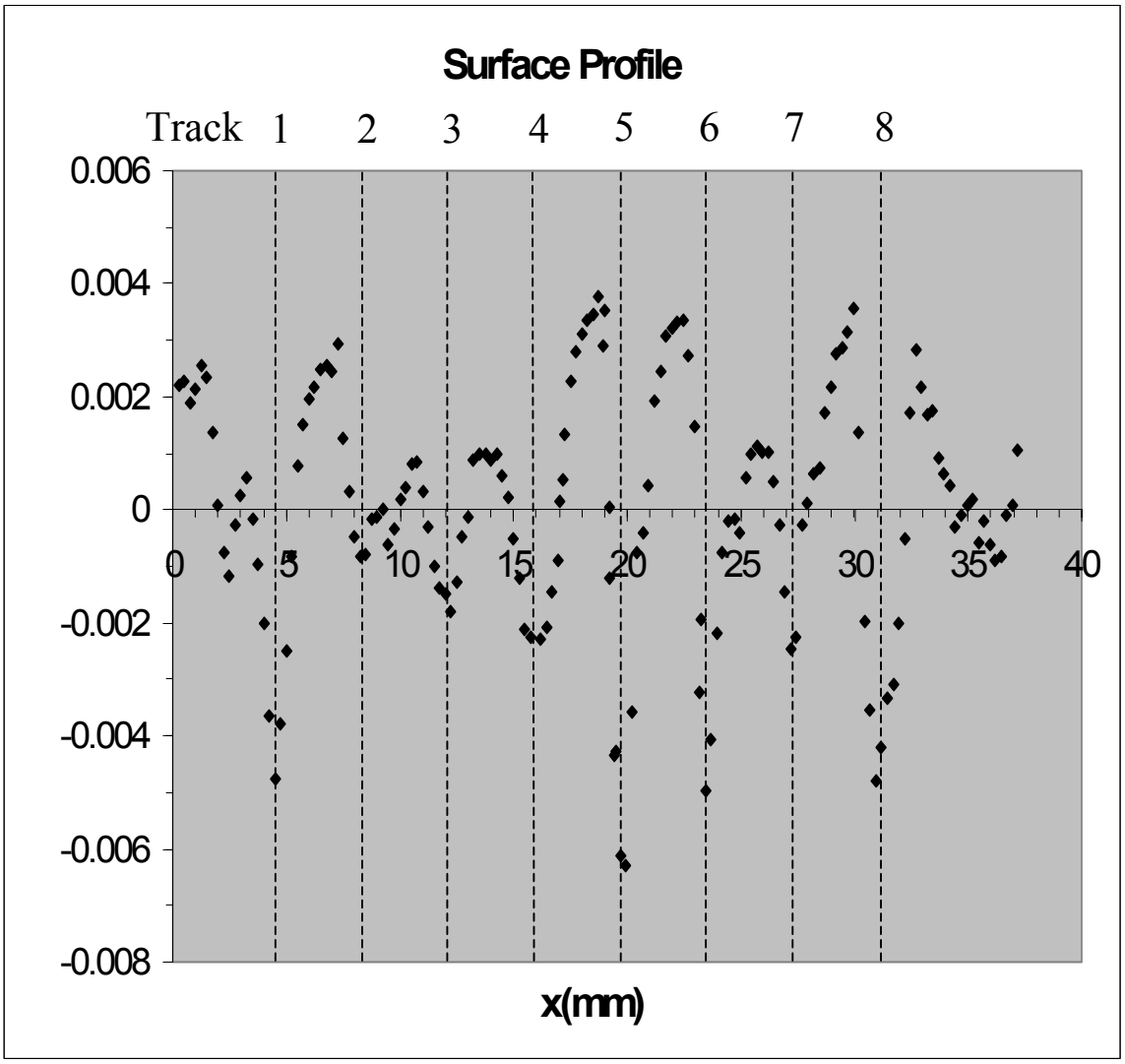

Figure 3.8b. Surface profile of the sample after the slow variation in surface height was removed by subtracting a polynomial function that had been fit to the profile from the data in Figure 3.8a.

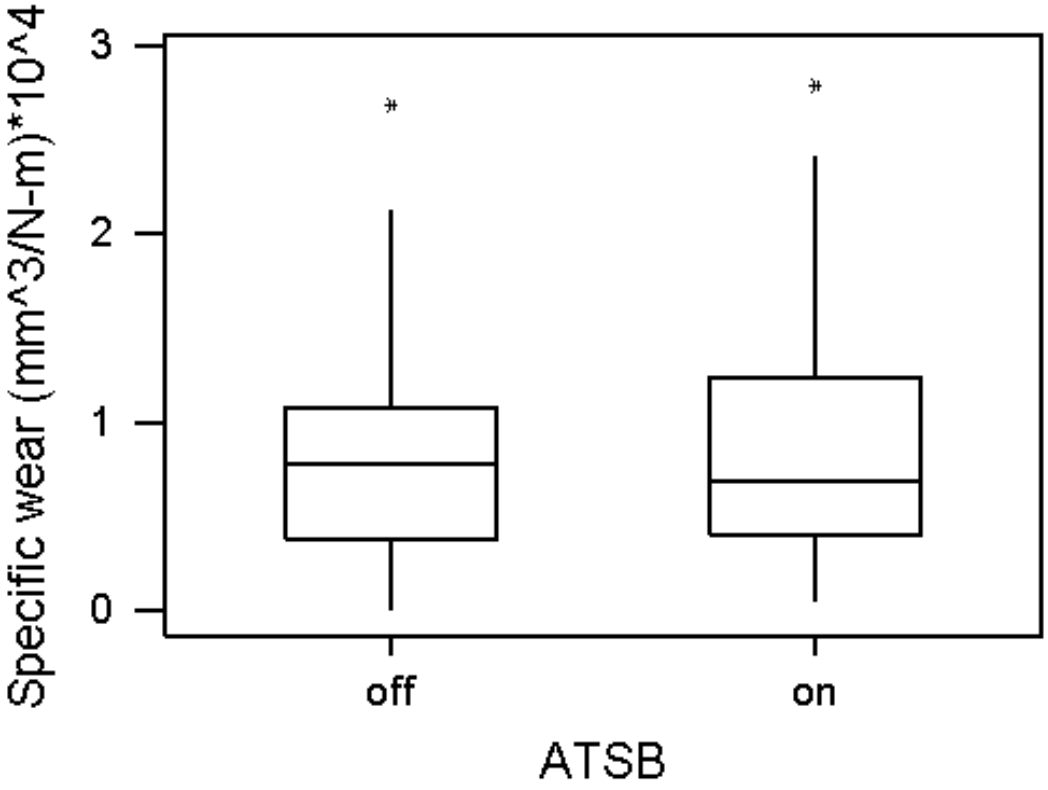

Figure 3.9a. Boxplot of the main effect of aluminum-tri-sec-butoxide (ATSB) gas on the specific wear.

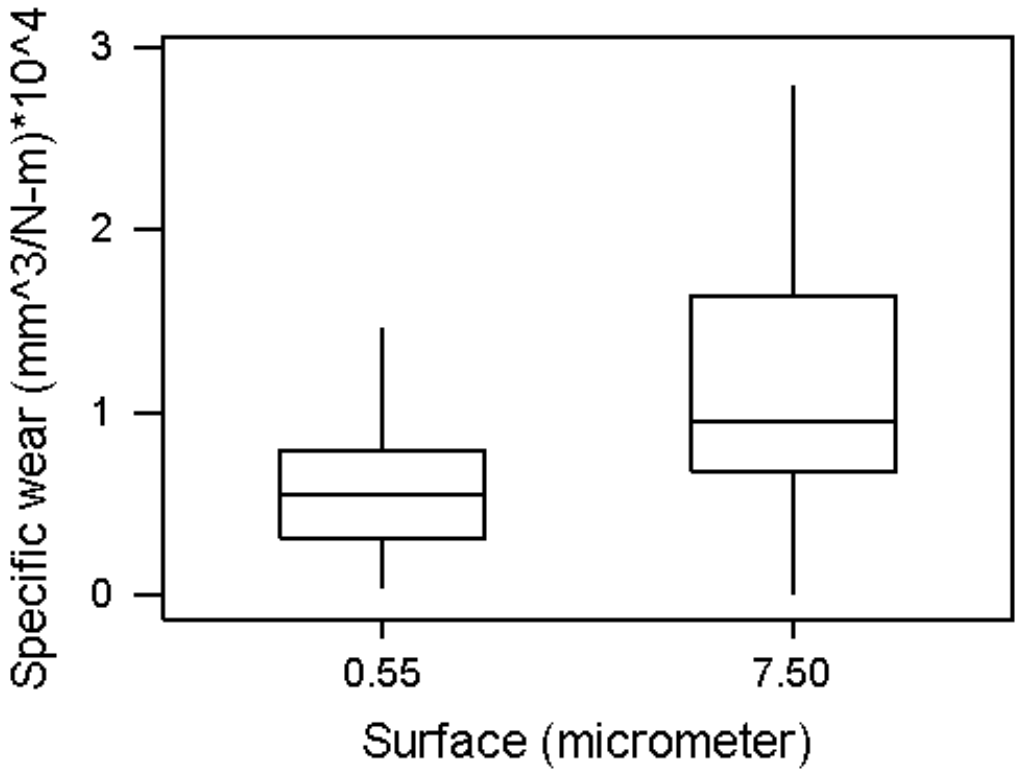

Figure 3.9b. Boxplot of the main effect of the surface roughness on the specific wear.

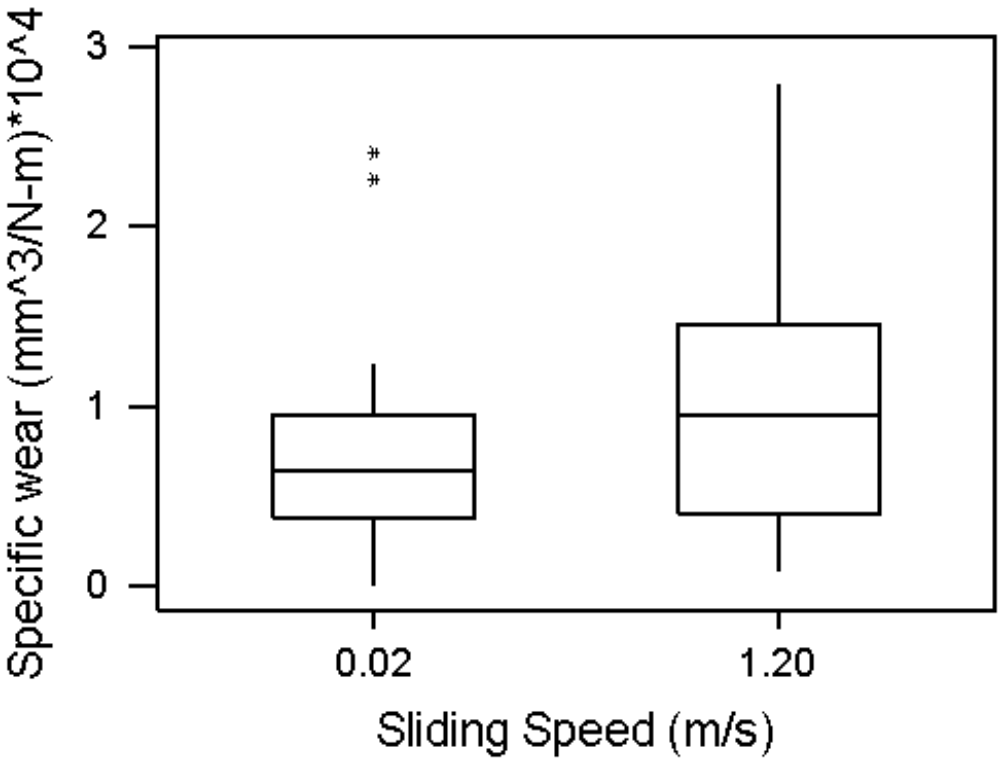

Figure 3.9c. Boxplot of the main effect of the sliding speed on the specific wear.

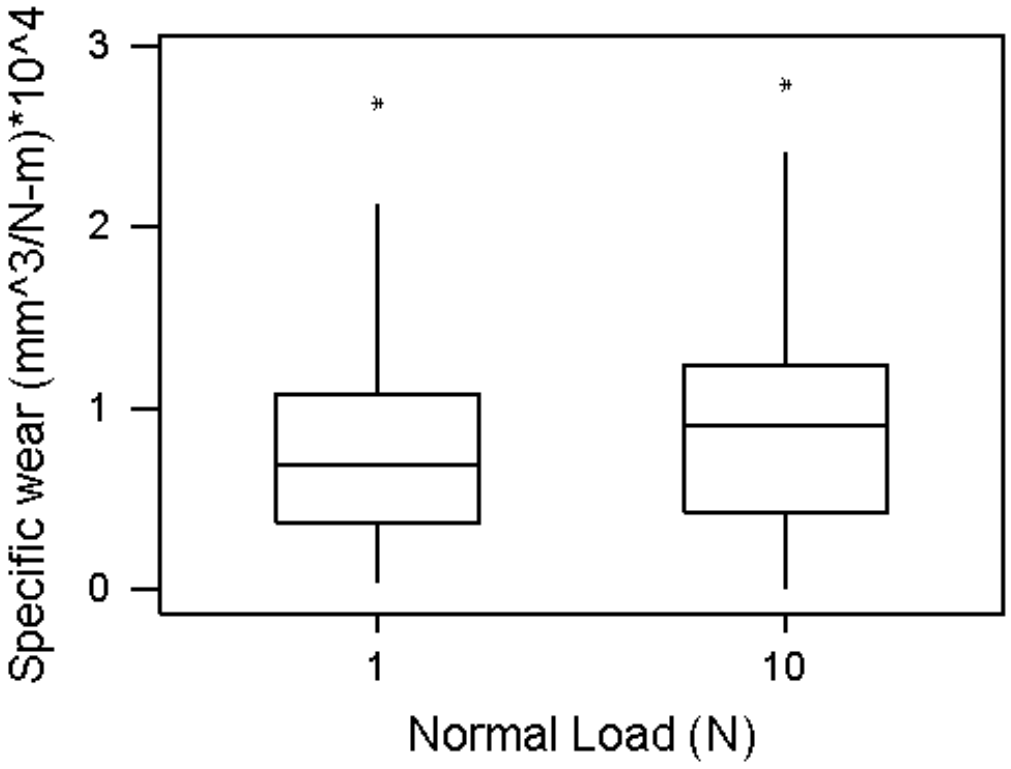

Figure 3.9d. Boxplot of the main effect of the normal load on the specific wear.

The analysis of variance for the split-plot measurement of specific wear is given in Table 3.2. Standard statistical tests applied to the data set confirm that it is consistent with a normal error distribution. In order to determine if the main effects of the various factors and the second order interactions [20] between the factors had a statistically significant influence on specific wear, we applied the F-test to the mean squares of the factors and the second order interactions. A value of F_0 much greater than one suggests that the variation in specific wear with factor or interaction levels is a real effect and not due solely to statistical fluctuation. The P-value is the cumulative of the F distribution from F_0 to infinity and $1 - P$ is a quantitative measure of the significance of the factor or interaction.

The F-test for the sub-plot factor ATSB gas is given by the ratio of the mean squares for the ATSB factor to the gas*blocks interaction mean squares (the sub-plot error for the ATSB factor) and equals $F_0 = 1.7$. The P-value for this ratio is $P = 0.28$ implying a significance level for this factor of 72% which does not support the hypothesis that the presence of ATSB affects the specific wear.

The surface roughness and speed factors have the largest variation in specific wear as a function of level as seen in Figure 3.9b and 3.9c. The F-test for the whole plot variable surface roughness is given by the ratio of the mean square variation in specific wear for this factor to the mean square interaction surface*blocks (the whole plot error) and $F_0 = 10.4$. The corresponding P-value is 0.05 and strongly supports (95% significance level) that the mean surface wear does depend on surface roughness. The test for the subplot variable speed is given by the ratio of the speed mean squares to the speed*blocks interaction mean squares (the subplot error for speed) and $F_0 = 6.2$. The corresponding P-value for this variable is $P = 0.09$ and supports (91% significance level) that the specific wear also depends on speed. Applying the same test to the sub-plot variable load and similar tests to the second order interactions between plot and subplot

Source of variation	Sum of squares	Degrees of freedom	Mean squares	F_0	P
Sample-to-Sample (Blocks)	1.52	3	0.51		
Surface Roughness (Surface)	5.41	1	5.41	10.4	0.05
Blocks*Surface (Whole-plot error)	1.56	3	0.52		
Gas	0.21	1	0.21	1.7	0.28
Blocks*Gas(Subplot error)	0.37	3	0.12		
Surface*Gas	0.07	1	0.07	0.22	0.67
Blocks*Surface*Gas(Interaction error)	1.02	3	0.34		
Load	0.40	1	0.40	0.48	0.54
Blocks*Load	2.51	3	0.84		
Surface*Load	0.03	1	0.03	1.6	0.30
Blocks*Surface*Load	0.05	3	0.02		
Speed	1.39	1	1.39	6.2	0.09
Blocks*Speed	0.67	3	0.22		
Surface*Speed	0.08	1	0.08	0.10	0.77
Blocks*Surface*Speed	2.44	3	0.81		
Gas*Speed	0.28	1	0.28	1.6	0.30
Gas*Speed*Surface*Blocks	0.53	3	0.18		
Speed*Load	0.40	1	0.40	1.6	0.30
Speed*Load*Surface*Blocks	0.77	3	0.26		
Gas*Load	0.46	1	0.46	2.0	0.25
Gas*Load*Surface*Blocks	0.69	3	0.23		

Table 3.2. Analysis of variance for the split-plot measurement of specific wear.

variables, we find no other statistically significant effects on wear ($P > 0.10$ for these factors and interactions).

3.3.2 Coefficient of friction

The main effects of each factor on the coefficient of friction are shown in Figure 3.10a-d as boxplots. The main effect of ATSB gas on the coefficient of friction is statistically insignificant, but the second order interaction between the ATSB gas factor and the sliding speed, shown in Figure 3.11, is statistically significant as will be discussed below. The existence of a substantial second order interaction between two factors can give rise to misleadingly small main effects for them and provides notice that the functional dependence of the response on the two factors may be relatively complex. The interaction plot for ATSB gas and speed indicates that the presence of ATSB reduces friction by 21% at low speed and increases friction by 26% at high speed.

The main effects of surface roughness and load are statistically significant and have comparable influence on the coefficient of friction. The coefficient of friction is a factor of two smaller for smooth samples relative to the coefficient of friction of rough samples. A more startling result is that the coefficient of friction decreases by over a factor of two when the load increases by a factor of ten. The second order interactions between the factors are not statistically significant except for the interaction, noted earlier, between ATSB gas presence and sliding speed.

The analysis of variance for the split-plot measurements of the coefficient of friction is given in Table 3.3. Standard statistical tests applied to the data set confirm that it is consistent with a normal error distribution. The F-test for the second order interaction between the presence or absence of ATSB and the factor sliding speed gives $F_0 = 5.4$ and a P-value of 0.10. This implies a significance level of 90% for this interaction,

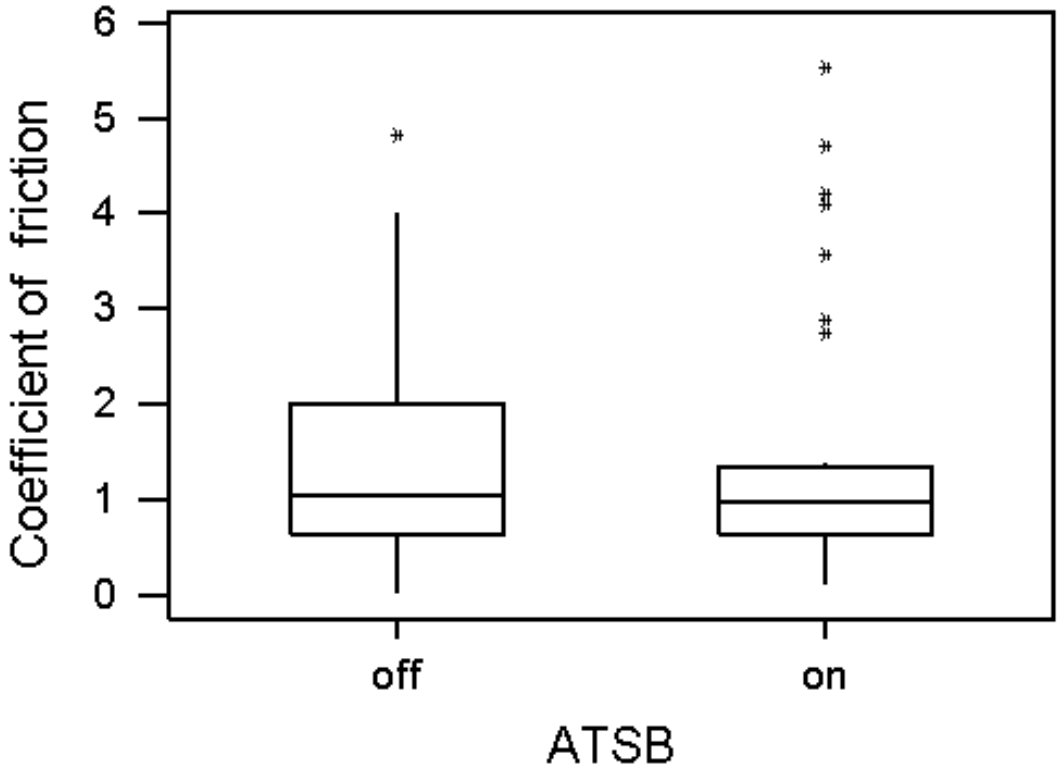

Figure 3.10a. Boxplot of the main effect of aluminum-tri-sec-butoxide (ATSB) gas on the coefficient of friction.

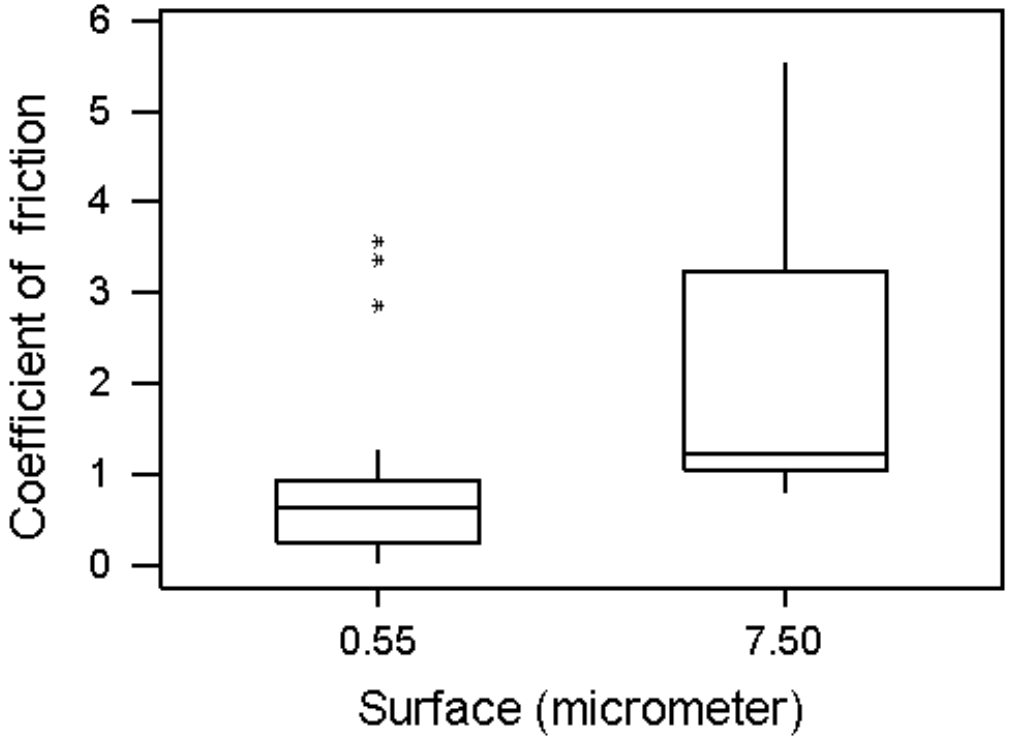

Figure 3.10b. Boxplot of the main effect of surface roughness on the coefficient of friction.

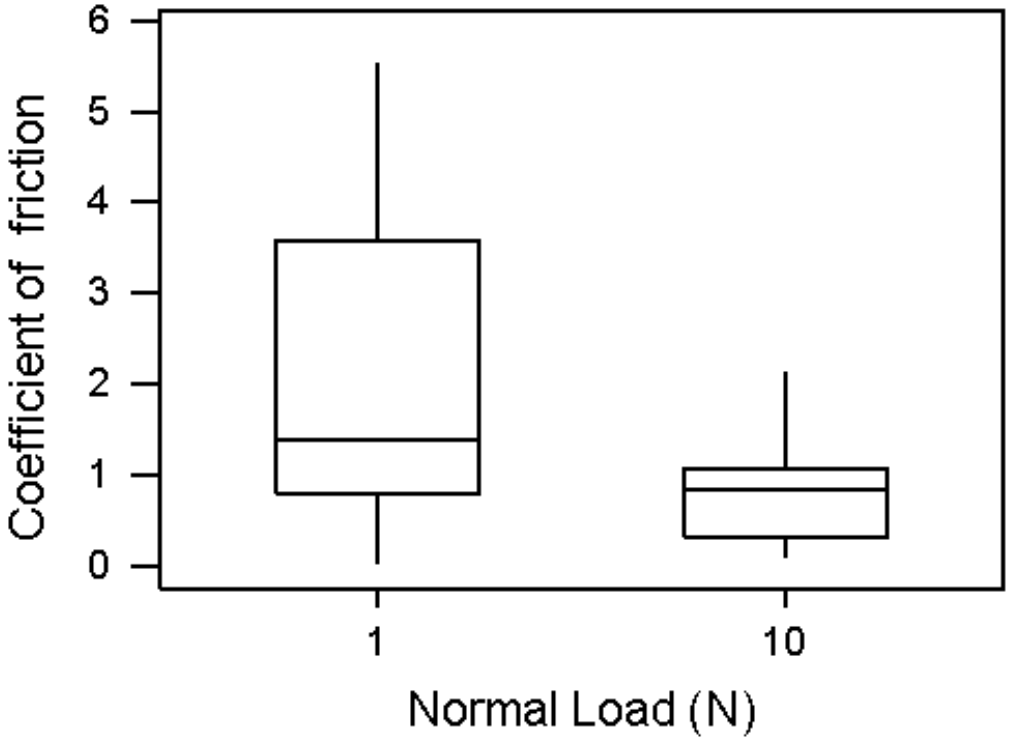

Figure 3.10c. Boxplot of the main effect of the normal load on the coefficient of friction.

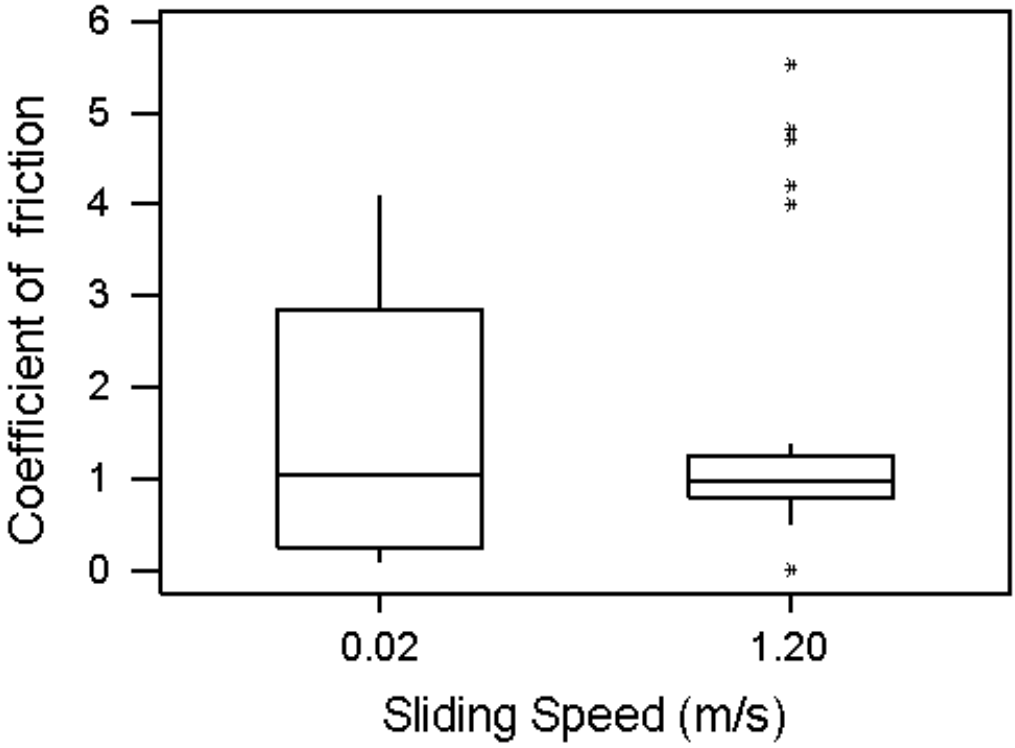

Figure 3.10d. Boxplot of the main effect of the sliding speed on the coefficient of friction.

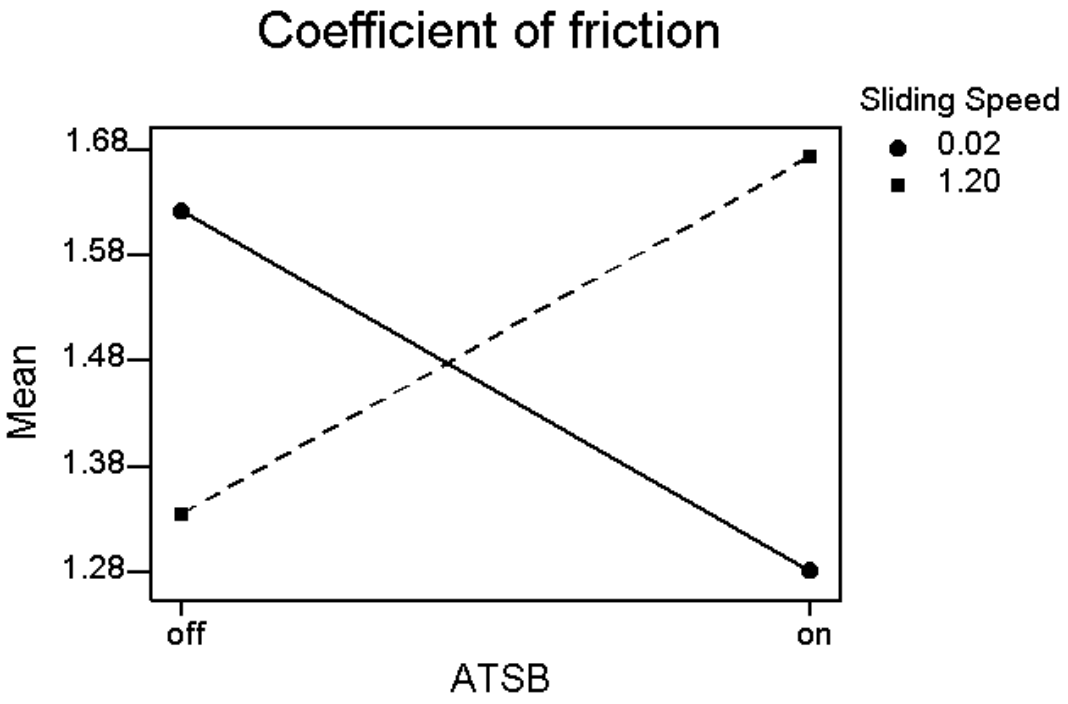

Figure 3.11. The second-order interaction effect between aluminum-tri-sec-butoxide (ATSB) gas and the sliding speed.

Source of variation	Sum of squares	Degrees of freedom	Mean squares	F_0	P
Sample-to-Sample (Blocks)	8.9	3	3.0		
Surface Roughness (Surface)	21	1	21	9.1	0.06
Blocks*Surface (Whole-plot error)	7.0	3	2.3		
Gas	<0.001	1	0.0	0.0	1
Blocks*Gas(Subplot error)	1.7	3	0.59		
Surface*Gas	1.2	1	1.2	1.0	0.39
Blocks*Surface*Gas(Interaction error)	3.5	3	1.2		
Load	30	1	30	18	0.02
Blocks*Load	5.1	3	1.7		
Surface*Load	3.8	1	3.8	2.2	0.23
Blocks*Surface*Load	5.2	3	1.7		
Speed	0.04	1	0.04	0.1	0.77
Blocks*Speed	1.2	3	0.41		
Surface*Speed	1.4	1	1.4	2.2	0.23
Blocks*Surface*Speed	1.9	3	0.64		
Gas*Speed	1.84	1	1.84	5.38	0.10
Gas*Speed*Surface*Blocks	1.03	3	0.34		
Speed*Load	0.39	1	0.39	0.34	0.60
Speed*Load*Surface*Blocks	3.44	3	1.15		
Gas*Load	0.09	1	0.09	0.11	0.76
Gas*Load*Surface*Blocks	2.43	3	0.81		

Table 3.3. Analysis of variance for the split-plot measurement of the coefficient of friction.

which supports the hypothesis that the presence of ATSB and the factor sliding speed do affect the coefficient of friction, but that the influences of these two factors on the coefficient of friction are interdependent.

The main effects of surface roughness and load on the coefficient of friction are also statistically significant. Applying the F-test to the coefficient of friction for the factor surface roughness, we find $F_0 = 9.1$ and a P-value of 0.06 giving a significance level of 94% that the coefficient of friction does depend on surface roughness. Similarly, for the factor load, the F-test gives $F_0 = 18$ and a P-value of 0.02 giving a significance level of 98% that the coefficient of friction depends on load. Applying the F-test to all other second order interactions besides gas*speed, we find no statistically significant effect on the coefficient of friction ($P > 0.10$ for these other second order interactions).

3.4 Discussion and Conclusions

3.4.1 Specific wear

Neither the main effect of the organometallic vapor ATSB on the specific wear of alumina-on-alumina, nor the effect on specific wear of second order interactions between the presence of ATSB and the other three factors (surface, speed, and load) were significant at a level greater than 75%. The lack of significant wear reduction by the presence of ATSB may be due to several reasons including: (1) insufficient ATSB in the boundary region, (2) insufficient energy to initiate the necessary reactions, (3) one or more slow reaction rates that created bottlenecks for creation of fresh material, and (4) poor adherence of fresh material on the contact surfaces. Further research will be required to understand why some condensation reactions occur under boundary lubrication conditions while others do not.

The specific wear did depend on initial surface roughness and speed to a statistically significant extent. Considerable research on the wear of alumina has demonstrated the existence of a mild wear to severe wear transition as a function of normal contact load, sliding distance, sliding speed, and temperature [Jahanmir and Dong [16] and references therein]. The transition can be over several orders of magnitudes from specific wear rates of less than 10^{-6} mm^3/N-m to rates that are over 10^{-4} mm^3/N-m. Our results for the specific wear, in the range 10^{-5} mm^3/N-m to 3×10^{-4} mm^3/N-m, are in the transition region from mild to severe wear. In this wear region, we found that the factors surface roughness and sliding speed had a statistically significant effect on specific wear, but that the normal load and sliding distance do not have a statistically significant effect.

Adachi et al. [17] studied the wear of alumina pin on alumina disk over a range of factor levels that overlapped our study. The initial roughness and mean grain size of their samples were $R_y \approx 3$ μm and $D_g = 5$ μm, respectively. As a function of the load and

sliding speed, they obtained wear maps for two different pin radii that delineated regions of mild (specific wear < 10^{-6} mm^3/N-m) and severe wear (specific wear > 10^{-6} mm^3/N-m). The mild-to-severe boundaries (pin radius = 4 mm) for velocity and load were approximately 0.2 m/s and 60 N, respectively. The boundaries were at higher speed and lower load for the smaller pin radius of 2 mm. Our results for a ball of radius 6.2 mm are consistent with the velocity, but not the load boundaries of Adachi et al. For loads of 1 N and 10 N, we find severe wear whereas Adachi et al. report mild wear in this region of load.

A study by Blomberg et al. [21] of alumina wear for dry sliding as a function of normal load and sliding velocity also overlaps our study. Their boundary between mild and severe wear is a line with intercepts at roughly a speed of 6 m/s and a load of 100 N. In the entire region of overlap with our study, sliding velocity less than 2 m/s and load less than 10 N, they find mild wear in disagreement with our findings that the specific wear is greater than 10^{-5} mm^3/N-m (transition region between mild and severe wear). The difference between their results and ours could be due to the different geometry of their test apparatus; theirs simulated a flat-on-flat contact geometry while ours was closer to a ball-on-flat geometry. But a more likely explanation for the difference is the fact that they used hydraulic loading of one flat to minimize vibration of the test flats against each other. This would tend to move their mild-to-severe wear boundaries to larger values of load and speed than would exist in the absence of damping.

3.4.2 Coefficient of friction

The median coefficient of friction as a function of the four variables surface roughness, presence of ATSB, sliding speed, and normal load varied between 1.0 and 2.0 in the transition region from mild to severe wear of our study. The main effect of ATSB being present or absent from the carrier gas was not statistically significant. But there was a statistically significant interaction between the presence ATSB and the sliding speed. At low speed (0.02 m/s), the mean coefficient of friction decreased from 1.63 when ATSB was absent to 1.28 when it was present. At high speed (1.2 m/s), the mean coefficient of friction increased from 1.33 when ATSB was absent to 1.67 when ATSB was present. This interaction between the presence of ATSB and the sliding velocity may be due to water produced as a by-product of the condensation reaction of ATSB on the alumina surface.

Several studies of the effect of humidity and water on the wear and friction of alumina have given conflicting results [22]. Two competing processes are thought to contribute to the ambiguity. Water accelerates crack growth resulting in increased microfracture and stimulating wear and friction, but water also reacts with the alumina surface to form a lubricious aluminum hydroxide film that reduces microfracture and friction. Our observation of an interaction between ATSB and sliding velocity may be evidence that the level of sliding velocity can shift the balance between these two processes. That is, at high velocity, the wear and friction are dominated by the acceleration of crack growth from the presence of water created when ATSB reacts with the alumina surface, while at low velocity, friction is reduced by the formation of an aluminum hydroxide film from the ATSB reacting with the surface.

The effects of surface roughness and normal load on the median coefficient of friction were also statistically significant. Not surprisingly, the median coefficient of friction for rough samples (2.1) was larger than the median coefficient of friction for smooth samples

(0.9). But the decrease in the median coefficient of friction with an increase in load is more puzzling. The change in the median coefficient of friction from 2.2 when the normal load is 1 N to 0.8 when the load is 10 N is roughly a factor of 0.4 which is consistent with the load being distributed over the area of an elastic (Hertzian) pressure contact. For Hertzian contact, the coefficient of friction is predicted to vary at low loads (below the yield point) as W^{-n} where n = 1/3 for a circular contact and n = 1/2 for a cylindrical (line) contact. The observation of Hertzian behavior is rare for dry sliding because the pressure is normally distributed over a finite number of asperity contacts rather than over the apparent area of contact. We have no explanation for this apparent inconsistency.

References

[1] V. A. C. Haanappel, H. D. van Corbach, T. Fransen, and P. J. Gellings, *Thin Solid Films*, 230 (1993), 138-144.

[2] P.G. Fox, *J. Mater. Sci*., 10 (1975), 340 – 360.

[3] Gerhard Heinicke, *Tribochemistry*, Akademie - Verlag, Berlin, 1984.

[4] John J. Gilman, *Science*, 274 (1996), 65.

[5] P. A. Thiessen, *Grundlagen der Tribochemie*, Wiss. Berlin Abh. Deut. Akad, Berlin, 1967.

[6] M.J. Furey and C. Kajdas, *Proc. Of the 4th Int.l Symp. On Ceramic Materials and Components for Engines*, Goteborg, Sweden, June 10-12, 1991, ed. by R. Carlsson, T. Johansson, and L. Kahlman, Elsevier Applied Science, London (1992), 1211-1218.

[7] B.S. Tripathy, M.J. Furey, and C. Kajdas, *Wear,* 181-183 (1995), 138-147.

[8] I. L. Singer, *MRS Bulletin*, (June 1998), 37-40.

[9] I.L. Singer, *Langmuir,* 12 (1996), 4486-4491.

[10] I. L. Singer, Th. Le Mogne, Ch. Donnet, and J-M Martin, *Tribol. Trans.* 39 (1996), 950-956.

[11] W.S. Rees (ed.), *CVD of Nonmetals*, VCH, New York, 1996.

[12] Chemical Vapor Deposition, *Advanced Materials*, Vol.2, 1996.

[13] J. Mort and F. Jansen (eds.), *Plasma Deposited Thin Films*, CRC, Boca Raton, 1986.

[14] L.A. Ryabova, *Current Topics in Material Science*, Vol. 5, ed. by E. Kaldis, North-Holland, New York, 1981, 587-641.

[15] Douglas C. Montgomery, Design and Analysis of Experiments, Fourth Edition (Wiley, New York, 1997), p. 521.

[16] S. Jahanmir and X. Dong, *J. Tribol.*, 114 (1992), 403-411.

[17] K. Adachi, K. Kato, and N. Chen, *Wear*, 203-204 (1997), 291-301.

[18] "Blocking is a technique used to increase the precision of an experiment. A block is a portion of the experimental material that should be more homogeneous than the entire set of material. Blocking involves making comparisons among the conditions of interest in the experiment within each block." Douglas C. Montgomery, Design and Analysis of Experiments, Fourth Edition (Wiley, New York, 1997), p. 13.

[19] The box plot (or box and whisker plot) is a convenient way to display data. The middle line in the boxplot for a specific factor A and treatment level a (a can take two values in our experiment; eg. rough or smooth, lo speeed or hi speed, etc.) is the median value of the response variable (specific wear or coefficient of friction) over all treatment combinations and replications of treatment combinations having that particular treatment level of factor A. The bottom and top of the box are the first (Q1) and third (Q3) quartiles, respectively, for the data. The whiskers (vertical lines) extend to the lower limit [Q1 - 1.5 (Q3-Q1)] and upper limit [Q3 +1.5 (Q3 - Q1)] of the data. Outlier data points outside these limits are marked by a star. The main effect of the factor A on the response

variable is the difference between the mean value of the response variable when the treatment level a is "hi" and the mean value of the response variable when the treatment level a is "lo". For a normal error distribution, the mean and median are equal.

[20] An interaction effect for the dependent response variable $y_{i,\,j\ldots}$ (i, j … enumerate the treatment levels for the different factors) between two factors A and B with two levels for each factor a = hi, lo and b = hi, lo is given by

$$\text{interaction } A*B = (\underline{y}_{a=hi,\,b=hi} - \underline{y}_{a=hi,\,b=lo} - \underline{y}_{a=lo,\,b=hi} + \underline{y}_{a=lo,\,b=lo})/2$$

where $\underline{y}_{a,b}$ is the average response over all other factors for the given treatment levels a and b. If the response is the sum of a functional of A alone plus a functional of B alone, then the interaction is zero.

[21] A.Blomberg, M. Olsson and S. Hogmark, Wear 17 (1994), 77-89.

[22] J.K. Lancaster, Y. A-H Marshal and A.G. Atkins, J. Phys. D: Appl. Phys. 25 (1992), A205-A211.

Acknowledgement

This material is based upon work supported by the National Science Foundation under Grant No. CMS-9625625.

Vita

Dan A. Mazilu was born on December 25th, 1971 in Iasi, Romania. He received his Bachelor of Science degree in Engineering Physics in June 1995 from Alexandru Ioan Cuza University of Iasi, Romania. As an undergraduate student, he was an exchange student at the University of Nebraska at Omaha with the Samantha Smith Memorial Exchange Program, from January to August 1994.

In 1996, he received a TEMPUS scholarship at the Catholic University of Leuven in Belgium and in June of the same year he received his Master of Science degree in Physics from Alexandru Ioan Cuza University of Iasi, Romania.

In August 1996 he came to the State University of New York at Buffalo as a graduate student in the Physics Department and he transferred to Virginia Tech in January 1997. He received a Master of Science degree in Physics in December 1998 from Virginia Tech and he has continued since then his doctoral studies.